REPORT DOCUMENTATION PAGE

Form Approved OMB No. 0704-0188

1. AGENCY USE ONLY (Leave blank)	2. REPORT DATE	3. REPORT TYPE AND DATES COVERED
	1995	Final Report

4. TITLE AND SUBTITLE

Investigation of Feel System and Control Sensitivity Characteristics Influencing P-I-O of Unmaneuverable Aircraft

5. FUNDING NUMBERS

F6170894W0315

6. AUTHOR(S)

Dr. Victor Rodchenko

7. PERFORMING ORGANIZATION NAME(S) AND ADDRESS(ES)

TsAGI, Central Aerohydrodynamic Institute
Zhukovsky 3, 60
Moscow 140160
Russia

8. PERFORMING ORGANIZATION REPORT NUMBER

N/A

9. SPONSORING/MONITORING AGENCY NAME(S) AND ADDRESS(ES)

EOARD
PSC 802 BOX 14
FPO 09499-0200

10. SPONSORING/MONITORING AGENCY REPORT NUMBER

SPC 94-4027

11. SUPPLEMENTARY NOTES

12a. DISTRIBUTION/AVAILABILITY STATEMENT

Approved for public release; distribution is unlimited.

12b. DISTRIBUTION CODE

A

13. ABSTRACT (Maximum 200 words)

This report results from a contract tasking TsAGI, Central Aerohydrodynamic Institute as follows: Investigate the pilot-induced-oscillation (PIO) tendency depending upon control sensitivity characteristics, damping of lever loading, lever mass and loading gradient at different flight regimes and dynamic performance using flight simulators.

14. SUBJECT TERMS

Nil

15. NUMBER OF PAGES

82

16. PRICE CODE

N/A

17. SECURITY CLASSIFICATION OF REPORT	18. SECURITY CLASSIFICATION OF THIS PAGE	19. SECURITY CLASSIFICATION OF ABSTRACT	20. LIMITATION OF ABSTRACT
UNCLASSIFIED	UNCLASSIFIED	UNCLASSIFIED	UL

TSAGI Central Aerohydrodynamic Institute

SPC -94-4027

INVESTIGATION OF FEEL SYSTEM AND CONTROL SENSITIVITY CHARACTERISTICS INFLUENCING P-I-O OF UNMANEUVERABLE AIRCRAFT

Project manager

Victor V Rodchenko, Ph.D.

Executors:

Victor V.Rodchenko
Larisa E.Zaichik
Yury P.Yashin
Victor V.Lyasnikov
Alexander M.Galyuchenko
Igor W.Rufov

Zhukovsky, 1995

CONTENTS

ABSTRACT

Presented are the results of studies aimed at revealing regularities of the effect of control sensitivity and feel system characteristics on low- and high-frequency PIO and developing methods of evaluating this effect. The study has been performed at TsAGI in compliance with the AF sponsored research contract SPC-94-4027.

The technique of PIO investigation on a flight simulator has been refined. Effect of simulator motion on PIO has been studied. It has been shown that PIO ground-based simulation should be conducted on a moving-base simulator, because the motion cues can influence greatly the PIO tendency in the modeled conditions (in some cases it becomes greater, in others it decreases). A method of pilot dynamic performance identification, which allows us to obtain, from the experiments directly, a common pilot describing function and, at the same time, dynamic performance of closed loop limb-manipulator system.

The experiments were conducted to study the effect of feel system and command sensitivity characteristics on low-frequency PIO. Obtained are the experimental results concerning the optimum feel system and command sensitivity characteristics for a tracking task, and pilot ratings worsening in the case of the characteristics deviation from their optimum values. The criterion is proposed for the estimation of manipulator feel system and command sensitivity influence on PIO. The criterion allows a designer, firstly, to define the optimum control sensitivity values for the given feel system characteristics for a tracking task, and, secondly, to estimate, in terms of the PIO tendency, pilot ratings worsening while command sensitivity and feel system characteristics deviating from their optimum values.

High frequency PIO occurring for certain feel system characteristics, aircraft dynamic performance, structural elastic mode have been studied, and the reasons of the phenomenon arising have been considered. It has been shown that for an unmaneuverable aircraft one of the causes of high frequency PIO can be the aircraft elastic modes coupled with limb-manipulator dynamics. The degree of the coupling depends on the elastic mode amplitude peak value, type of manipulator and its feel system, command sensitivity characteristics and aircraft dynamic performance. The influence of accelerations experienced by a pilot plays a significant role in PIO phenomenon. To analyze high-frequency oscillations in the roll axis the mathematical pilot-aircraft system model can, with a good reason, be used.

NOMENCLATURE

F, X - manipulator force and displacement (kg, mm)

F_{n_z}, X_{n_z} - longitudinal command-response gradients (control sensitivity characteristics, kg/g, mm/g)

F_p, X_p - lateral command-response gradients (kg/deg/sec, mm/deg/sec)

F^x, F_{br} - feel system gradient and breakout force (kg/mm, kg)

n_z, n_y - normal and lateral accelerations

n_{Z_α} - normal acceleration per unit angle of attack (g/rad)

α, β - angle of attack and sideslip angle (rad)

θ, ϕ, ψ - pitch, roll and yaw angles (rad)

q, p, r - pitch, roll, yaw rates (rad/sec)

V - flight velocity (m/sec)

T_R - roll mode time constant (sec)

Y_p, Y_c - transfer functions models of pilot and controlled element

Y_{n_z} - X/n_z - transfer function

Z, Y - aerodynamic forces along z- and y- axes

M, L, N - pitching, rolling and yawing aerodynamic moments

$\delta_a, \delta_e, \delta_r$ - deflection of aileron, elevator and rudder (deg)

$Z_\alpha, \ldots, Y_\beta, \ldots, M_\alpha, \ldots, L_\beta, \ldots, N_\beta, \ldots$ - force and moment aerodynamic dimensionless derivatives

INTRODUCTION

Pilot-induced-oscillation phenomenon (PIO) has been the problem of considerable importance for modern aircraft. This problem crops up while developing almost every new aircraft. However, no effective design or experimental methods have been yet developed to predict a PIO tendency at an early stage of aircraft designing and tests. MIL-F-8785C for example, just states that an aircraft will not have a PIO tendency, but provides no guidance in the area of precluding PIO tendency by design [1] . So the great attention has been paid recently to investigation of this problem both in this country and abroad [1–16].

A PIO tendency depends on aircraft dynamic performance, as well as on manipulator feel system characteristics and command - response gradients. The greater success was achieved in studying the effect of aircraft dynamic performance (time delay, actuator rate limiting, etc.) on the ordinary low-frequency, up to 1 Hz, PIO (works of D.McRuer, T.Neal, R.Smith, R.Hoh[4–7] and others). For studying and precluding this type of PIO there are well developed and widely used methods based on a pilot-vehicle mathematical model; the methods allow a designer to estimate the dynamic performance admissible in terms of pilot-vehicle system stability. A number of criteria are developed to investigate the latent PIO causes due to abrupt changes in dynamic performance or in flying conditions (presence of a catalyst: failures, stress situations, switching from one control loop over to another, etc.). The common drawback of the approaches is that they do not take into account the effect of feel system and control sensitivity characteristics on PIO. These characteristics are usually considered to be optimum and, as a rule, they are considered optimum for a tracking task. However, neither the optimum values of the characteristics nor any methodology for their definition are ever shown. These drawbacks diminish considerably the approaches usefulness since in reality the feel system characteristics and command gradients can greatly differ from the optimum values.

Along with low-frequency PIO, high-frequency oscillations (about 1.5-3 Hz), named *ratchet*, have become possible. Especially great attention has been paid recently to the ratchet in the roll axis, discovered on quite a number of aircraft with small roll mode time constants. As it is shown in many publications (see [8,9] and others), ratchet, as well as low-frequency PIO, occurs as a result of pilot / aircraft interaction. The main cause of ratchet was peaking in amplitude of a limb-manipulator describing function in high frequencies region. The presence of the peaks, their values and frequencies, depend on manipulator feel system and command sensitivity characteristics. However, this dependence and a ratchet phenomenon as a whole have not been sufficiently studied yet. Special attention should be paid to ratchet coupling with structural modes of an airframe (CH-53, F-111, C-17 [3] and others), since there is a tendency in modern aircraft to diminish their structural stiffness that results in coupling of airframe structural modes and limb-manipulator dynamic performance.

A number of publications on an effect of manipulator feel system and command sensitivity characteristics on handling qualities [17–22] have appeared recently.

Nevertheless, this problem, in terms of PIO tendency especially, is insufficiently studied yet, and at present there are no methods to estimate the above mentioned effect.

While developing controllability criteria and theoretical methods of PIO tendency estimation, it is also important to improve the experimental methods of investigation. Complexity of PIO ground-based investigation is determined by the fact that aircraft oscillation tendency manifests itself irregularly and depends not only on aircraft characteristics, but on the piloting task and pilot physiological state. Therefore, it is necessary to improve methods of PIO modeling and experimental data processing to study both evident and latent causes of PIO.

The goals of the work are:

- development of PIO investigation methods on a ground-based simulator,
- studying the effect of manipulator feel system and command sensitivity characteristics on low-frequency PIO and creating the criterion of the effect estimation,
- studying the effect of limb-manipulator dynamic performance coupled with structural elastic modes on high-frequency oscillation aircraft, and the development of a technique to estimate the effect.

Besides, a few experiments in cooperation with MAI and FRI were conducted on TsAGI Flight Simulator FS-102 as a part of work under the contracts with Wright Laboratory. For those purposes, the Tu-154M in-flight simulator dynamics was modeled in FS-102, the tracking task indicator was modeled on the special "book-size" display, the flight test technique was worked out and in-flight simulator model parameters were selected, the test-pilots were trained. The results of this part of the work are not considered in the present report, since they are referred to in the reports of MAI and FRI.

Chapter 1

EXPERIMENTAL INVESTIGATION TECHNIQUE

1.1 Flight Simulator

The experimental part of the work was conducted on flight simulator FS-102. The simulator is intended, mainly, for investigation of stability and controllability of unmaneuverable aircraft. This simulator was selected because its structure and system parameters give an opportunity to study, more completely, the effect of different flight factors on PIO: to reproduce linear and angular accelerations along all degrees of freedom, to change quickly manipulator types and their characteristics and the kinds of flight information displayed, and other flight conditions.

The photos of the simulator and its systems are presented in fig.1.1-1.3. The simulator has following principal characteristics:

- Visual system: single-channel, optical collimating system, computer-generated image of a runway and its vicinity (fig.1.2).
- Motion system (fig.1.1): of synergetic type, 6DOF with the travel limits:

  - vertical ± 1.2 m, longitudinal and lateral directions ± 1.5 m;

  - roll ± 30 deg, pitch ± 40 deg, yaw ± 60 deg.
- Pilot cockpit (fig.1.2): two seats, the equipment ordinary for unmaneuverable aircraft.
- Piloting displays (fig.1.2): In the instrument desk there are the ordinary piloting indicators and two special displays installed. On the first of them, the right one, there are different indicators reproduced which display the current values of angle-of-attack, normal acceleration, airspeed, altitude, vertical speed. The left display (fig.1.3) was used as an indicator for the tracking task simulation (fig.1.4) while studying PIO phenomenon.
- Control manipulators: changeable. The spring central stick and electro-hydraulic side stick (fig.1.3) were mostly used in the experiments (the characteristics are presented in fig.1.5, 1.6). In several experiments the electro-hydraulic central stick with widely changeable characteristics was used. Using these manipulators was determined by simultaneous works which were to be conducted by MAI and FRI using these types of manipulators.

1.2 The Technique of PIO Simulation.

1.2.1 Piloting Task and Other Experimental Conditions.

Piloting task. For experimental investigation of PIO the tracking task was used (the diagram is represented in fig.1.4). This type of piloting task was selected due to its

methodological advantages. First, only in the case of persistent handling under disturbance input conditions, pilot describing functions can be identified. It is impossible to develop theoretical methods of controllability or investigate PIO problems without these functions. Second, it was this very piloting task that was used to develop a number of existing methods to study controllability as a whole and criteria for PIO tendency evaluation in particular. Therefore, when considering this piloting task, there is a possibility to compare the results of theoretical and experimental investigations; it results in improving the theoretical methods of controllability investigation, on the one hand, and, on the other hand, in simplifying the experimental results analysis. Third, the tracking task is easy to simulate and it is easy for both pilots and operators to be trained, its modeling does not require complex experimental equipment and experimental conditions; results obtained in different works, on flight simulators and in flying conditions, are easy to reproduce and compare. Finally, the pilot-aircraft system responses defined for this piloting task can be a sort of basic standard for PIO tendency evaluating. This very task was used to conduct unique flight tests within different programs (LAHOS and others). In the present work this task was used as well for the joint experiments (TsAGI, MAI, FRI) carried out to develop a technique of PIO analyzing.

In addition to the tracking task, a landing approach was modeled in the course of experiments. The experimental conditions for a landing approach task correspond to those defined in the report [22] and, therefore, in this report are not referred to.

Tracking task indication type. While performing a pitch tracking task, a pilot was instructed to keep the pitch tracking error e (i.e. the difference between the pitch predetermined by a certain disturbance input function i and the current pitch value θ) (fig.1.4) within the limits represented in the indicator as lines. The lines were to be the permissible range of the tracking error. An indication of the lines and the tracking error were reproduced in the attitude indicator together with an indication of the current values of pitch, roll and yaw, altitude, vertical speed and others. Angles of pitch and roll were reproduced in full scale. The image of the attitude indicator was generated on a computer and then reproduced on a special "book-size" display (fig.1.3), which was installed in the instrumentation desk of the simulator cockpit. Two types of indication were considered (fig.1.7a,b). In the first case (fig.1.7a) the mark of the tracking error moved while the lines were fixed. In the second case (fig.1.7b) the error mark was fixed about the central line of the attitude indicator while the lines moved, i.e. were deflected in accordance with the pitch angle.

The investigation results showed that pilots adaptability was absolutely the same in both cases of error indication. Piloting accuracy does not depend on the type of indication either. However, for the operators, who participated in the experiments as well, the first type of indication seemed to be easier to comprehend and to use in practice. Therefore, the first indication type was chosen for further investigation (fig.1.7a).

To simulate a roll tracking task, the roll error mark was presented on the display and the error was to be nulled by a pilot while performing the tracking. For this case no precision limits were displayed.

Disturbance input and aircraft dynamics. Pitch and roll force functions manifested themselves as sum of sines (SOS):

$$F(t) = \sum_{i=1}^{i=15} A_i \sin \omega_i t$$

Magnitudes A_i and frequencies ω_i used in the pitch and roll loop correspond to those plotted in fig.1.8. Higher force function frequencies for the roll in comparison with the pitch are accounted for by the fact that in the longitudinal channel low-frequency oscillations were studied, while in the lateral channel high-frequency oscillations were considered.

In a few experiments some LAHOS dynamic configurations were modeled for the results to be later compared with the results of MAI and FRI studies. In the present work LAHOS configurations *1-4, 2-1, 2-10, 3-3, 4-10* and others were considered.

In other experiments both longitudinal and lateral aircraft motion was modeled in accordance with the equations given in part 3.2.

Three test-pilots, one former military pilot and one operator participated in the experiments.

1.2.2 An Effect of Motion Cues on PIO

The conducted investigations of acceleration effect on PIO phenomenon and available publications as well, show, that motion cues play a significant role in PIO. The degree of this effect depends on quite a number of factors: control channel, aircraft performance, flying task and others.

Let us consider first the experimental results of motion cues effect on roll control, see fig.1.9.-1.12. Fig.1.9 illustrates roll damping influence ($1/T_R$) on roll tracking precision. It is seen that simulator motion diminishes a roll error considerably. The positive role of motion cueing is especially evident at low values of roll damping, where a PIO tendency is observed. In fig.1.10 the data on roll rate magnitudes of the oscillations occurred at low negative roll damping values are shown. The data were obtained earlier on TsAGI's simulator with and without motion system for various fields of view [11]. It is seen that angular accelerations influence greatly PIO. Due to the simulator motion the roll rate oscillation magnitude decreases 3-5 times.

That positive effect of simulator motion on handling quality can be illustrated by the pilot describing function presented in fig.1.11. The data show that in the case of both moving and unmoving simulator, the pilot behaviour can be described quite well by the function

$$Y_p = K_p(T_l s + 1)e^{-s\tau}.$$

However, as a simulator moves pilot pure time delay decreases (in this case, from $\tau = 0.26$ sec to $\tau = 0.19$ sec). Due to time delay decreasing a pilot-aircraft system stability margin increases, that allows a pilot to raise his gain (in our case from $K_p = 4.5$ to $K_p = 7.5$). For this reason in the case of moving simulator roll error compensation improves and PIO probability decreases.

In some cases motion cues can, on the contrary, promote PIO. Roll high frequency oscillations can be an illustration of this effect. In fig.1.12 time histories obtained on a moving/unmoving simulator for the aircraft model with certain elastic modes are shown. (The results of the experiments will be considered in detail in chapter 3.) It is seen, that oscillations appear only on a moving simulator. Neither in the previous investigations [9] nor in the present one the attempts to reproduce ratchet cases in real flight have been successful on unmoving simulators. This fact points out once more to the essential role of motion cues in high frequency oscillations phenomenon.

In the longitudinal channel an effect of motion cueing on piloting and a PIO tendency is not so evident. Nevertheless, according to the comments of the evaluation pilots, simulator motion makes simulation conditions seem more realistic. The pilots noted that in some cases motion cues intensify a PIO tendency, in others they do not influence the tendency or mitigate it. Motion cues influence piloting precision in the same way as they affect PIO.

A possibility of a negative effect of accelerations on PIO is consistent, for example, with R.Smith's criterion [5]. In accordance with the criterion the frequency can exist at which the power spectral density of the pilot's normal acceleration due to pitch attitude tracking is sufficiently narrowband. If such a frequency exists, there is a high probability in high gain tracking task pilot will switch from tracking pitch to tracking the normal acceleration he feels at that frequency. If phase margin of the pilot-felt normal acceleration to stick force dynamics is less than zero, then the aircraft will have a tendency to PIO at that frequency.

The positive effect of cockpit motion on piloting is usually displayed while the accelerations are reproduced with regard to the distance between the cockpit position and center-of-gravity $l \gg 0$) and especially while there is no PIO tendency observed.

The effect of cockpit motion on pitch tracking may disappear at $l = 0$, which can be attributed to the fact that motion cues do not give a pilot any additional information in comparison with visual ones. It has been shown that in the case of an aircraft of a traditional configuration motion cues do not practically lead visual cues due to the inseparable connection of a normal acceleration and a pitch angle at pilot activity frequencies

$$\frac{n_z}{\theta} = \frac{n_{z_\alpha} s}{s + n_{z_\alpha} g / V}$$

and due to the fact that the acceleration in c.g. does not significantly lead a pitch angle. Pitch acceleration feeling and its using by a pilot are hampered due to the strong effect of normal accelerations acting in combination with a pitch acceleration.

In view of the distance between the pilot cockpit and c.g., the n_{z_p}/θ - transfer function takes the form

$$\frac{n_{z_p}}{\theta} = \frac{n_{z_\alpha} s}{s + n_{z_\alpha} g/V} + \frac{l}{g} s^2 .$$

It is seen from this equation, that an acceleration leads a pitch angle and, therefore, motion cues can produce a favourable effect on controlling. If the aircraft tends to oscillate in pitch, simulating a normal acceleration can worsen these oscillations, as it was observed in several experiments.

Thus, the data considered above show that motion cues can influence piloting and a PIO tendency greatly. Three cases should be defined: motion cues producing a positive effect on piloting and mitigating a PIO tendency; motions cues producing no effect at all; motion cues intensifying a PIO tendency. At present there are no theoretical methods to estimate a degree of this effect for all possible cases. Therefore, experimental investigations of PIO should be conducted on moving-base flight simulators. It can be mentioned also, that a moving-base simulator has some methodological advantages in comparison with an in-flight simulator. For example, on a moving - base simulator there is a possibility to change acceleration conditions (scaling, separate switching on different degrees of freedom, etc.) without changing other flying conditions, which is impossible in real flight due to the inseparable unity of motion and visual cues and other types of flying information. Therefore, for a study of motion cues effect on PIO phenomenon, a moving-base simulator is preferable to an in-flight simulator.

1.3 Experimental Data Processing

In the work both subjective and objective methods of experimental data processing were used.

Pilot rating scales used. In the work two pilot rating scales were used: PIO rating scale (PIOR) and Cooper-Harper's pilot rating scale (PR). The PIOR scale was used to illustrate that pilot ratings worsen due to PIO tendency intensification as command sensitivity increases or feel system gradients decrease in comparison with their optimum values. However, for the final rating the PR-scale was used, since it is a multipurpose scale adapted for evaluation of controllability in different flight conditions, including a PIO tendency. The scale is well known for experts in stability and controllability problems and pilots engaged in the experiments. It is important also that this scale is used for standardization of handling qualities in Specifications in different countries.

Each studied aircraft configuration was flown no less than 3 - 5 times. The ratings obtained were averaged. In accordance with the technique stated in [13], the confidence

interval of rating arithmetic mean for 3-5 runs does not exceed PR = 0.7-1. For the aircraft configurations of Level 1, the confidence interval is about PR = 0.5.

The technique of pilot describing function identification. In the study the run-time histories processing was carried out according to the technique for a single-loop tracking task [13].

In this study an attempt was made to develop an experimental technique of an identification of a pilot describing function as a whole and, in particular, its partial corresponding to the dynamics of a limb-manipulator system. The block diagram of the pilot-aircraft system for this case is shown in fig.1.13. The model does not contradict the modern pilot behaviour models, for example, the McRuer's model presented in fig.1.14. In this diagram and further the following notations are applied:

- e - tracking error displayed on an indicator and observed by a pilot (command stimulus),
- i - disturbance input (sum-of-sines forcing function),
- θ, ϕ - current state variables (for example, pitch or roll angle),
- F - stick force, kg
- X - stick displacement, mm
- f - force disturbance generated in feel system,
- Y_{cns} - transfer function model of central nervous system,
- Y_{lm} - transfer function model of closed-loop limb-manipulator system,
- Y_{ns} - transfer function model of neuromuscular system,
- Y_p - pilot transfer function model ($Y_p = Y_{cns} \times Y_{lm}$),
- Y_{fs} - feel system transfer function model,
- Y_c - transfer function model of the controlled element (for example, stick displacement (X, mm) referred to pitch or roll (θ, ϕ, deg)),
- n_e - pilot remnant transferred to visual input,
- n_x - limb-manipulator system remnant transferred to force.

As it is seen from the diagram, a pilot-aircraft system incorporating a neuromuscular system is a two-loop model. In order to identify simultaneously two transfer functions in this system (Y_p and its partial Y_{lm}), the inputs i and f should be uncorrelated. Let us consider each of them to be Gaussian white noise passing through a linear filter. In accordance with the remnant definition given in [13], remnants n_e and n_x are considered uncorrelated with the inputs i and f.

To identify the transfer function models the Fourier transform algorithm was used. According to this algorithm, a stick displacement and a tracking error can be described as follows

$$\begin{aligned} X(j\omega) &= X_i(j\omega) + X_{n_e}(j\omega) + X_f(j\omega) + X_{n_x}(j\omega) \\ E(j\omega) &= E_i(j\omega) + E_{n_e}(j\omega) + E_f(j\omega) + E_{n_x}(j\omega) \end{aligned} \qquad (1.1)$$

Subscripts i, n_e, f, n_x here and further, refer to the processes in a closed-loop pilot-aircraft system, caused by $i(t), n_e(t), f(t), n_x(t)$.

With the use of the transfer functions shown in diagram 1.13, eq.(1.1) takes the following form (for the sake of brevity, $j\omega$ is omitted):

$$X = \frac{Y_p}{\Delta} I + \frac{Y_p}{\Delta} N_e + \frac{Y_{fs}}{\Delta(1+Y_{ns}Y_{fs})} F + \frac{1}{1+Y_{ns}Y_{fs}} N_x$$
$$E = \frac{1}{\Delta} I - \frac{Y_p Y_c}{\Delta} N_e - \frac{Y_{fs}Y_c}{(1+Y_{ns}Y_{fs})\Delta} F - \frac{Y_c}{(1+Y_{ns}Y_{fs})\Delta} N_x \qquad (1.2)$$

where $\Delta = 1 + Y_p Y_c$.

Now, taking into account that i, f, n_e, n_x are uncorrelated, one can obtain the following power spectra

$$S_{xi} = \frac{Y_p}{\Delta} S_{ii}$$
$$S_{ei} = \frac{1}{\Delta} S_{ii} \qquad (1.3)$$
$$S_{xf} = \frac{Y_{fs}}{\Delta(1+Y_{ns}Y_{fs})} S_{ff}$$

where $S_{ii}, S_{ff}, S_{cf}, S_{ef}$ - power spectra of inputs.

Having divided left and right hand parts of the first two equations, one has

$$Y_p(j\omega) = \frac{S_{xi}(j\omega)}{S_{ei}(j\omega)} \qquad (1.4)$$

Taking into account that

$$\delta = F + f,$$
$$Y_{fs}(j\omega) = \frac{S_{xi}}{S_{\delta i}},$$

from equations (1.3), it is easy to obtain

$$Y_{lm}(j\omega) = \frac{S_{xi}S_{ei}S_{ff} - S_{xf}S_{ii}S_{\delta i}}{S_{xi}S_{ei}S_{ff}}. \qquad (1.5)$$

As it is shown in[13], for a two-loop controlling task it is impossible to define separately the remnants n_e, n_x. It is possible to define their sum only. Let us consider that the remnant n_x as well as remnant n_e are transferred to command e. So, further we will consider only the sum of remnant n_e, transferred to e. It can be shown that the power spectrum of the remnant can be calculated as

$$Se_n e_n(j\omega) = \frac{S_{ee}S_{ii}^2 - S_{ii}S_{ei}^2}{S_{xi}^2} \qquad (1.6)$$

Thus, in the case of a two-loop controlling task, the describing functions Y_p, Y_{lm} and the pilot remnant $Se_n e_n$ can be determined by (1.4), (1.5), (1.6) .

As to the practical application of the method, the following fact should be mentioned. A pilot describing function is identified more precisely when an input function manifests itself as sum of sines. However, in the case of a two-loop task, the using of two input functions leads to some difficulties in the identification process. These difficulties are accounted for by the difficulty in reproducing two uncorrelated input functions. Taking this into account, it has been proposed to produce one of the inputs as SOS, and another input as white noise passing through a linear filter.

The first experience in using the method have given hopeful results. However, the method requires further developing.

Chapter 2

EFFECT OF FEEL SYSTEM AND COMMAND SENSITIVITY CHARACTERISTICS ON LOW-FREQUENCY P I O

Command sensitivity and feel system characteristics are the main factors affecting PIO phenomenon. This fact is mentioned in a number of publications. It is enough to say, that great attention is paid to this problem in Specifications, for example, MIL. It is for PIO precluding that the requirements for minimum values of these characteristics are specified in them. Nevertheless, the documents available show the effect of control sensitivity and feel system characteristics on PIO insufficiently and in kind only. It is known that complex interaction of such factors as dynamic performance, feel system characteristics and piloting task influences a degree of this effect considerably. However, reliable methods of the effect evaluation have not been developed yet. One of possible approaches to this problem is considered in this chapter.

2.1 Effect of Command-Response Gradients

In fig.2.1, 2.2 the pilot ratings are plotted against the command-response gradients for longitudinal and lateral channels. The relations have been obtained for different dynamic performance for an aircraft with a central stick. The PIORs presented there together with the PRs show, that pilot ratings deterioration in the case of command-response gradients decreasing is correlated with PIO tendency intensified. These and quite a number of other data available show that regularities of the effect of control sensitivity and feel system characteristics on handling qualities and PIO, being referred to their optimum value, are the same for different piloting conditions, aircraft classes, control channels, piloting tasks, dynamic performance and manipulator feel systems (fig.2.3). (The above mentioned conditions affect only optimum values of command-response gradients. This effect will be considered in greater detail in part 2.3.)

As it is seen from the given data, an increase of control sensitivity (command-response gradients decrease) over optimum values, leads to PIO tendency arising. At small deviations from optimum values the tendency is slight. It becomes considerable if control sensitivity characteristics are more than 2 times greater in comparison with optimum values. For example, if sensitivity increase is 2 times the PRs and the PIORs deteriorate by 0.6. If sensitivity increase is 4 times the PR-ratings deteriorate by 2-2.5, the PIOR-ratings deteriorate by 2.

A dependence of pilot ratings on dimensionless command gradients $(F_{n_z}/F_{n_z}^{opt}, F_p/F_p^{opt}, \ldots)$ is approximately the same for different conditions not only in kind, but in degree as well. The degree of pilot ratings deterioration if the command-response gradients are below their optimum values, can be described by the relation (feel system characteristics are considered optimum):

for Cooper-Harper scale

$$\Delta PR = \begin{cases} -6\lg\dfrac{F_r}{F_r^{opt}} - 1.5, & at\ \dfrac{F_r}{F_r^{opt}} \le 0.5 \\ 6\lg^2\dfrac{F_r}{F_r^{opt}}, & at\ 0.5 \le \dfrac{F_r}{F_r^{opt}} \le 1.0 \end{cases}$$

For PIO scale (2.1)

$$\Delta PIOR = \begin{cases} -4\lg\dfrac{F_r}{F_r^{opt}} - 0.5, & at\ \dfrac{F_r}{F_r^{opt}} \le 0.5 \\ 6\lg^2\dfrac{F_r}{F_r^{opt}}, & at\ 0.5 \le \dfrac{F_r}{F_r^{opt}} \le 1.0 \end{cases}$$

It should be mentioned also, that if dynamic performance causes no PIO tendency, control sensitivity decreasing (command gradient values increasing) causes only Cooper-Harper pilot ratings variation, while PIO ratings do not change. It is accounted for by the fact, that command gradients increase over their optimum values does not result in PIO tendency intensification. Controllability worsening in this case is due to piloting precision deterioration and heavy controlling, but not to PIO tendency (fig.2.1 - 2.3). If dynamic performance is a cause of PIO tendency, control sensitivity reducing can mitigate it.

It is evident, that eq.(2.1) describes growth of PIO tendency only approximately. In each particular case, PIO severity may differ from this empirical relation, as it is shown in fig.2.4. This tendency could be evaluated more precisely studying pilot behaviour models in terms of command gradients decrease. Unfortunately, the models and controllability criteria developed so far (McRuer, Neal-Smith, et al) do not clearify this tendency pecularities. In fact, they assume that as aircraft gain deviates from its optimum value, a pilot changes his gain in inverse proportion to it so, that $Y_p Y_c$ describing function remains unchanged. Therefore, models of this type do not take into account the fact that as command sensitivity increases a pilot-aircraft system becomes more oscillating. To define possible ways of eliminating this drawback of the modern pilot models, special investigations of pilot adaptability to a high aircraft gain were conducted in the present work.

In fig.2.5 the pilot and pilot-aircraft describing functions obtained for the tracking task with various command sensitivity gradients are plotted. The analysis of these and other data obtained during the experiments, shows the following: if control sensitivity increase exeeds 2 times, a pilot-aircraft cut-off (crossover) frequency becomes somewhat higher, i.e. control sensitivity variation interferes with pilot adaptability. The interference becomes considerable at high frequencies. As it is seen in fig.2.5, at frequencies of 0,7-1 Hz, the magnitudes of pilot describing functions are practically the same in spite of the great difference in aircraft gains. The pilot phase remains equal over a wide frequency range for all aircraft gains.

This pilot peculiarity may be a result of different muscles of an arm being engaged in deflecting a certain manipulator and their having different dynamics and displacement

ranges. Wide-ranged manipulator displacements, which are low-frequency as a rule, are produced mainly by a shoulder and a forearm. Due to this fact, pilot adaptability is higher at low frequencies. High-frequency deflections of manipulator are produced by muscles of a hand, having more narrow displacements limits. It is these limits that restrain the pilot high-frequency adaptability to aircraft gain variations.

Due to this human peculiarity noticeable changes take place in a closed-loop pilot-aircraft describing function. As it is seen in fig.2.5 , the amplitude peak increases. The peak is often used (Neal-Smith, et al) as a standard of an aircraft tendency to PIO. Thus, an increase of control sensitivity leads to increasing a pilot-aircraft cut-off frequency and rising a pilot amplitude ratio in a high frequency band. This, in turn, leads to peaking in a pilot-aircraft system and, therefore, increasing the system oscillability. This is a possible if not a sole cause of PIO tendency arising under increased control sensitivity. This fact should be paid much more attention to in the future.

2.2 Effect of Feel-System Characteristics

The main feel system parameters are manipulator gradient F^x and breakout force F_{br}. PIO determined by abrupt changes in force gradient values have been considered in a number of works (see [15,16]). An effect of force gradients and breakout on PIO is considered in the present work. Its regularities have not been sufficiently presented in publications yet, though these parameters are paid great attention to.

Fig.2.6;2.7 are plots of pilot ratings and force gradients for different force breakouts. The results presented were obtained for both central and side sticks for optimum aircraft control sensitivity characteristics. These and other data available brought us to the following results.

Force gradient F^x and breakout force F_{br} qualitative influence on PIO is the same for different manipulators, aircraft dynamics and piloting tasks. There are certain optimum values of manipulator force gradients for each manipulator type and control channel. In the case of any deviations of force gradients from their optimum values the aircraft tends to oscillate and pilot ratings worsen; but it is force gradient values decreasing that plays a decisive role in PIO tendency severity and pilot ratings worsening. For low force gradient values a certain additional value of force breakout mitigates a PIO tendency and improves controllability, due to the fact that too low gradient values hamper pilot's measuring control forces. In this case the lack of control forces is compensated by some additional breakout.

It should be mentioned that for low gradient values an effect of control sensitivity characteristics on PIO is also greater, what has been shown in the experiments, see fig.2.8. This results in changing relation (2.1): for low gradient values, deviations of control sensitivity from its optimum value lead to more considerable pilot ratings worsening as compared to (2.1).

If gradients and breakouts are referred to their optimum values (fig.2.9), the dependence of pilot ratings on these referred values is about the same in degree for

different manipulators and control channels. The latter fact is determined by the theoretical approach to optimization of control sensitivity and feel system characteristics presented in [22]. According to the approach, for a pilot there exist certain desirable ranges of force F_* and displacement X_* for every control manipulator. The optimum gradient value (for F_{br}=0) is about

$$F_{opt}^{x} = {F_*}/{X_*}. \tag{2.2}$$

If pilot forces and displacements differ from their desirable values, controllability deterioration degree is determined by ${F}/{F_*}$ and ${X}/{X_*}$. This dependence remains the same for different manipulators and control channels. For slight deviations of ${F}/{F_*}$ and ${X}/{X_*}$ from *1* the dependence can be described by the equation

$$\Delta PR = f \lg^2 {F}/{F_*} + g \lg^2 {X}/{X_*}, \tag{2.3}$$

where *f, g* are constant for different manipulators.

For optimum control sensitivity and low values of gradient and breakout force, a manipulator displacement range does not depend greatly on F^X and F_{br}. So, it can be assumed that

$$X=X_*. \tag{2.4}$$

For optimum values of gradients and F_{br}= 0, the manipulator force range is close to desirable F_* . If gradient values decrease and breakout values increase force range values change according to

$$F = \frac{F^x}{F_{opt}^x} \cdot F_* + F_{br}. \tag{2.5}$$

Having inserted (2.5) into (2.3) and taking into consideration (2.2) and (2.4), we have

$$\Delta PR = f \lg^2 \left({F^X}/{F_{opt}^x} + {F_{br}}/{F_{opt}^x X_*} \right).$$

It can be seen from the equation that if gradients deviate from their optimum values, pilot ratings deterioration is determined by ${F^X}/{F_{opt}^x}$ and ${F_{br}}/{F_{opt}^x X_*}$ only, regardless of breakout values and the manipulator type.

Thus, longitudinal PIO tendency severity due to deviations of feel system and control sensitivity characteristics from their optimum values can be evaluated with the function

plotted in fig.2.9. Optimum gradient values and X_* for different manipulator types are presented in the same figure.

2.3 Design Criterion for Evaluation of Feel-System and Command Sensitivity Characteristics Effect on PIO

An essence of the criterion proposed here is the following:

1. With the help of the criteria available (T.Neal, R.Smith, R.Hoh and others) severity of PIO tendency is evaluated for optimum values of feel system and control sensitivity characteristics.

2. In accordance with the technique stated below, the tracking task optimum values of control sensitivity characteristics are evaluated for given feel system characteristics and aircraft dynamic performance.

3. With the help of the function in fig.2.9 a degree of PIO tendency increase is evaluated for control sensitivity and feel system characteristics deviating from their optimum values.

To develop the technique of optimum values selecting for control sensitivity characteristics, the investigations have been conducted to define the regularities of an effect of dynamic performance and feel system characteristics on optimum values of command-response gradients for the tracking task conditions. The analysis of data obtained shows that the relation of optimum command-response gradients to aircraft dynamics and manipulator feel system characteristics is the same in its nature for the tracking task and for the ordinary flying task (landing approach, cruise). This relation for the main flying tasks was considered in great detail in[22] and, therefore, in this work is not refferred to. To illustrate the relation of optimum command gradients to aircraft dynamic performance, fig.2.10 presents the optimum command-response gradients X_{n_z} which have been obtained in the experiments for five different LAHOS configurations. Having compared configurations *2-1* and *5-11* which have approximately equal damping ratio, one could see that if natural short-period mode frequency increases, optimum command-response gradients X_{n_z} increase too. The comparison of configurations *2-1* and *3-3* shows that damping ratio increase results in increasing optimum X_{n_z}.

The experimental data obtained allow us to assume that optimum command-response gradients for a tracking task as well as for other piloting tasks can be defined by A-criterion [22]. For the longitudinal channel the criterion takes the form:

$$\left[\left[1+\frac{V_0}{n_{z_\alpha} g}\sqrt{\omega_*^2+\left(\frac{n_{z_\alpha} g}{V}\right)^2}\right]\cdot\left|Y_{n_z}(j\omega_*, X_{n_z}^{opt})\right|\right]^{-1} = A\left(F^X, F_{br}, \ldots\right). \qquad (2.6)$$

To show that A-criterion application is well-grounded for a tracking task as well as for landing approach, aircraft describing functions are plotted in fig.2.11. These functions were defined for optimum values of X_{n_z} for the same LAHOS configurations as presented in fig.2.10. It can be seen that in spite of different configurations dynamics their transfer function amplitude ratio curves meet at about the same point demonstrating the physical nature of A-criterion (2.6).

But quantitatively optimum values of command gradients depend on a piloting task. See, for example, fig.2.10 where the optimum command gradients for some LAHOS configurations are shown for the tracking task and landing approach.

It obvious that the difference in optimum values of command-response gradients for different piloting tasks can be considerable; quantitatively this difference depends on aircraft dynamic performance.

Relation (2.6) shows optimum command gradients values in kind and in degree, if the parameters in (2.6) are specified. The comparison of the calculated and experimental data has shown that the values of the parameters in (2.6), but for ω_*, do not depend on a piloting task. And as it has been shown in [22] the value of Vo can be put equal to 140m/sec for all flight conditions of an unmaneuverable aircraft. The parameter A depends on a manipulator type and its feel system characteristics. The values of A for central and side sticks of an unmaneuverable aircraft are shown in fig.2.12.

The charateristic frequency ω_* depends only on a piloting task and an aircraft class. It is 1.2-1.5 rad/sec (or 0.7 rad/sec for a landing approach task), see fig.2.11, for an unmaneuverable aircraft with the input disturbance shown in fig.1.8.

Thus, optimum command-response gradients values for a tracking task on an unmaneuverable aircraft with central or side sticks can be calculated using (2.6), where A values correspond to those shown in fig.2.12 and ω_* is about 1.2-1.5 rad/sec.

Some additional studies may clearify a relation of parameter A to manipulator feel system characteristics and specify the characteristic frequency ω_* in order to define optimum command gradient values for other control channels, manipulators and aircraft classes for a tracking task.

Chapter 3

INVESTIGATION OF LIMB-MANIPULATOR DYNAMIC INTERACTION WITH ROLL CONTROL OF "ELASTIC" AIRCRAFT

3.1 Statement of The Problem.

In view of change-over to fly-by-wire system on modern unmaneuverable aircraft a necessity disappeared for a pilot to apply great forces to move a control linkage. Therefore, small-inertia manipulators have come into use on unmaneuverable aircraft (small-mass wheels, mini-wheels, central and side sticks: Tu-204, A-320, A-340, etc.). For these types of manipulators high frequency resonant peaks (1-3 Hz) in limb-manipulator system describing function are typical. As to roll mode time constants, their low values are not characteristic of unmaneuverable aircraft. For unmaneuverable aircraft the values about $T_R = 0.5$sec or more are typical. Therefore, for unmaneuverable aircraft, in contrast to maneuverable ones, high frequency peaking in limb-manipulator system and, consequently, *ratchet* phenomenon due to only unfavourable limb-manipulator system characteristics is hardly probable.

But for a modern unmaneuverable aircraft noticeable peaking in aircraft describing function in a frequency band about 2-3 Hz is typical due to airframe elasticity. It is accounted for by the fact that attempts of reducing airframe weight, installing engines on a wing, increasing aircraft dimensions lead to a tendency of decreasing aircraft elastic mode frequency and increasing elastic mode amplitudes on modern and prospective aircraft. As a result, in peak frequencies aircraft dynamics differs from traditional one, which could be described by roll mode only. In 2-3 Hz frequency band a resonant peak appears in roll amplitude ratio; considerable lateral accelerations can arise while roll controlling. (It is seen from flight data given in fig.3.1 and transfer function models responses shown in fig.3.2a,b.) Due to this fact, high-frequency oscillations of ratchet type become possible on unmaneuverable aircraft as well, in spite of high roll mode constant values. These oscillations were observed, for example, in flight tests of one of Russian unmaneuverable aircraft (fig.3.1).

It should be mentioned that the phenomenon in question may present a problem for a maneuverable aircraft, since high frequency oscillations caused by structural elasticity appear on maneuverable aircraft as well. This type of oscillations appeared, for example, on a relatively light military aircraft F-111 with external stores loading [3].

This chapter of the report aims at theoretical and experimental validation of a possibility of roll high-frequency oscillations caused by a pilot for a certain combination of manipulator characteristics, structural elasticity and unmaneuverable aircraft dynamics.

3.2 Unmaneuverable Aircraft Lateral Motion Model Coupled with Elastic Modes

Simplified linearized equations of aircraft lateral motion coupled with structural elastic modes can be written as follows:

$$\begin{cases} \dot{\beta} = Y_\beta \beta + \dfrac{g\cos\theta}{V}\phi + r\cos\alpha + p\sin\alpha + Y_{\delta_a}\delta_a + Y_{\delta_r}\delta_r + Y_\beta \dfrac{w}{V} \\ \dot{r} = N_\beta \beta + N_r r + N_p p + N_{\delta_a}\delta_a + N_{\delta_r}\delta_r + N_\beta \dfrac{w}{V} \\ \dot{p} = L_\beta \beta + L_r r + L_p p + L_{\delta_a}\delta_a + L_{\delta_r}\delta_r + L_\beta \dfrac{w}{V} \\ \dot{\phi} = p - r\tan\theta \\ \ddot{\xi} + (D_K + D_A)\dot{\xi} + (G + B_A)\xi = R_a\delta_a + R_r\delta_r + R_w\delta_w \end{cases} \qquad (3.1)$$

where $\xi = \xi(t)$ - is a vector of aircraft structural modes coordinates of dimension Nt, where Nt is a number of structural modes considered,

w - is a side wind gust velocity.

The terms describing dynamic interaction of structural modes and rigid aircraft motion are excluded from the motion equations considered. The influence of static elastic deformation of an airframe is taken into account by means of special corrections of aerodynamic coefficients in motion equations (3.1) which describe an aircraft as a rigid body.

The matrix of aircraft structural stiffness G is diagonal, it consists of squares of structural mode natural frequencies in vacuum; the matrix of structural damping D_K is diagonal as well. Matrices G and D_K do not depend on flight conditions. Matrices of aerodynamic stiffness B_A, aerodynamic damping D_A and "control surfaces efficiency" R_a, R_r, R_w change due to flight conditions changing and depend on dynamic pressure and flight velocity V in a first approximation.

Roll rate $\hat{p}$, yaw rate $\hat{r}$ and side acceleration $\hat{n}_y$ affecting a pilot or registered by control system sensors (located at a point with the coordinates xs, zs) are computed according to the following equations:

$$\hat{p}(t, x) = p(t) + \sum_{i=1}^{N_t} \varphi_i(x)\dot{\xi}_i(t)$$

$$\hat{r}(t, x) = r(t) + \sum_{i=1}^{N_t} \psi_i(x)\dot{\xi}_i(t)$$

$$\hat{n}_y(t, x, z) = \frac{V}{g}\left[\dot{\beta}(t) - r(t)\cos\alpha - p(t)\sin\alpha\right] - \phi(t) -$$

$$-\frac{x}{g}\dot{r}(t) + \frac{z}{g}\dot{p}(t) + \frac{1}{g}\sum_{i=1}^{N_t}\left[f_i(x) + z\varphi_i(x)\right]\ddot{\xi}_i(t)$$

where

$f_i(x)$, $\varphi_i(x)$, $\psi_i(x)$	-	structural i-mode values :
$f_i(x)$	-	fuselage deformation along the y-axis, m;
$\varphi_i(x)$	-	fuselage torsion angle with respect to the x-axis, rad;
$\psi_i(x)$	-	fuselage bending angle with respect to the z-axis, rad;
xs, zs	-	coordinates of the point considered, m.

A first approximation of elastic aircraft mathematical model takes into account 4 structural modes. Matrices $\hat{D}_A, \hat{B}_A, \hat{R}_a, \hat{R}_r, \hat{R}_w$ for cruise conditions (H=11300m, M=0.825, q=1047kg/m^2 , V = 243 m/sec) for aircraft weight 83000kg have the forms:

$$\hat{D}_A = \begin{bmatrix} 1.49 & 0.244 & -.178 & 0.0 \\ 0.376 & 0.212 & 0.234 & 0.0 \\ 0.108 & 0.306 & 0.628 & 0.0 \\ 0.0 & 0.0 & 0.0 & 0.26 \end{bmatrix}, \hat{B}_A = \begin{bmatrix} 47.2 & 5.95 & -14.6 & 0.0 \\ 0.052 & 3.73 & 7.96 & 0.0 \\ 15.7 & 5.24 & 21.0 & 0.0 \\ 0.0 & 0.0 & 0.0 & 6.26 \end{bmatrix}$$

$$\hat{R}_a = \begin{bmatrix} 34.9 \\ 33.3 \\ 63.5 \\ 29.4 \end{bmatrix}, \hat{R}_r = \begin{bmatrix} 69.5 \\ 1.20 \\ -28.1 \\ 0.262 \end{bmatrix}, \hat{R}_w = \begin{bmatrix} 4555.7 \\ 27.0 \\ 51.0 \\ 37.0 \end{bmatrix}$$

Diagonal matrices G, D_K are the following:

$$G = \begin{bmatrix} 173.4 & 0.0 & 0.0 & 0.0 \\ 0.0 & 221.9 & 0.0 & 0.0 \\ 0.0 & 0.0 & 244.3 & 0.0 \\ 0.0 & 0.0 & 0.0 & 683.2 \end{bmatrix}, D_K = \begin{bmatrix} 0.211 & 0.0 & 0.0 & 0.0 \\ 0.0 & 0.238 & 0.0 & 0.0 \\ 0.0 & 0.0 & 0.250 & 0.0 \\ 0.0 & 0.0 & 0.0 & 0.418 \end{bmatrix}.$$

As a result for cruise flight conditions structural modes equations can be written as follows:

$$\begin{bmatrix} \ddot{\xi}_1 \\ \ddot{\xi}_2 \\ \ddot{\xi}_3 \\ \ddot{\xi}_4 \end{bmatrix} + \begin{bmatrix} 1.703 & 0.244 & -.178 & 0.0 \\ 0.376 & 0.450 & 0.234 & 0.0 \\ 0.108 & 0.306 & 0.878 & 0.0 \\ 0.0 & 0.0 & 0.0 & 0.678 \end{bmatrix} \times \begin{bmatrix} \dot{\xi}_1 \\ \dot{\xi}_2 \\ \dot{\xi}_3 \\ \dot{\xi}_4 \end{bmatrix} + \begin{bmatrix} 220.6 & 5.95 & -14.6 & 0.0 \\ 0.052 & 225.6 & 7.96 & 0.0 \\ -15.7 & 5.24 & 265.3 & 0.0 \\ 0.0 & 0.0 & 0.0 & 689.5 \end{bmatrix} \times \begin{bmatrix} \xi_1 \\ \xi_2 \\ \xi_3 \\ \xi_4 \end{bmatrix} =$$

$$= \begin{bmatrix} 34.9 \\ 33.3 \\ 63.5 \\ 29.4 \end{bmatrix} \delta_a + \begin{bmatrix} 69.5 \\ 1.20 \\ -28.1 \\ 0.262 \end{bmatrix} \delta_r + \begin{bmatrix} 45.7 \\ 27.0 \\ 51.0 \\ 37.0 \end{bmatrix} w$$

For cruise flight condition the values of aerodynamic derivatives of rigid aircraft equations considering static corrections for structural elasticity are given in the following table:

derivative	*Y*	*L*	*N*
β	-0.1	-3.75	-2.2
p	0	-0.9	-0.076
r	0	-0.3	-0.33
δa	0	-0.8	0
δr	-0.02	-0.75	-1.05

Values of structural modes in different fuselage points are equal to

- in a cockpit

$$f = [-0.155 \quad 0.219 \quad -0.293 \quad -0.971]$$
$$\varphi = [0.0374 \quad 0.0148 \quad -0.021 \quad 0.0027]$$
$$\psi = [0.0093 \quad -0.0092 \quad 0.0276 \quad 0.109]$$

- in a control system sensors location

$$f = [-0.0323 \quad 0.116 \quad 0.035 \quad 0.135]$$
$$\varphi = [0.0326 \quad 0.0107 \quad -0.0185 \quad 0.00455]$$
$$\psi = [0.0048 \quad -0.00015 \quad 0.016 \quad 0.017]$$

n_y/δ_a, p/δ_a - transfer functions models responses measured in a cockpit are presented in fig.3.2.a,b.

Block-diagrams of lateral control system selected for simulation are given in fig.3.3.

Feed-back and feed-forward gains of control system for cruise flight conditions are equal to the following:

$$K_q = 3.0 \text{ sec}; \quad K_{n_z} = 0.087 \ {}^{\text{rad}}/_{\text{sec}}; \quad K_p = 0.6 \text{ sec}; \quad K_r = 1.0 \text{ sec};$$
$$K_e = 0.0017 \ {}^{\text{rad}}/_{\text{mm}}; \quad K_a = 0.0052 \ {}^{\text{rad}}/_{\text{mm}}; \quad K_r = 0.003 \ {}^{\text{rad}}/_{\text{mm}}$$

Coordinates of control system sensors are $x_S = 4.6$ m, $z_S = 0$.

Longitudinal aircraft motion model for simulation is described with the following equations:

$$\begin{cases} \dot{\alpha} = -Z_\alpha \alpha + q - Z_{\delta_e} \delta_e \\ \dot{q} = M_\alpha \alpha + M_q q + M_{\dot{\alpha}} \dot{\alpha} + M_{\delta_e} \delta_e \end{cases}$$
$$n_z(t, x) = \frac{V}{g}[q(t) - \dot{\alpha}(t)] + \frac{x}{g}\dot{q}(t)$$

Aerodynamic coefficients accounting for static corrections for structural elasticity are given in the following table:

derivative	Z	M
α	0.691	-2.034
p	-	-0.533
α	-	-0.221
δe	0.030	-2.38

Transfer functions models of side acceleration and roll rate referenced to an aileron deflection take the forms:

$$\frac{n_y}{\delta_e} = -0.187\frac{(s+1.62)(s^2+0.88s+1.59)}{(s+0.83)(s^2+0.54s+2.2)}\frac{(s-7.2)(s+5.5)}{(s^2+1.6s+219)}\times$$
$$\times\frac{(s^2+0.71s+227)}{(s^2+0.41s+222)}\frac{(s^2-6.3s+555)}{(s^2+s+270)}\frac{(s^2+4.4s+631)}{(s^2+0.63s+678)}$$
$$\frac{p}{\delta_e} = \frac{2.44}{(s+0.83)}\frac{(s^2+0.44s+2.27)}{(s^2+0.54s+2.2)}\frac{(s^2+0.21s+221)}{(s^2+1.6s+219)}\frac{(s^2+1.19s+250)}{(s^2+0.41s+222)}\times$$
$$\times\frac{(s+9.3)(s-8.66)}{(s^2+s+270)}\frac{(s^2+0.678s+690)}{(s^2+0.63s+678)}$$

3.3 Experimental Results

The results of high-frequency pilot assisted oscillations modeling are considered in this part of the work.

The experiments modeling aircraft dynamics on a flight simulator (see part 3.2) show the following:

1. Aircraft elastic mode influence high-frequency oscillations in pilot-aircraft system to a considerable extent.

High-frequency oscillations were regularly observed in the course of experiments on the moving-base simulator for both step roll manipulator input and permanent manipulator deflections determined by a tracking task. This fact was mentioned by all the three pilots who took part in the experiments. In fig.3.4, 3.5 the time histories for an elastic and rigid aircraft are given; the moving-base simulator was flown by one of the pilots. The comparison of the given time histories shows that high-frequency oscillations appeared on the elastic aircraft only.

The oscillations frequency remained about 2.5 Hz in all the cases regardless of a pilot and his piloting manner. This frequency coincides with that obtained during flight tests (fig.3.1) and corresponds to the frequency of the first aircraft elastic mode (fig.3.2a,b). The latter fact proves it was aircraft elasticity that caused oscillations in both ground-based and in-flight experiments.

2. The magnitude of such high-frequency oscillations depends on a resonant peak magnitude in elastic aircraft transfer function responses.

It can be seen in fig.3.5-3.8 that as the first aircraft elastic mode peak becomes higher, the magnitudes of lateral and roll rate oscillations increase, the magnitudes being proportional to the elastic mode peak, see fig.3.9.

As it is shown in fig.3.10 the pilot ratings worsen as the peak magnitude increases. The threshold peak magnitude which corresponded to ratchet arising, was about 12,5% of the peak maximum value, according to the pilots. As the peak became higher, the pilots noticed the unfavourable effect of the accelerations. The attempts to counteract these disturbances failed. Smooth manipulator resetting to the neutral position or setting it free damped these oscillations.

3. Pilot-felt accelerations influence high-frequency oscillations considerably.

This follows from the comparison of the data obtained in the experiments while different degrees of freedom were engaged: roll and lateral displacement (fig.3.5), roll only (fig.3.11), no degrees of freedom switched on (fig.3.12).

The data showed and the pilots noticed that aircraft oscillations arose on a moving simulator only. An aircraft oscillation tendency was observed even while only the roll degree was switched on, but it was lateral accelerations that influenced this tendency greatly. An acceleration effect interfered with tracking task performing, thus, the piloting precision worsened.

4. The high-frequency oscillations are characteristic of both central and side sticks in spite of the latter having an armrest and a damping device, see time histories in fig.3.5-3.7 for the central stick and fig. 3.13, 3.15 for the side stick.

A tendency to high-frequency oscillations depends on the direction of forces applied. This scewness depends on the manipulator type. In the case of a central stick the tendency is greater ,while the stick is deflected to the right, but for a side stick it is vice versa, see fig.3.5 and 3.13. According to the pilots, difference in the type of scewness due to the type of a stick is accounted for by the fact that different muscle groups are engaged in controlling, these muscles having different dynamic and force characteristics. In the case of a central stick an arm and upper body are engaged, while in the case of a side stick with an arm on an armrest, only a forearm and a hand are used.

5. Aircraft command sensitivity affects high-frequency oscillations caused by structural elasticity to a considerable extent, which can be seen from the time histories (fig.3.5, 3.14, 3.15) and from the relation of pilot rating to command sensitivity as well (fig.3.16).

It should be mentioned that pilot ratings variation is accounted for by ratchet mainly, according to the pilots; if there is no ratchet observed aircraft gain variation does not influence pilot ratings. According to our data if aircraft gain is 2 times less in comparison with its optimum value, there are practically no high-frequency oscillations observed.

This peculiarity of command sensitivity effect on high-frequency oscillations caused by structural elasticity is in agreement with the data given in [9] concerning a command sensitivity effect on ratchet at low roll mode time constant values.

6. High-frequency oscillations are possible to simulate on a ground-based simulator with a motion system. It follows from all the data presented above.

According to the pilot who took part in the in-flight experiment (see time histories in fig.3.1) and in the ground-based experiments (see time histories in fig.3.17) high-frequency oscillations felt on the ground-based and in-flight simulators are basically the same. However, the oscillation tendency observed in flight experiments was less. It is accounted for by two facts: first, a miniwheel was used in flight while central and side sticks were used on a simulator; second, the command sensitivity characteristics differed.

It has been mentioned in some works (see, for example, [9]) that ratchet caused by low roll mode time constant values is difficult to reproduce on a ground-based simulator. As to high-frequency oscillations caused by structural elasticity, our experience shows that this type of oscillations is easily reproduced and, thus, can be studied on a simulator.

The experimental data concerning pilot describing functions will be considered in the next part.

3.4 Analysis of Pilot-Aircraft System Characteristics

To reveal causes of high-frequency PIO and ways to preclude this phenomenon let us consider the describing functions of a pilot and an open-loop pilot-aircraft system obtained in the course of the experiments, see fig.3.18-3.21. In these figures the approximation of these describing functions in terms of a pilot transfer function model is shown as well. The pilot transfer function is as follows

$$Y_p = K_p(T_l s+1)e^{-s\tau}Y_{lm} \tag{3.2}$$

where

K_p, T_l - pilot's gain and lead,

τ - pilot's equivalent time delay (as a combination of pilot's pure time delay and computer time delay).

In accordance with the diagram in fig.1.14 Y_{lm} - transfer function model ($T_N = 0$, $P_{sp} = \infty$) can be presented as

$$Y_{lm} = \frac{1}{T_1^2 s^2 + 2\xi_1 T_1 s+1}\frac{1}{T_2^2 s^2 + 2\xi_2 T_2 s+1} \tag{3.3}$$

Let us consider the pilot/pilot-aircraft describing functions in fig.3.18 and 3.19 for the case of roll motion described with

$$Y_c = {K_c}/{s}\,(T_R s+1) \tag{3.4}$$

It can be seen that there is noticeable peaking in amplitude ratio at high frequencies (1-3 Hz) which is determined by limb-manipulator system dynamics. As a result a resonant peak in an open-loop pilot-aircraft system appears at these frequencies if values of roll mode time constant are low (T_R = 0.1sec, fig.3.18). The same type of peaking was observed by other investigators who analyzed ratchet occurring on maneuverable aircraft in real flight. Some studies have shown (see [9], for example) that this peak magnitude is a measure of high-frequency PIO tendency caused by low roll mode time constant values. Roll high-frequency oscillations arise when a peak magnitude is about -6db or more. Thus, the more the peak magnitude, the greater the PIO tendency.

If roll mode time constant exceeds 0.5 sec which is typical of "rigid" unmaneuverable aircraft, resonant peaks are below -6db. This can be seen from the describing functions presented in fig.3.19 and 3.20: in the first case roll motion corresponded to eq.(3.4) where T_R = 0.5 sec; in the second case roll motion corresponded to eq. (3.1) where T_R = 1.2 sec (structural elasticity was not taken into account). Thus, for a rigid unmaneuverable aircraft no ratchet was observed neither in our experiments no in other studies.

The experiments were conducted for an elastic unmaneuverable aircraft with various elastic mode amplitudes and control sensitivity characteristics. The experiments showed that if a resonant peak in $\left|Y_p Y_c\right|$ exceeded -6db, high-frequency PIO arose. The pilot/pilot-aircraft describing functions are given in fig.3.22 for the case when structural elastic modes (see eq.(3.1)) corresponded to real ones. (As it has been mentioned above, in this case the PIO tendency was extreme.) It is seen that for this case the resonant peak magnitude was up to +6db.

These data has shown that the pilot and his neuromuscular system describing functions obtained in the experiments can be adequately approximated by transfer functions models (3.2), (3.3).

The above mentioned facts allow us to conclude that both high-frequency oscillations on unmaneuverable aircraft due to their structural elasticity and ratchet phenomenon on maneuverable aircraft due to low values of roll mode time constant can be studied on the basis of pilot-aircraft model responses.

The pilot-aircraft model responses can be defined empirically or derived from pilot and limb-manipulator transfer functions models (3.2), (3.3). In the latter case a pilot's pure time delay can be assumed constant, for example, τ =0.3 sec; parameters K_p and T_l can be derived from "crossover model" as the data in fig.3.18-3.21 prove:

$$Y_p(j\omega)Y_c(j\omega) = \frac{\omega_c}{j\omega} e^{-j\omega\tau},$$

where ω_c - pilot-aircraft crossover frequency ($\left|Y_p Y_c(j\omega_c)\right| = 1$) which does not depend on aircraft characteristics.

It should be mentioned that a limb-manipulator model has not been sufficiently developed yet. There is no clear idea of the order of a limb-manipulator model which would be adequate to analyze different cases of high-frequency PIO. It was concluded in [9] that a third-order transfer function model is enough to describe ratchet caused by low roll mode time constant. The pilot describing functions presented in fig.3.18-3.21 show that there are two resonant peaks in pilot's amplitude ratio at the frequencies exceeding 1 Hz. These describing functions can be matched to a transfer function model of the fourth order. Comparing the experimental and calculated data showed that an adequate approximation of pilot-aircraft describing functions as well as the resonant peaks is achieved if transfer function model (3.3) is applied. We may conclude that while studying high-frequency PIO a limb-manipulator transfer function such as (3.3) can be with a good reason applied.

It has been mentioned in the publications that parameters T_1, T_2, ξ_1, ξ_2 depend on a manipulator type and its feel system characteristics. They can be $T_{1,2}$ = 0.05 - 0.15 sec, $\xi_{1,2}$ = 0.05 - 1.0.

In our experiments these parameter magnitudes were $T_1 = 0.12\,\text{sec}$ ξ_1 = 0.2 sec, T_2 = 0.055 sec, ξ_2 = 0.1. However, these parameters adjustment rules determined by a manipulator type and feel system characteristics have not been developed yet. This hampers an application of mathematical models of a pilot-aircraft system for high-frequency PIO analysis. These rules are also necessary for describing limb-manipulator system dynamics while developing controllability criteria and analyzing low-frequency PIO. Further studies to develop such adjustment rules should be carried out.

The pilot mathematical model considered here disregards pilot-felt lateral accelerations. Therefore, influence of these accelerations on low- and high-frequency PIO should be studied in greater detail.

CONCLUSIONS

1. The technique of PIO experimental studies has been improved while modeling compensatory tracking task on a ground-based simulator.

   It has been proved that ground-based PIO studies should be conducted on a moving-base simulator, since motion cues felt by a pilot can influence a PIO tendency greatly (in some cases the tendency is mitigated, in others it is intensified).

   The technique has been improved to define, from experiments directly, a common pilot describing function and, at the same time, dynamic performance of closed loop limb-manipulator system. The technique suggests the use of two uncorrelated disturbance functions: one of them is the visual disturbance function, and the other is the manipulator force disturbance function generated in a feel system.

2. Main regularities of a feel system and control sensitivity characteristics effect on PIO have been revealed.

   It has been shown that a decrease of command-response gradients and force gradient in comparison with their optimum values leads to PIO tendency intensification. Greater values of breakout forces at low values of force gradients mitigate PIO tendency.

   As control sensitivity increases pilot gain adaptability to aircraft gain variation is upset. First, the pilot-aircraft model cut-off frequency becomes somewhat higher. Second, at the frequencies exceeding the cut-off value, pilot model amplitude ratio curves tend to converge. The amplitudes are practically the same when the frequency is about 0.7-1 Hz, in spite of the great difference in aircraft gains. The pilot phase remains about the same for all aircraft gains. This is accounted for by the fact that quite a number of muscle groups with various dynamic responses and displacement limits participate in deflecting a particular manipulator. This pilot peculiarity should be studied in greater detail further, as it could form the basis for a mathematical method to evaluate the control sensitivity effect on PIO.

   The criterion is proposed for an estimation of manipulator feel system and command sensitivity influence on PIO. The criterion allows a designer, firstly, to define optimum control sensitivity values for a tracking task for the given feel system characteristics, and, secondly, to estimate, in terms of PIO tendency, pilot ratings worsening in the case of characteristics deviation from their optimum values.

3. It has been shown that there is a tendency to high frequency oscillations on an unmaneuverable aircraft with certain characteristics of a manipulator, structural elasticity and aircraft dynamics.

   High frequency PIO is possible to imitate on a moving-base simulator. According to the pilot the high frequency oscillations felt on ground-based and in-flight simulators are essentially the same.

Aircraft elastic modes affect considerably high frequency oscillations in a pilot-aircraft system. Their mere arising and their intensity depends on the magnitude of the first aircraft elastic mode. Their frequency corresponds to the frequency of the first elastic mode.

High frequency PIO intensity depends on limb-manipulator system characteristics as well; these characteristics are determined by the manipulator type and its feel system parameters. High frequency PIO appeared in the experiments with both central and side control sticks. High frequency PIO tendency depends on the direction of forces applied. This skewness, in its turn, depends on the manipulator type. In the case of a central stick the tendency is greater in the right direction, in the case of a side stick it is greater in the left direction.

Aircraft command-response gradients influence high frequency oscillations caused by structural elasticity to a considerable extent. As aircraft gain increases and pilot adaptability gets upset, a resonant peak in an open loop pilot-aircraft system is higher and, therefore, a PIO tendency is intensified.

Roll and lateral accelerations felt by a pilot play an important role in high frequency oscillations phenomenon. High frequency oscillations were observed only on the simulator with a moving base.

Causes of high frequency PIO and ways of its precluding can be adequately studied by means of analyzing pilot-aircraft model describing functions.

REFERENCES

1. Bjorkman E.A., Silverthorn J.T., Calico R.A. Flight Test Evaluation of Techniques to Predict Longitudinal Pilot Induced Oscillations. - AIAA Guidance, Navigation and Control Conference, 1986. A Collection of Technical Papers, p.967-975.

2. Newell F.D. and Wasserman R. In-Flight Investigation of Pitch Acceleration and Normal Acceleration Bobweights. AFFDL-TR-69-3, April 1969.

3. K.McKay. Summary of an AGARD Workshop on Pilot Induced Oscillation. AIAA - 1994.

4. Neal T.R., Smith R.E. An in-flight investigation to develop system design criteria for fighter airplanes.-AFFDL-TR-70-74, vol.1.

5. Smith R.H. A Theory for londitudinal short period pilot induced occillations. - AFFDL-TR-77-57.

6. Hodgkinson J., Wood J.R., Hoh R.H. An alternative method of specifying bandwidth for flying qualities. -AIAA Paper No 82-1609.

7. Gibson J.C. Piloted Handling qualities design criteria for highorder flight control systems. -AGARD-CP-333, 1982.

8. Johnston, D.E. and D.T.McRuer. Investigation of Interactions Between Limb-Manipulator Dynamics and Effective Vehicle Roll Control Characteristics in Roll Tracking. NASA CR-3983, 1986.

9. Johnston D.E. and McRuer D.T. Investigation of Limb-Sidestick Dynamic Interaction with Roll Control. -AIAA Paper No 85-1853.

10. Устойчивость и управляемость самолетов на режимах взлета и посадки. Левин М.А. Обзор по материалам иностранной печати. ОНТИ ЦАГИ, 1990г.

11. Бюшгенс Г.С., Студнев Р.В. Аэродинамика самолета. Динамика продольного и бокового движения. М.: Машиностроение, 1979, 352 с.

12. Гуськов Ю.П., Загайнов Г.И. Управление полетом самолетов. М.: Машиностроение, 1980, 215 с.

13. Ефремов А.В., Оглоблин А.В., Предтеченский А.Н., Родченко В.В. Летчик, как динамическая система. М.: Машиностроение, 1992, 336 с.

14. Перебатов В.С. Особенности управления современным неманевренным самолетом по курсу. ВИМИ №DD0905, 1983.

15. I.I.Fedotov, A.Z.Tarasov, K.A.Tatarnikov. Aircraft Handling Qualities Research and Criteria Development for Nonstationary/Nonlinear Situations. Final report on AF sponsored research contract #SPC-94-4002.

16. Yu.B.Dubov, L.E.Zaichik, Yu.P.Yashin. The Investigation of Conditions Causing Pilot-Induced Oscillation in the Longitudinal Motion. Aircraft Flight Safety Conference, Zhukovsky, Russia, Aug. 31- Sept. 5, 1993.

17. Johnston, D.E. and B.L.Aponso. Design Considerations of Manipulator and Feel Systems Characteristics on Roll Tracking. NASA CR-4111, 1988.

18. Watson, D.C. and J.A.Schroeder. Effects of Stick Dynamics on Helicopter Flying Qualities. AIAA-90-3477-CP, presented at the AIAA Guidance, Navigation and Control Conference, Portland, OR, Aug.1990.

19. Morgan,J.M. An Initial Study Into the Influence of Control Stick Characteristics on the Handling Qualities of a Fly-By-Wire Helicopter. AGARD Flight Mechanics Panel Symposium on Flying Qualities, Quebec City, Canada, Oct.1990.

20. Hess, R.A. Analyzing Manipulator and Feel-System Effects in Aircraft Flight Control. IEEE Transactions on Systems, Man, and Cybernetics. Vol.20, No.4, July/Aug.1990, pp.923-931.

21. Rodger R.Smith. Effects of FCS Dynamics on Fighter Approach and Landing Longitudinal Flying Qualities. AFFDL-TR-78-122, vol.1.

22. V.V.Rodchenko, L.E.Zaichik, Yu.P.Yashin, V.S.Perebatov, V.V.Lyasnikov. Investigation of Controllability Criteria of Unmaneuverable Aircraft Equipped with a Side Stick. Final report on AF sponsored research contract #SPC-93-4046.

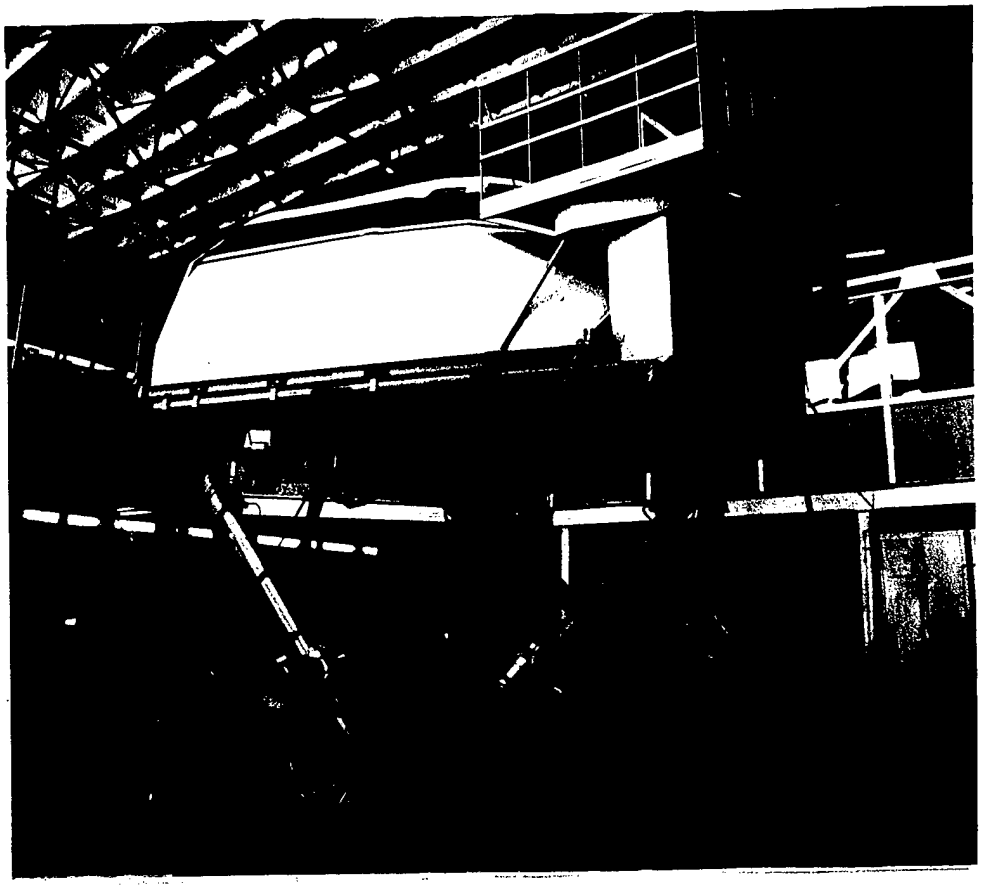

Fig.1.1. Flight Simulator FS-102

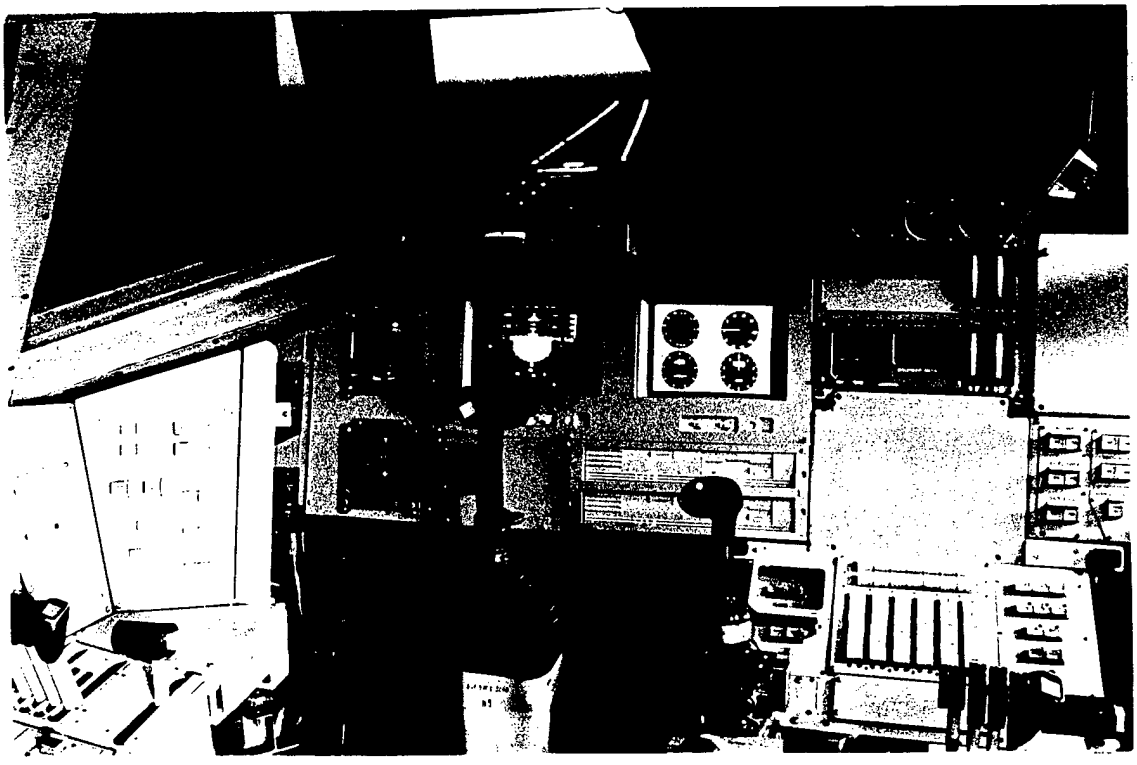

Fig.1.2. Cockpit Interior of Flight Simulator FS-102

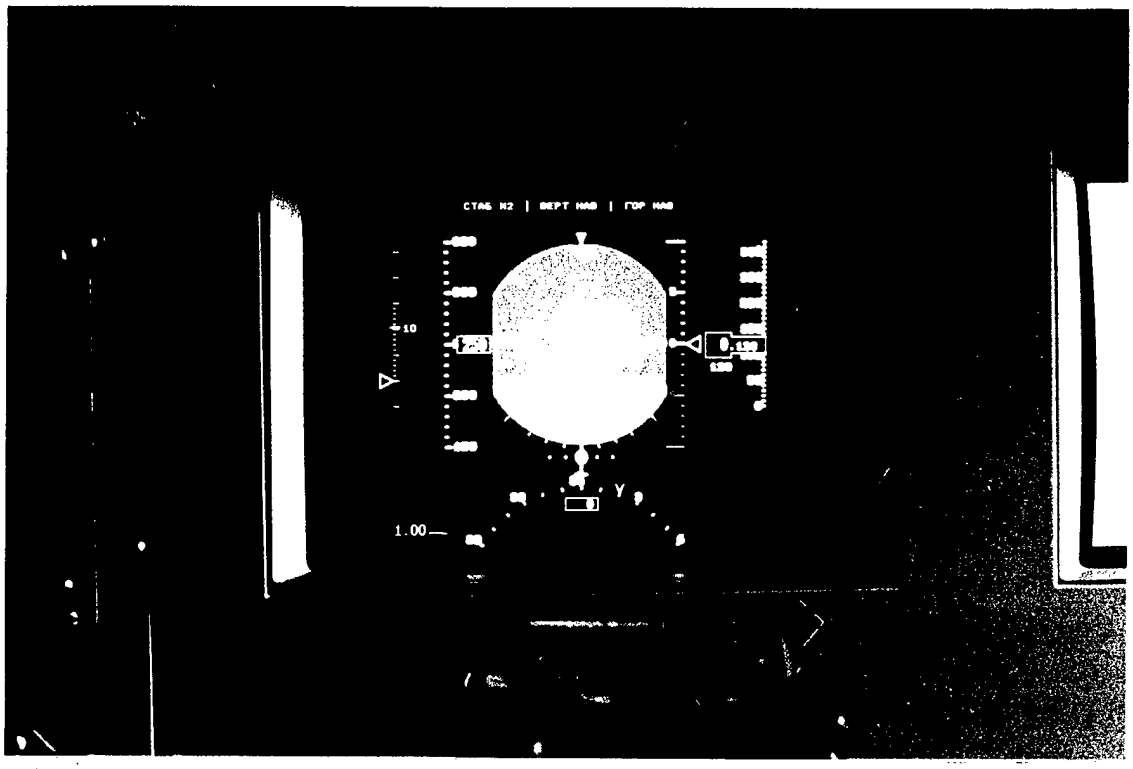

Fig.1.3. Tracking Task Indicator

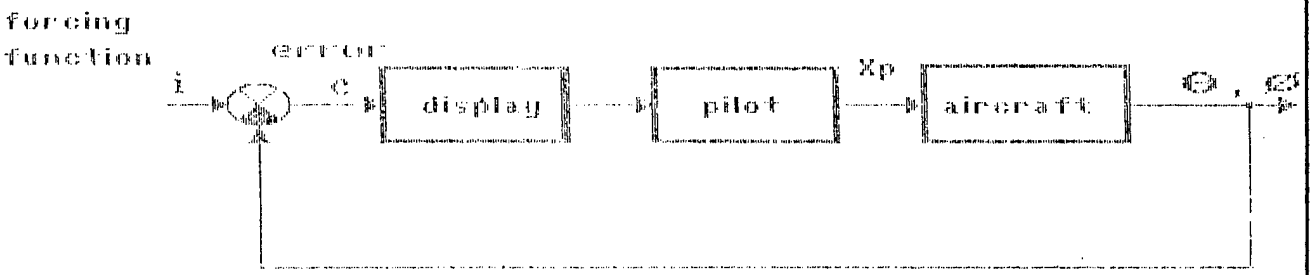

Fig. 1.4 Tracking task scheme.

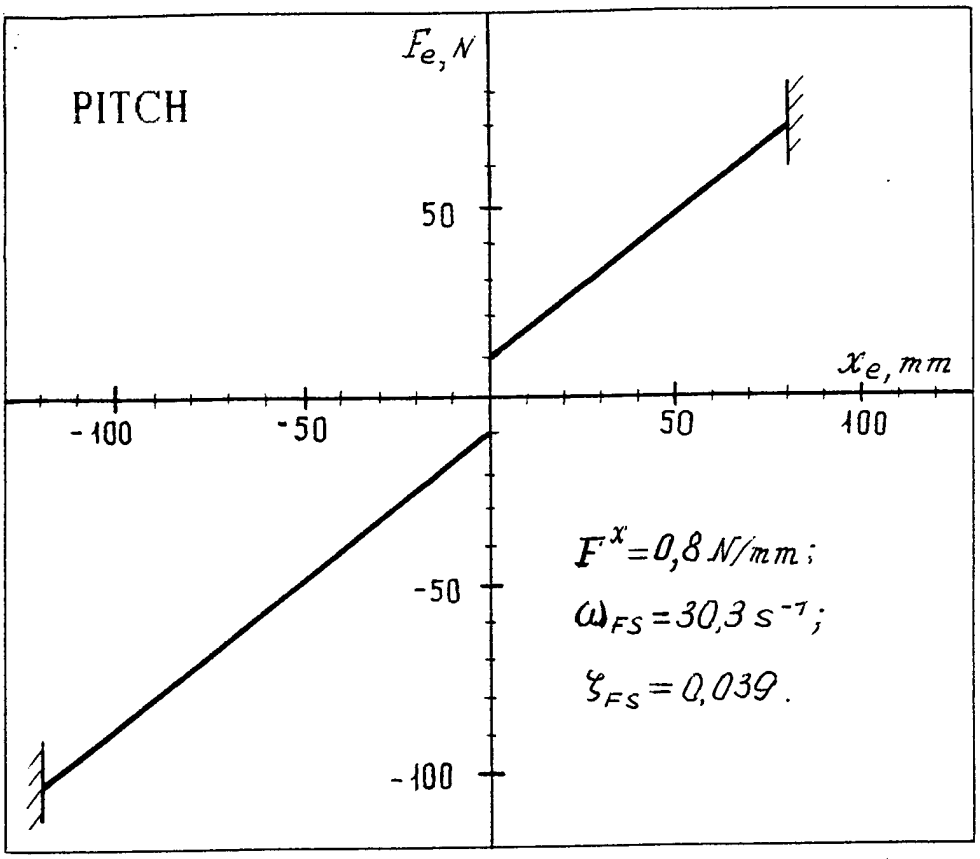

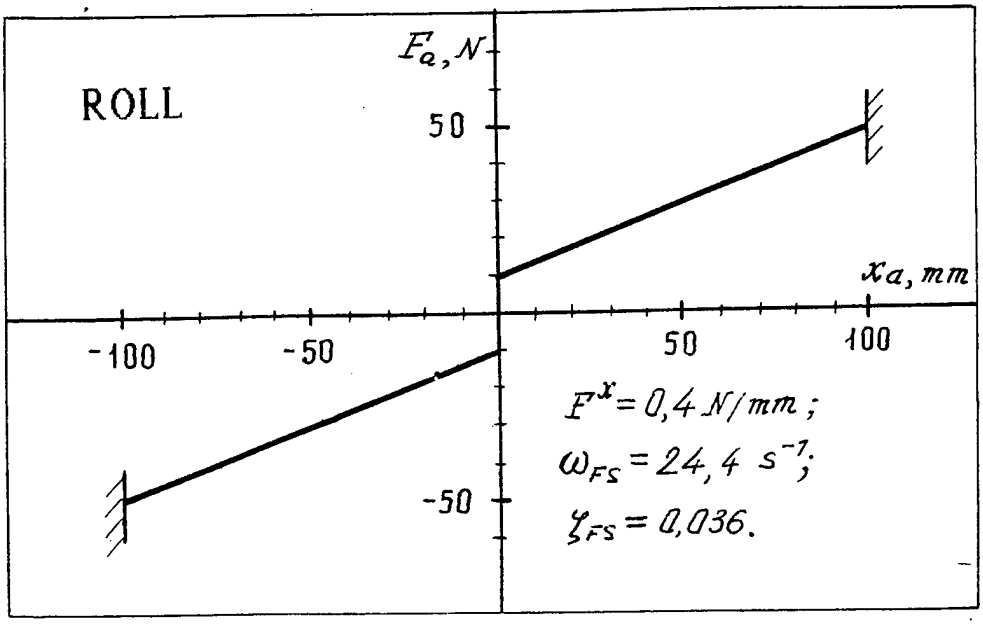

Fig.1.5. Central Stick Feel System Characteristics

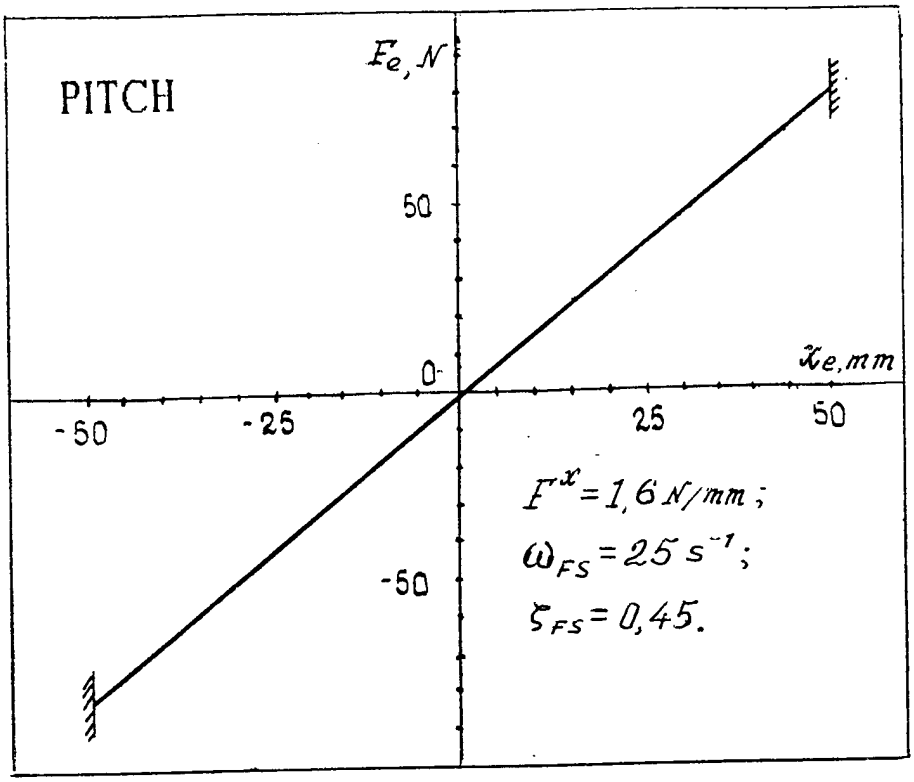

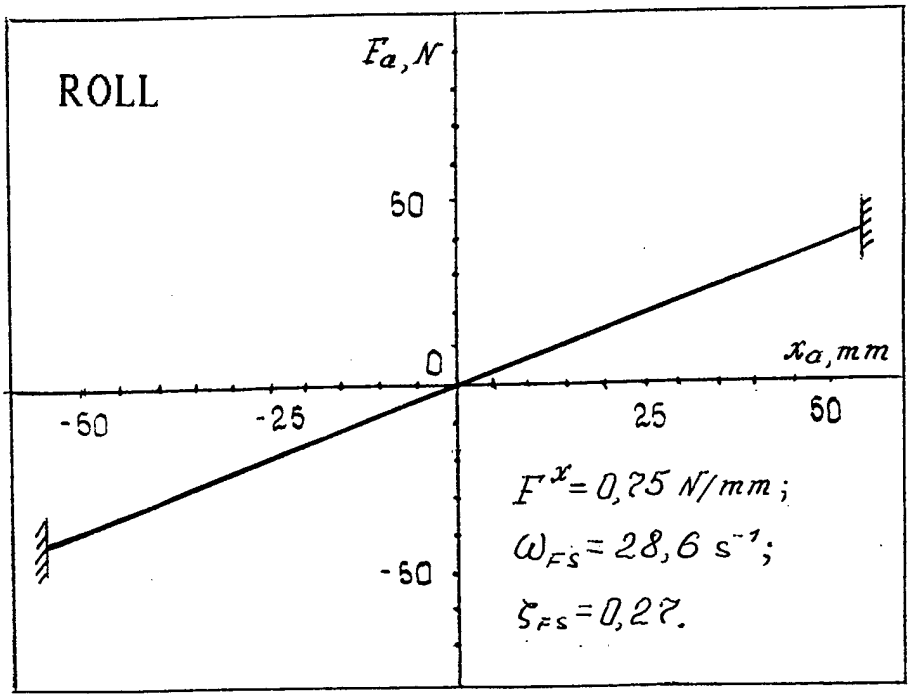

Fig.1.6. Side Stick Feel System Characteristics

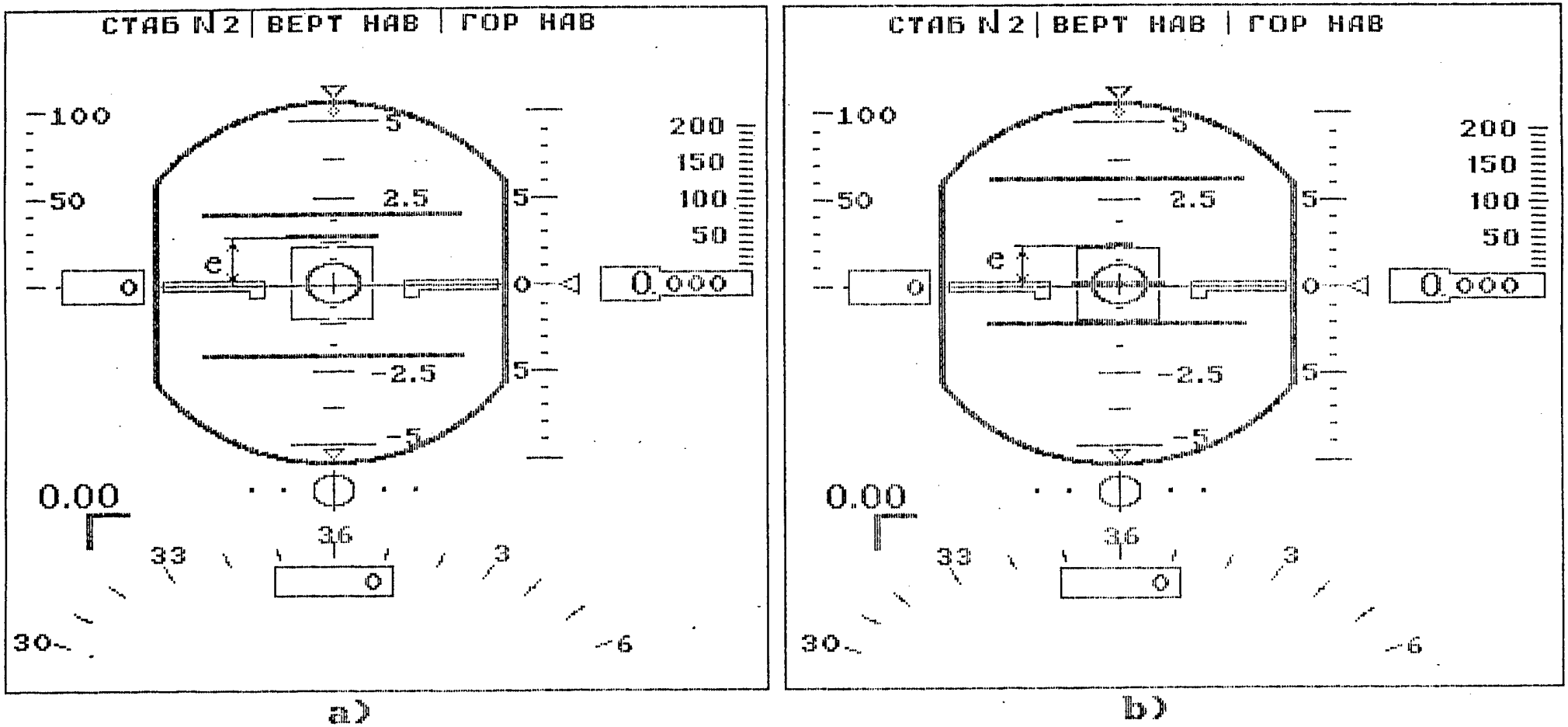

Fig. 1.7 Types of indication for the pitch tracking task.

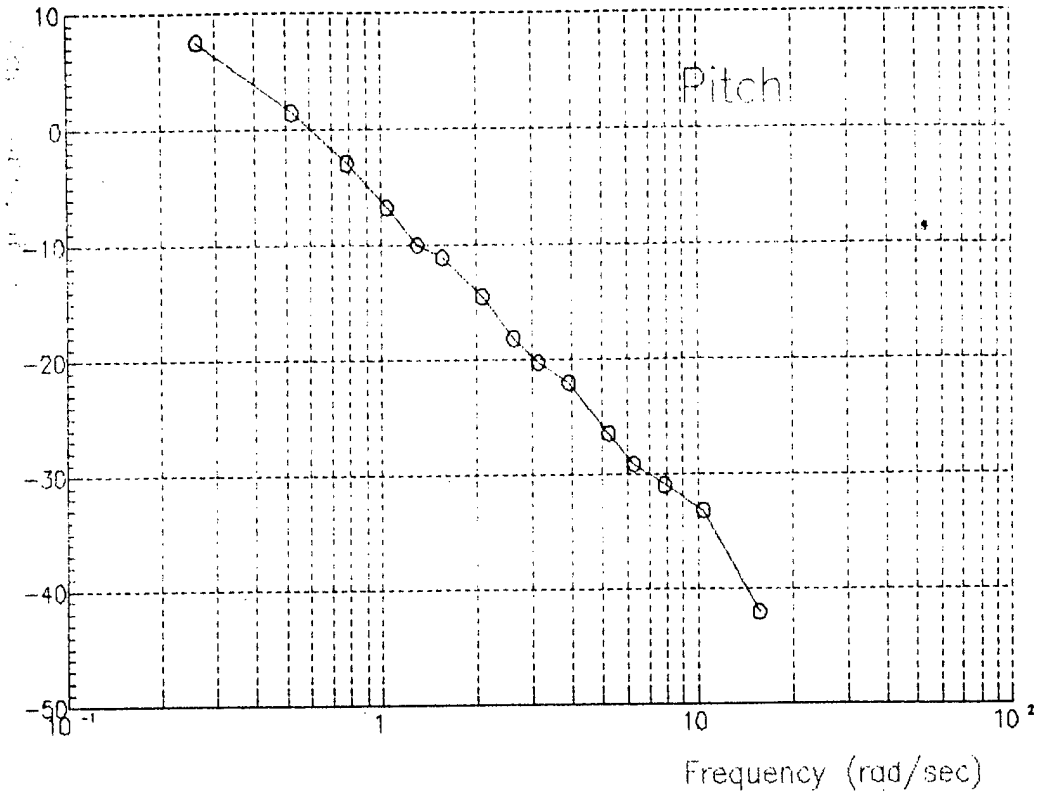

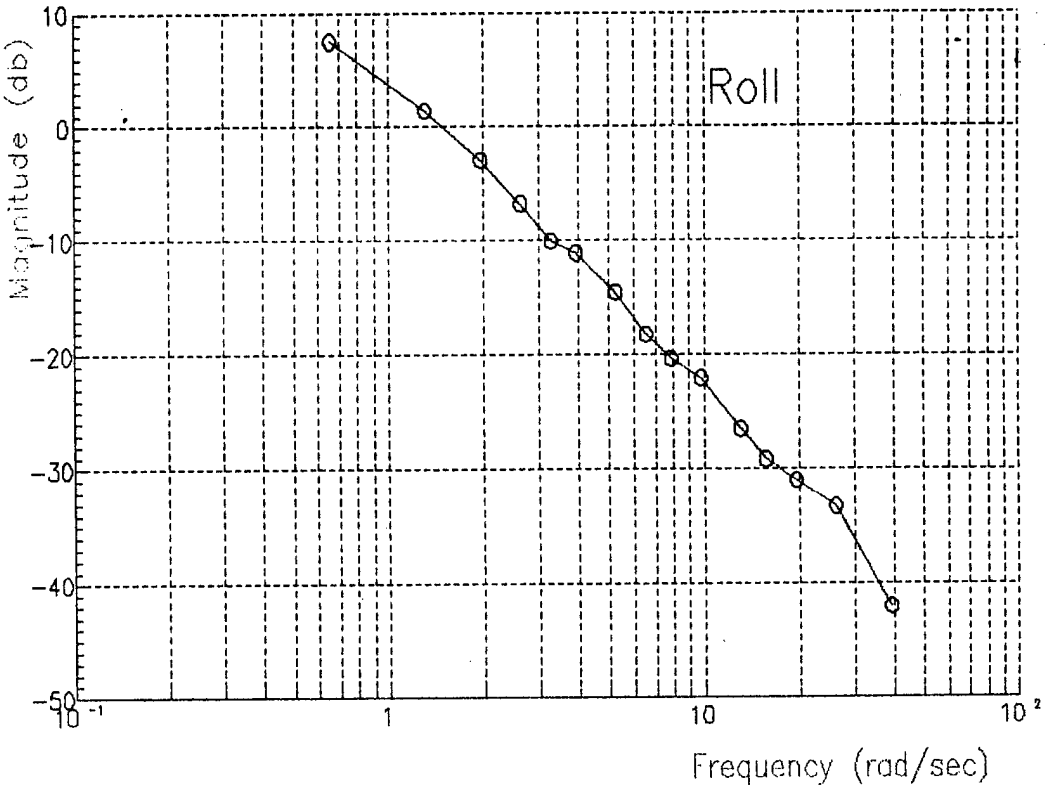

Fig.1.8 Forcing function spectral densities.

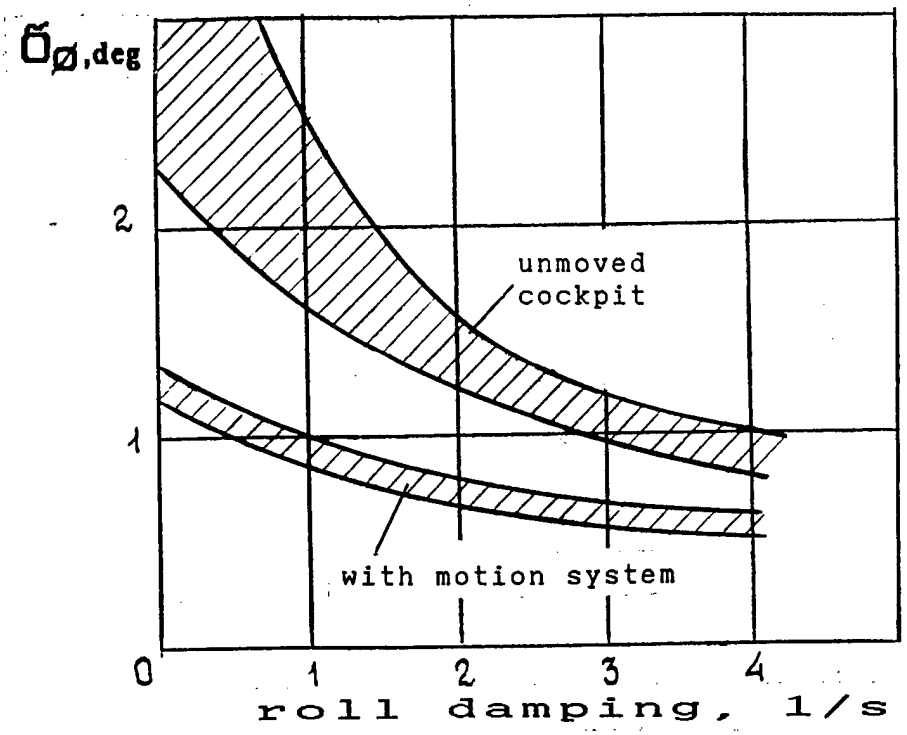

Fig.1.9. Motion Cues Influence on Roll Stabilization Precision

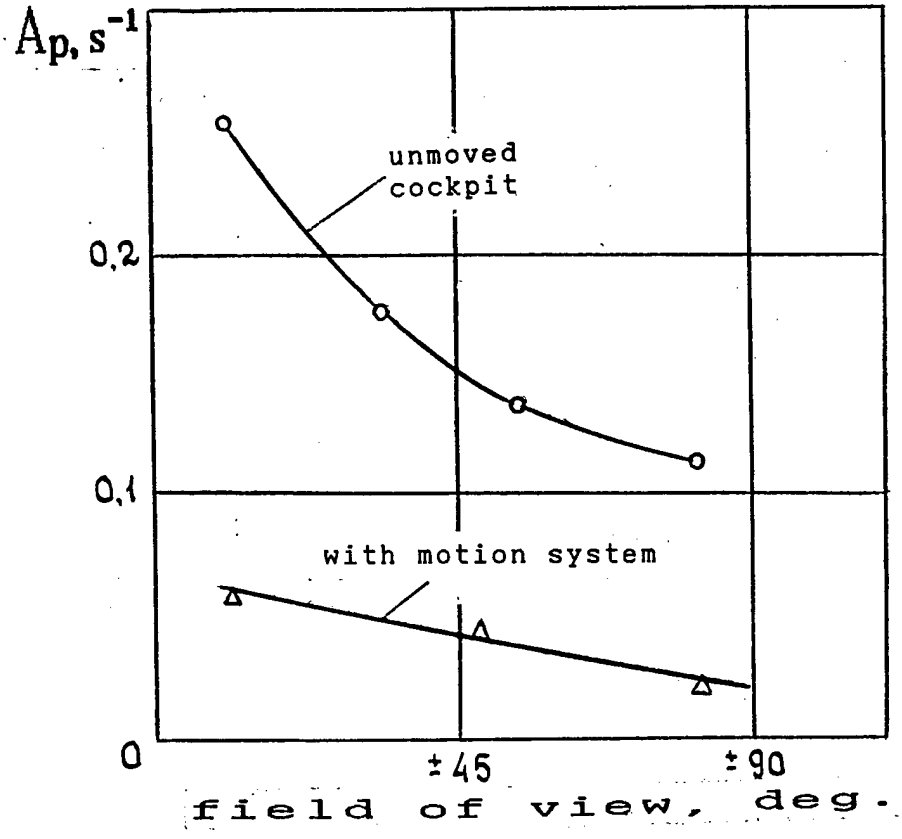

Fig.1.10. Motion Cues Influence on Roll Rate Magnitude of Roll Oscillations

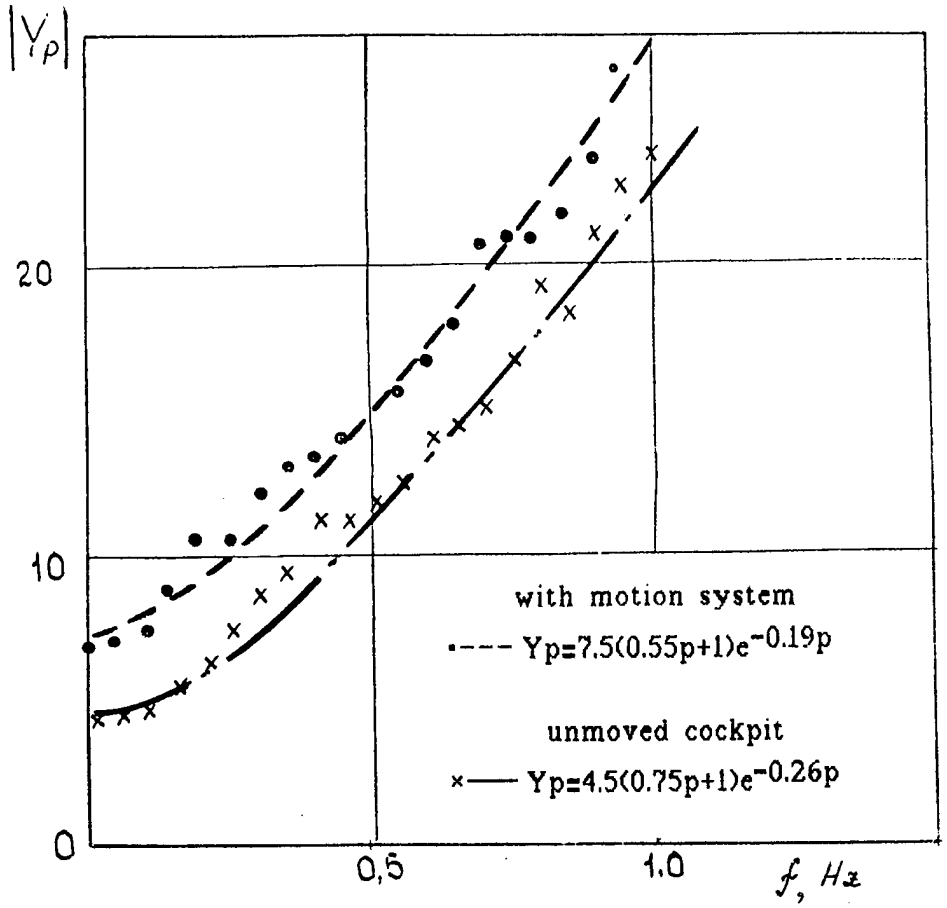

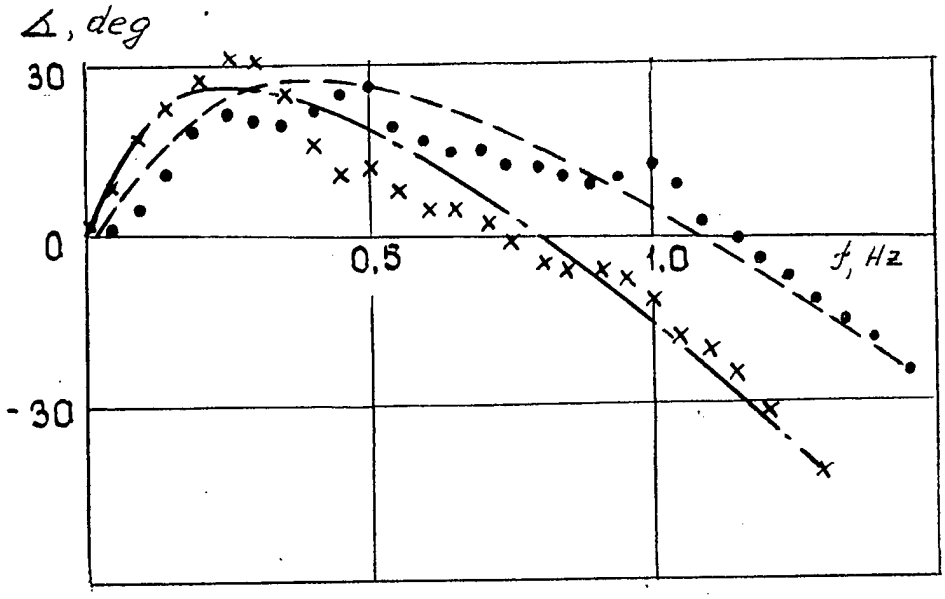

Fig.1.11. Motion Cues Influence
on Pilot Describing Function

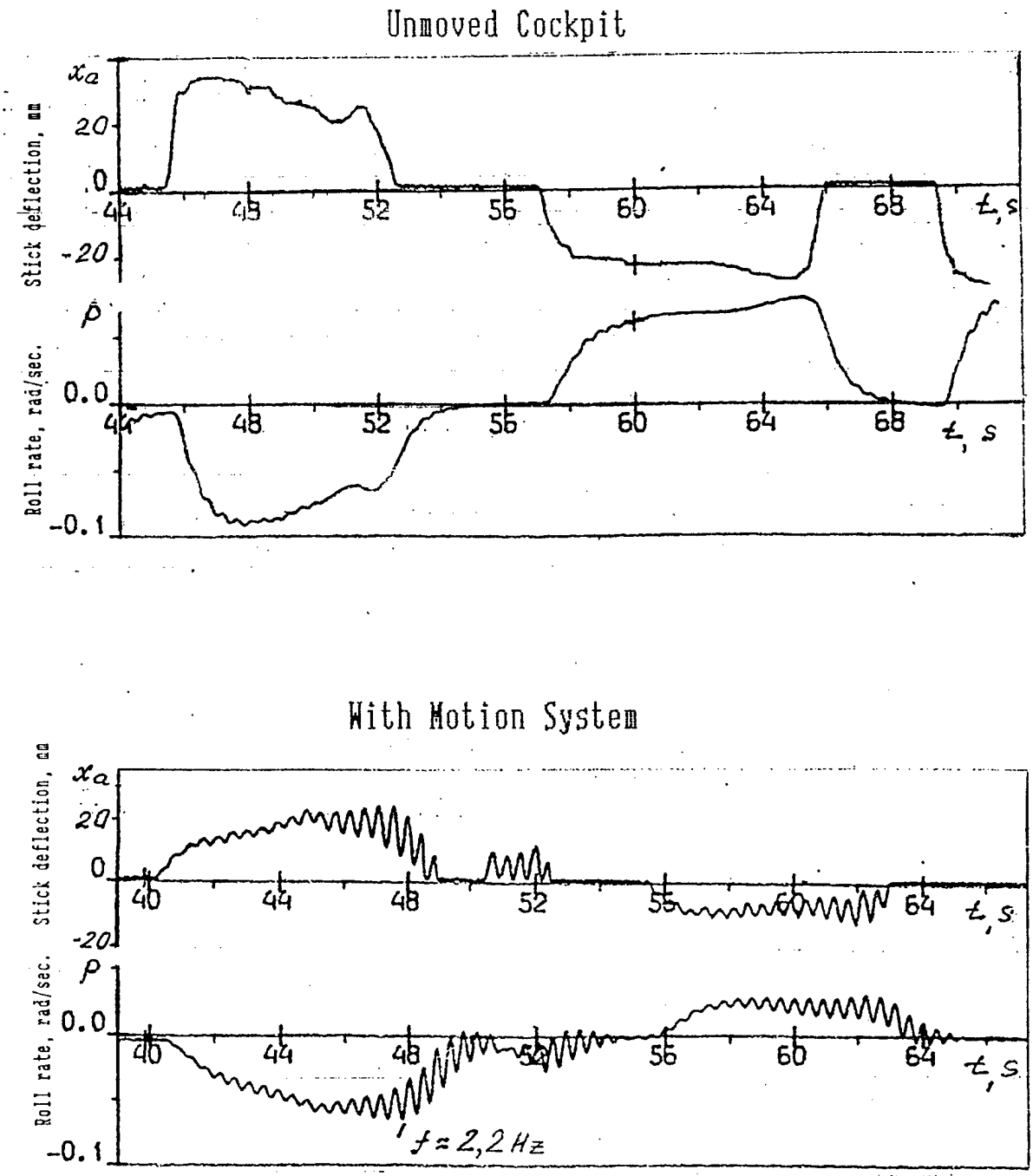

Fig.1.12. Cockpit Motion Influence on High-Frequency Roll Oscillation of Elastic Aircraft.

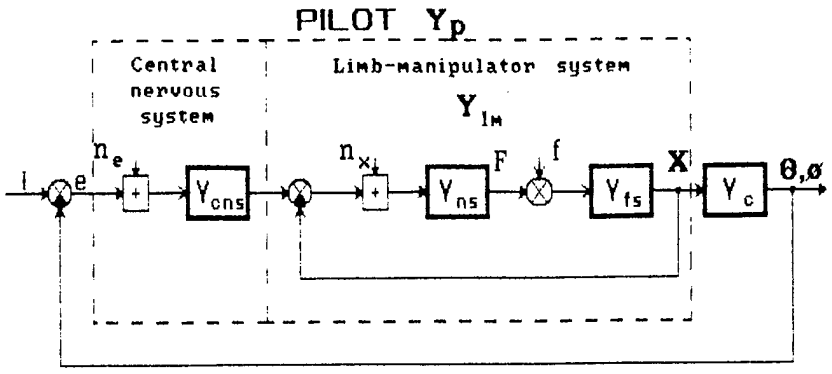

Fig.1.13 Diagram of pilot-aircraft system including closed loop limb-manipulator system.

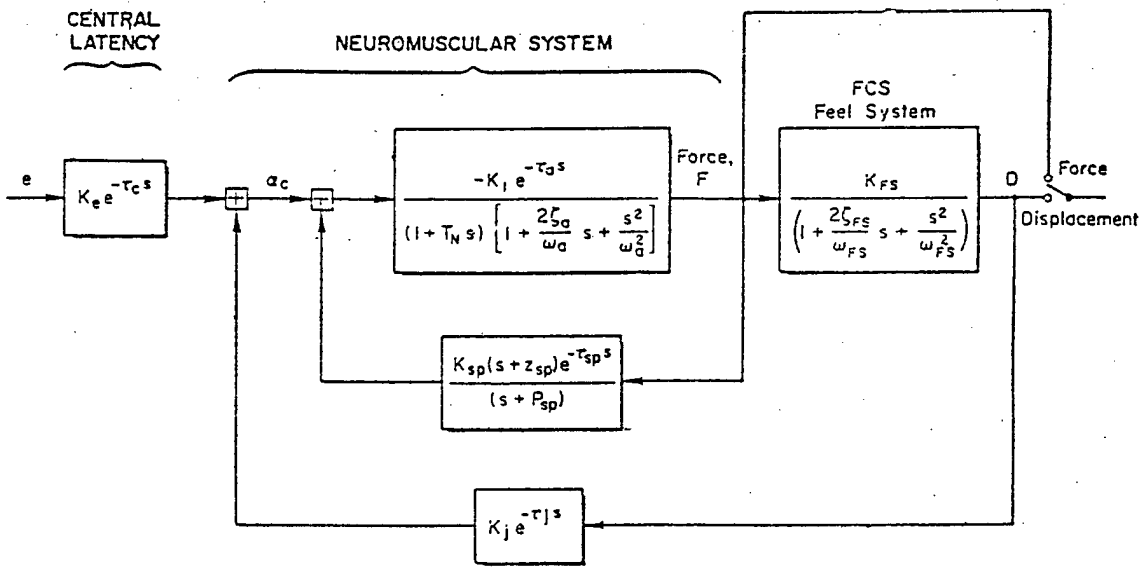

$$\frac{\text{Force}}{e} = \frac{K_p\left(1+\frac{s}{P_{sp}}\right)\left[1+\frac{2\zeta_{FS}s}{\omega_{FS}}+\left(\frac{s}{\omega_{FS}}\right)^2\right]e^{-\tau_p s}}{(1+T_N' s)\left[1+\frac{2\zeta_N' s}{\omega_N'}+\left(\frac{s}{\omega_N'}\right)^2\right]\left[1+\frac{2\zeta_{FS}' s}{\omega_{FS}'}+\left(\frac{s}{\omega_{FS}'}\right)^2\right]} \cdot \frac{\text{Displacement}}{e} = \frac{K_p\left(1+\frac{s}{P_{sp}}\right)e^{-\tau_p s}}{(1+T_N' s)\left[1+\frac{2\zeta_N' s}{\omega_N'}+\left(\frac{s}{\omega_N'}\right)^2\right]\left[1+\frac{2\zeta_{FS}' s}{\omega_{FS}'}+\left(\frac{s}{\omega_{FS}'}\right)^2\right]}$$

Fig.1.14. Pilot Closed-Loop Limb-Actuation With Feel System Dynamics

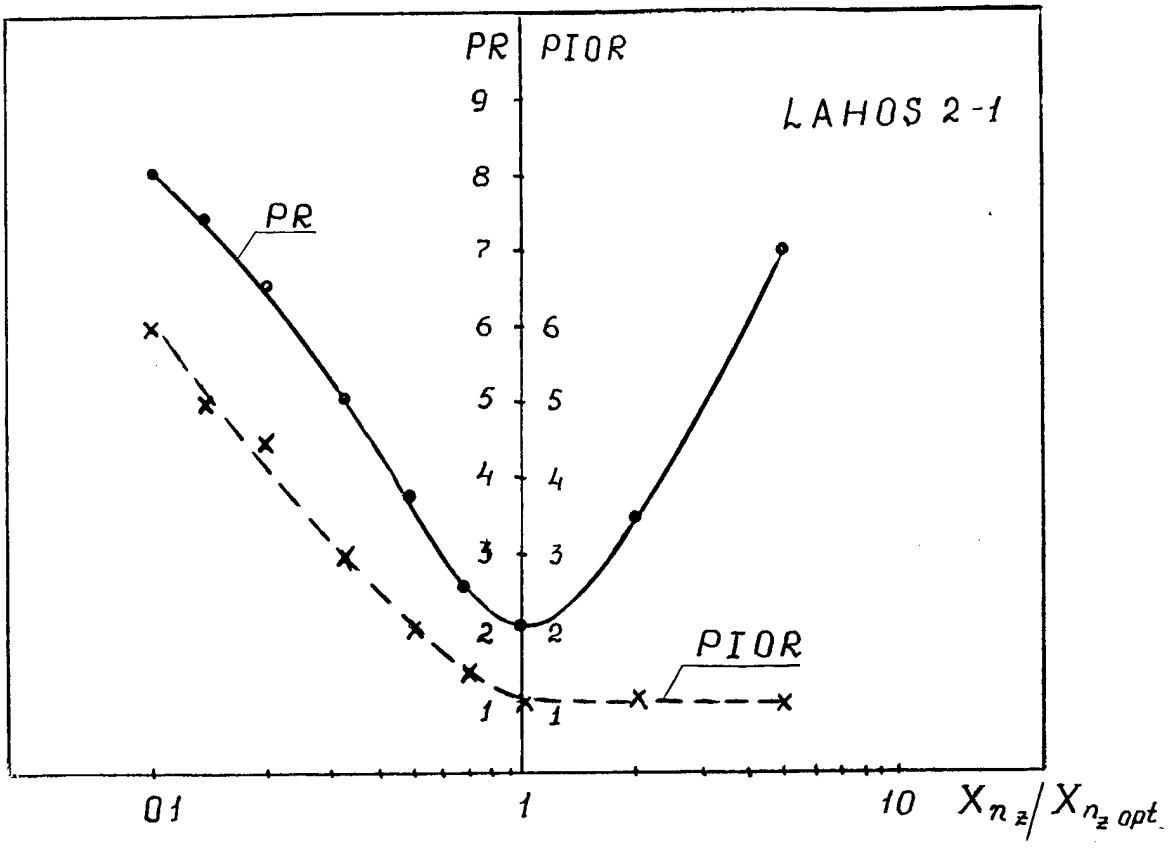

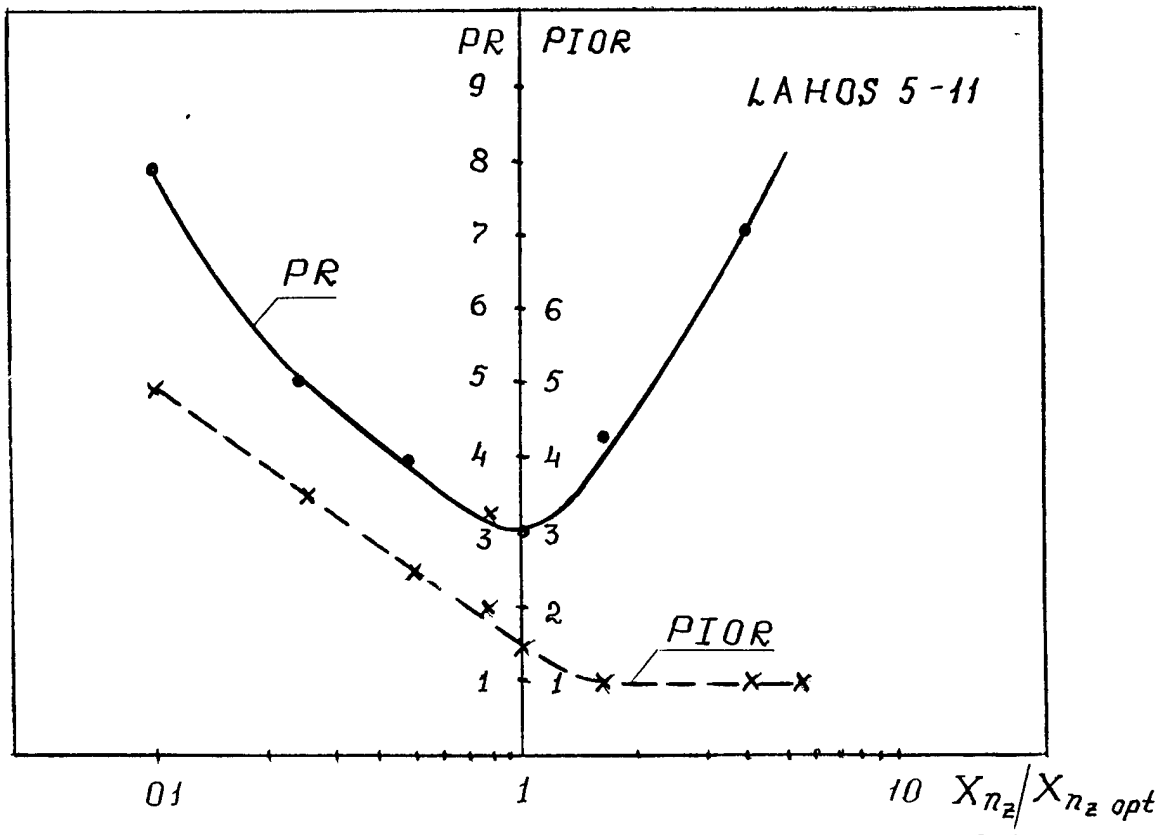

Fig.2.1. Command-Response Gradients Influence on Pilot Ratings (PR and PIOR) at different dynamic performance for an aircraft with a central stick.

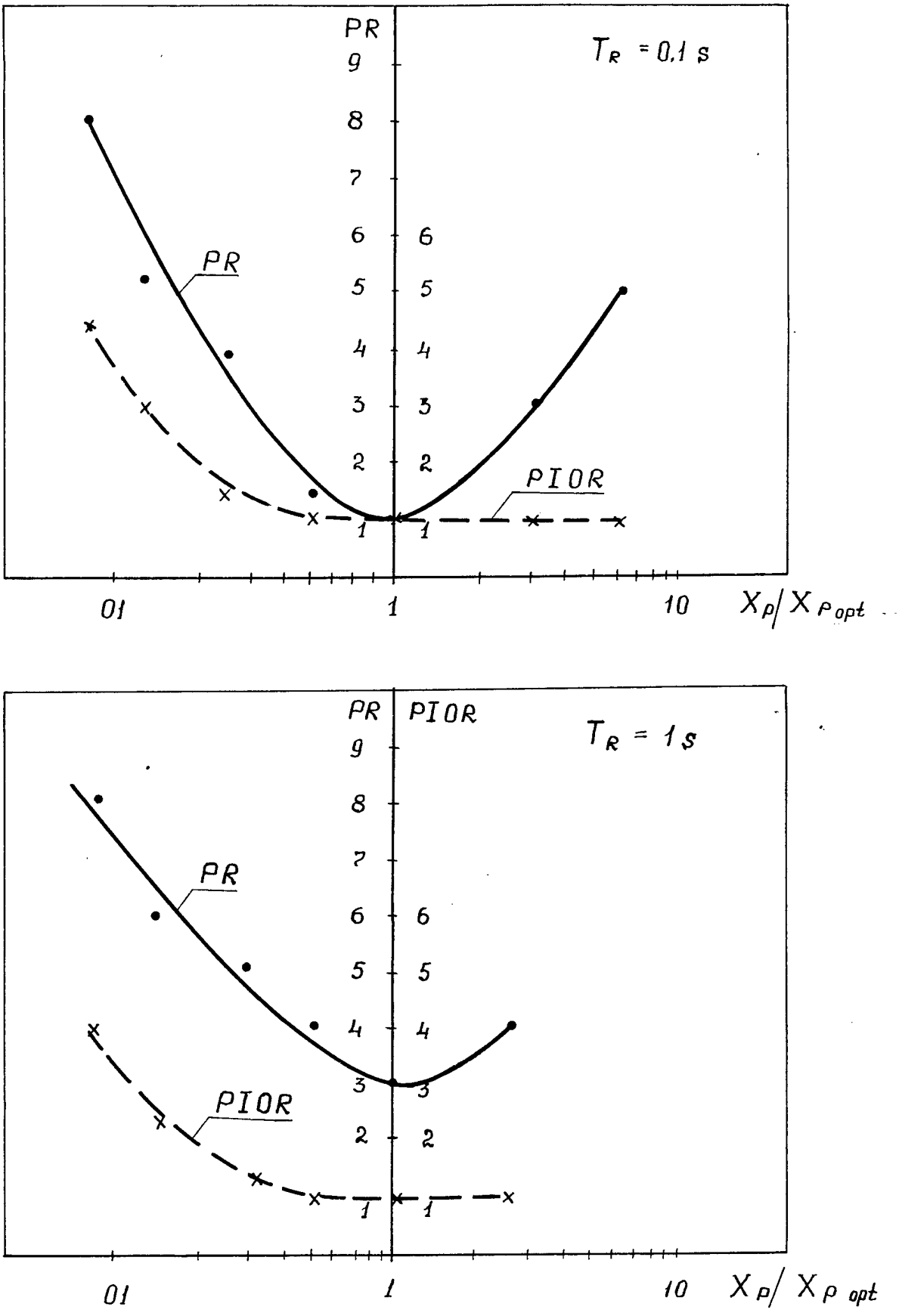

Fig.2.2. Lateral Command-Response Gradients Influence on Pilot Ratings (PR and PIOR) for two values of roll mode time constant for an aircraft with a central stick.

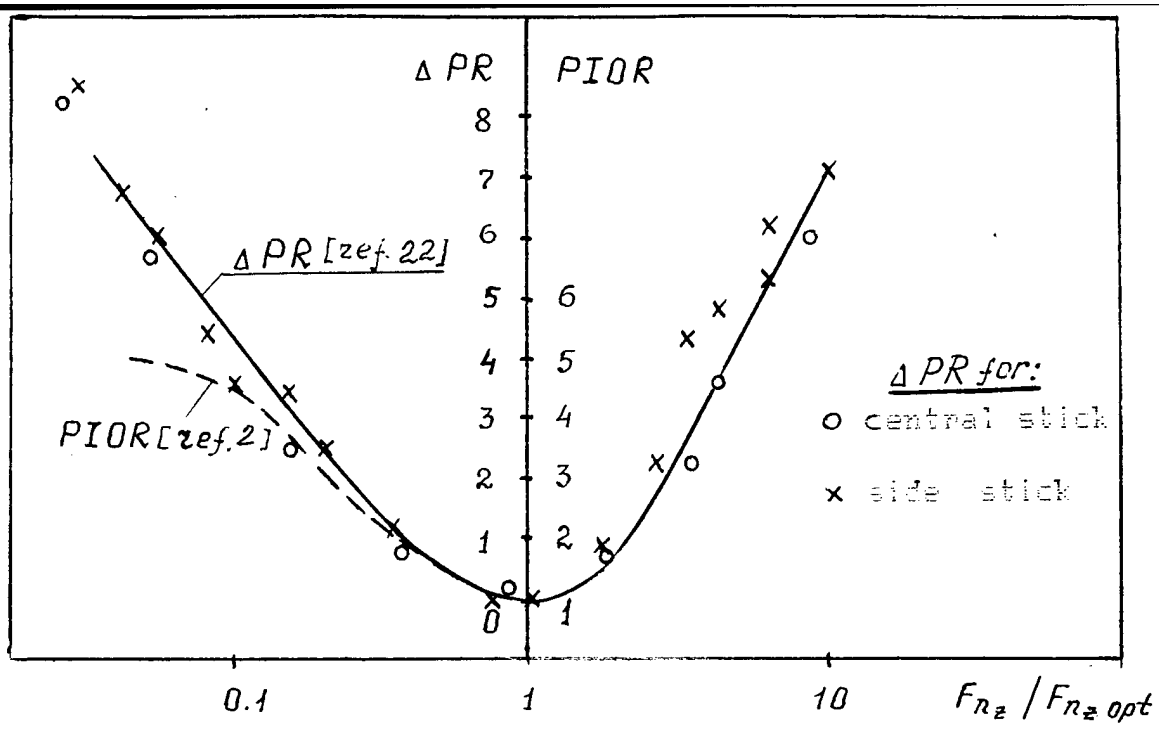

Fig.2.3. Longitudinal Command-Response Gradients Influence on PIORs and PR.

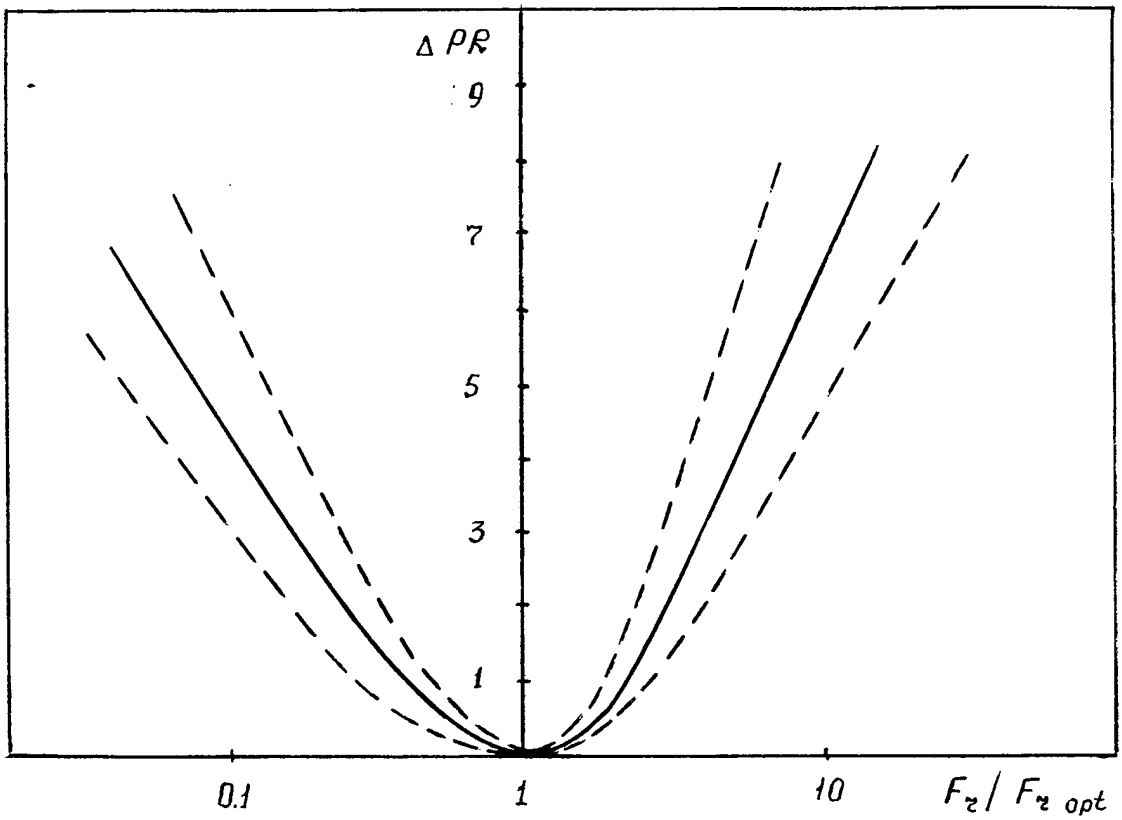

Fig.2.4. Limits of Pilot Ratings Worsening Variation PR at Command-Response Gradients Deflecting about their optimum values. [ref.22]

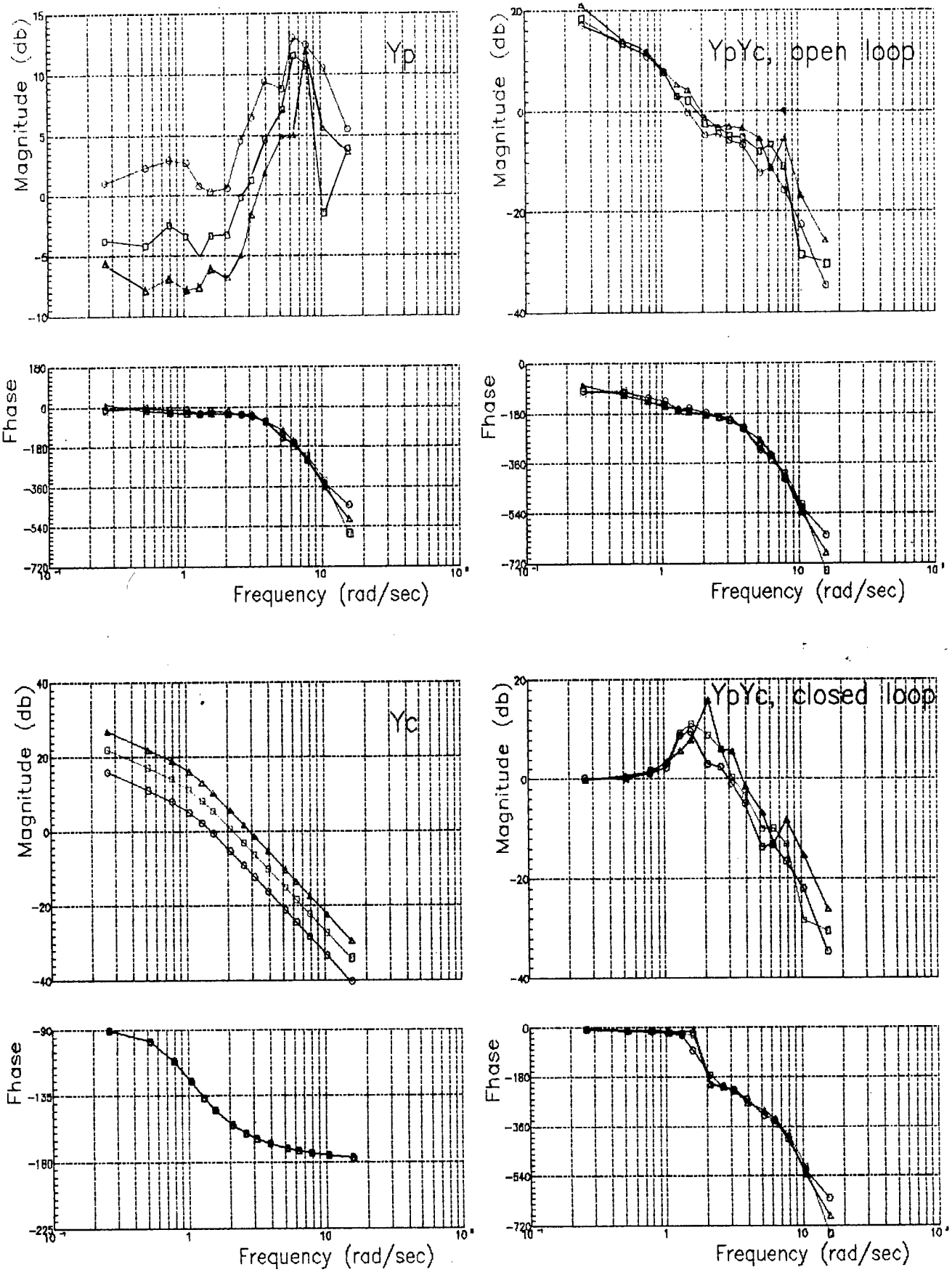

Fig.2.5 Pilot/Pilot–Aircraft describing functions for different aircraft gains /longitudinal channel '1–1' LAHOS/.

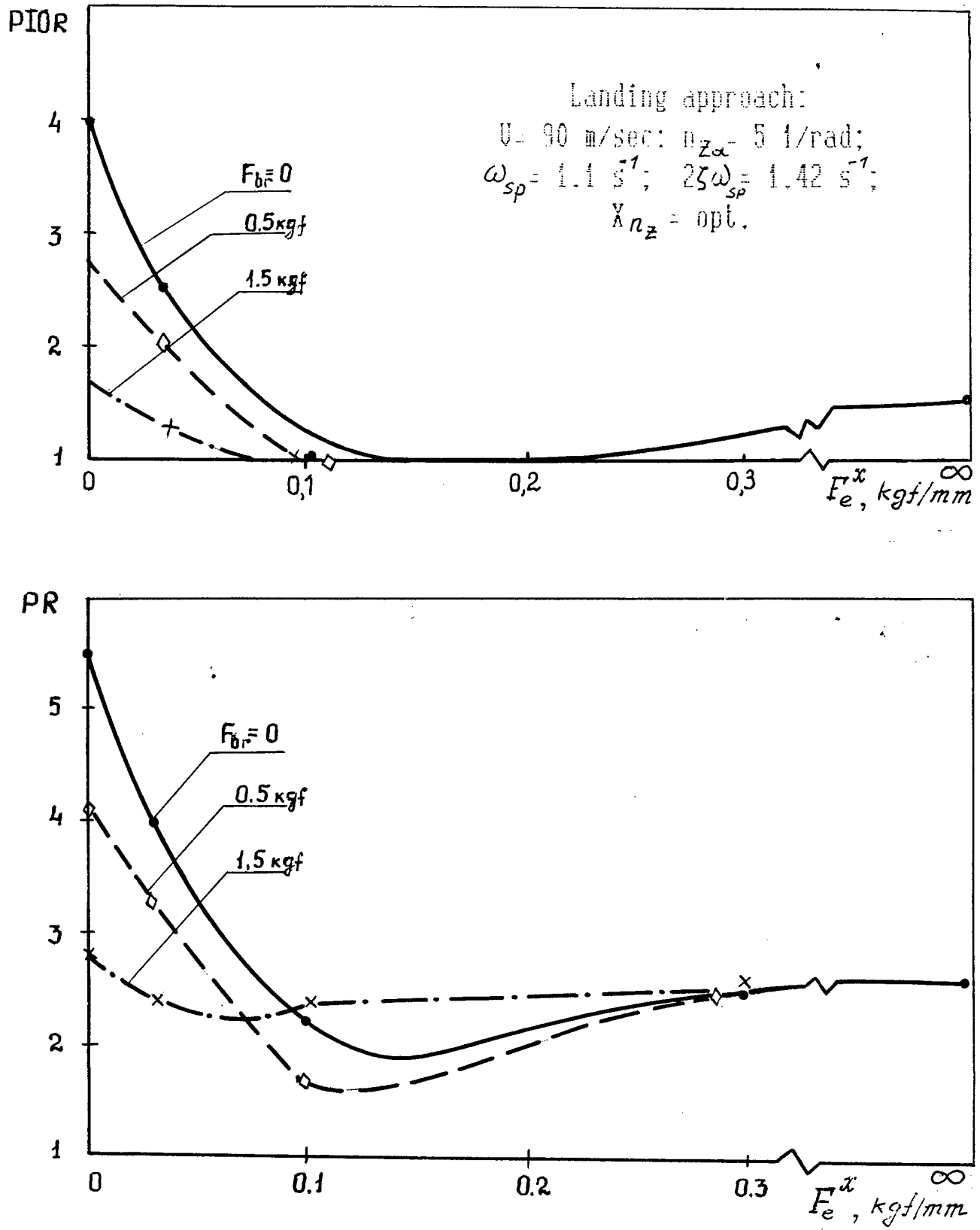

Fig.2.6. Longitudinal Feel System Gradient and Breakout Force Influence on PIOR and PR (central stick)

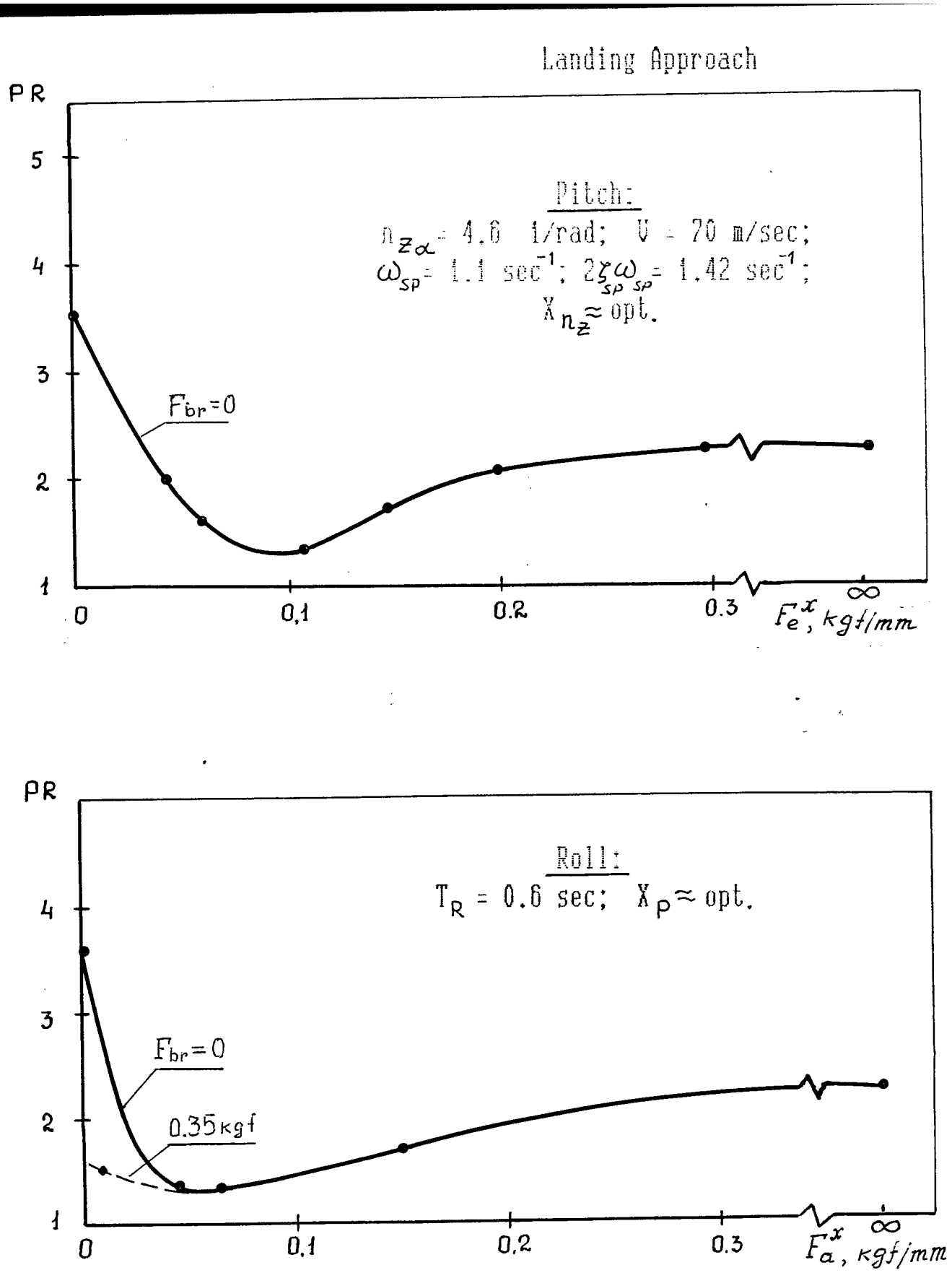

Fig.2.7. Pitch and Roll Feel System Gradients Influence on PR (side stick)

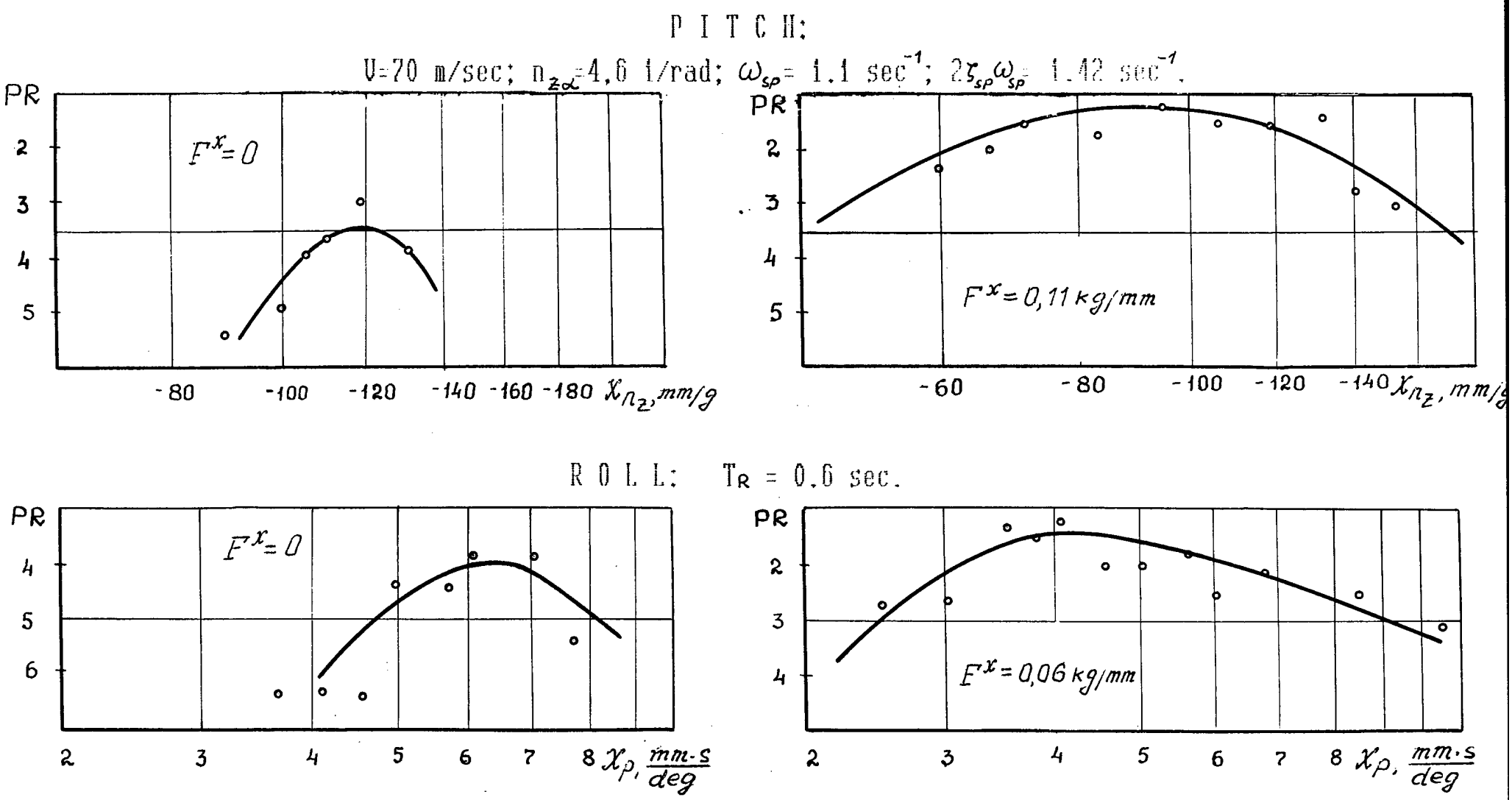

Fig.2.8 Influence of Feel System Gradients F^x and Command Response Gradients X_{n_z} and X_p on Pilot Ratings (side stick)

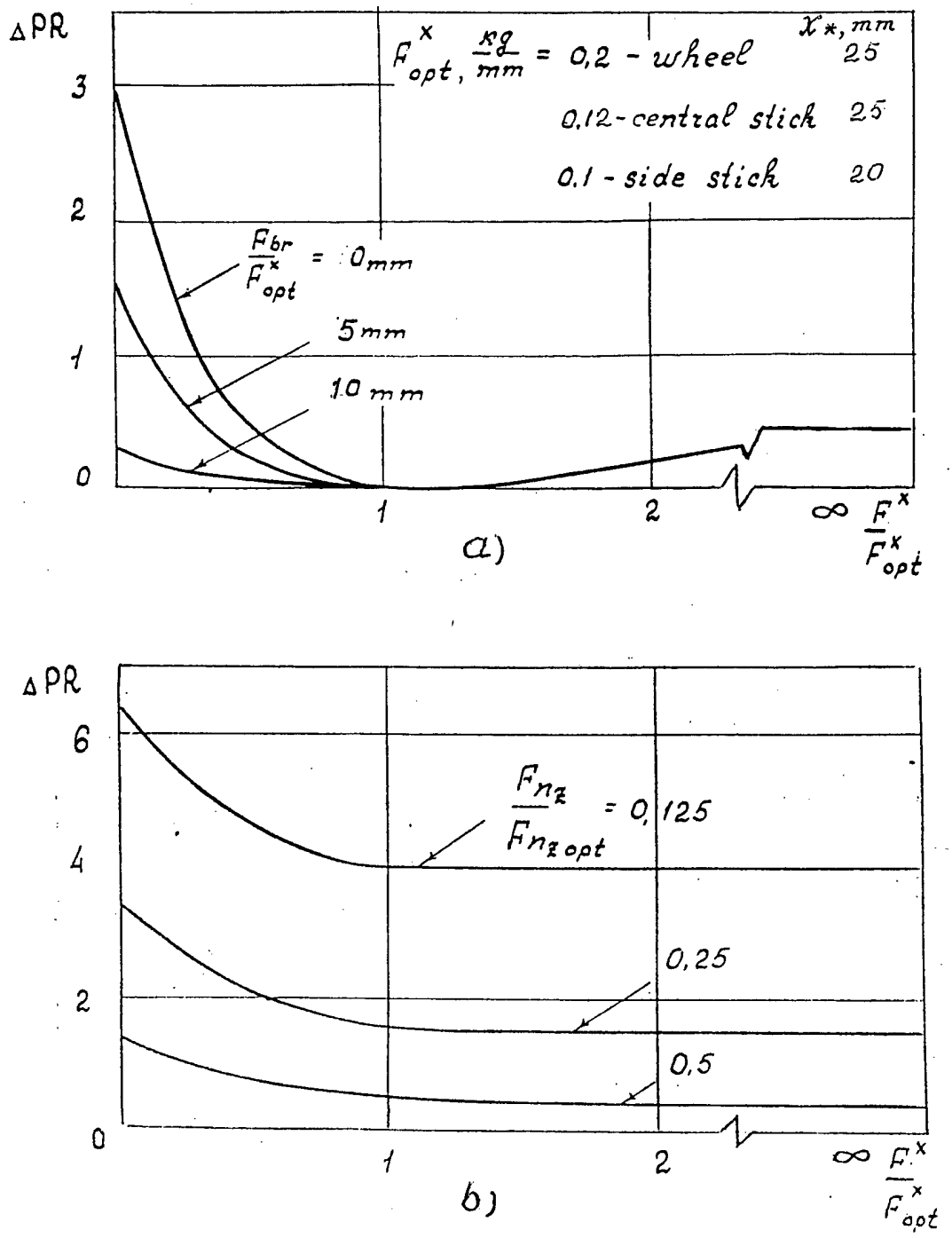

Fig.2.9 Pilot Ratings Deterioration Degree due to PIO Tendency Increasing in the case of Feel System (a) and Control Sensitivity (b) Characteristics Deviation from Their Optimum Values.

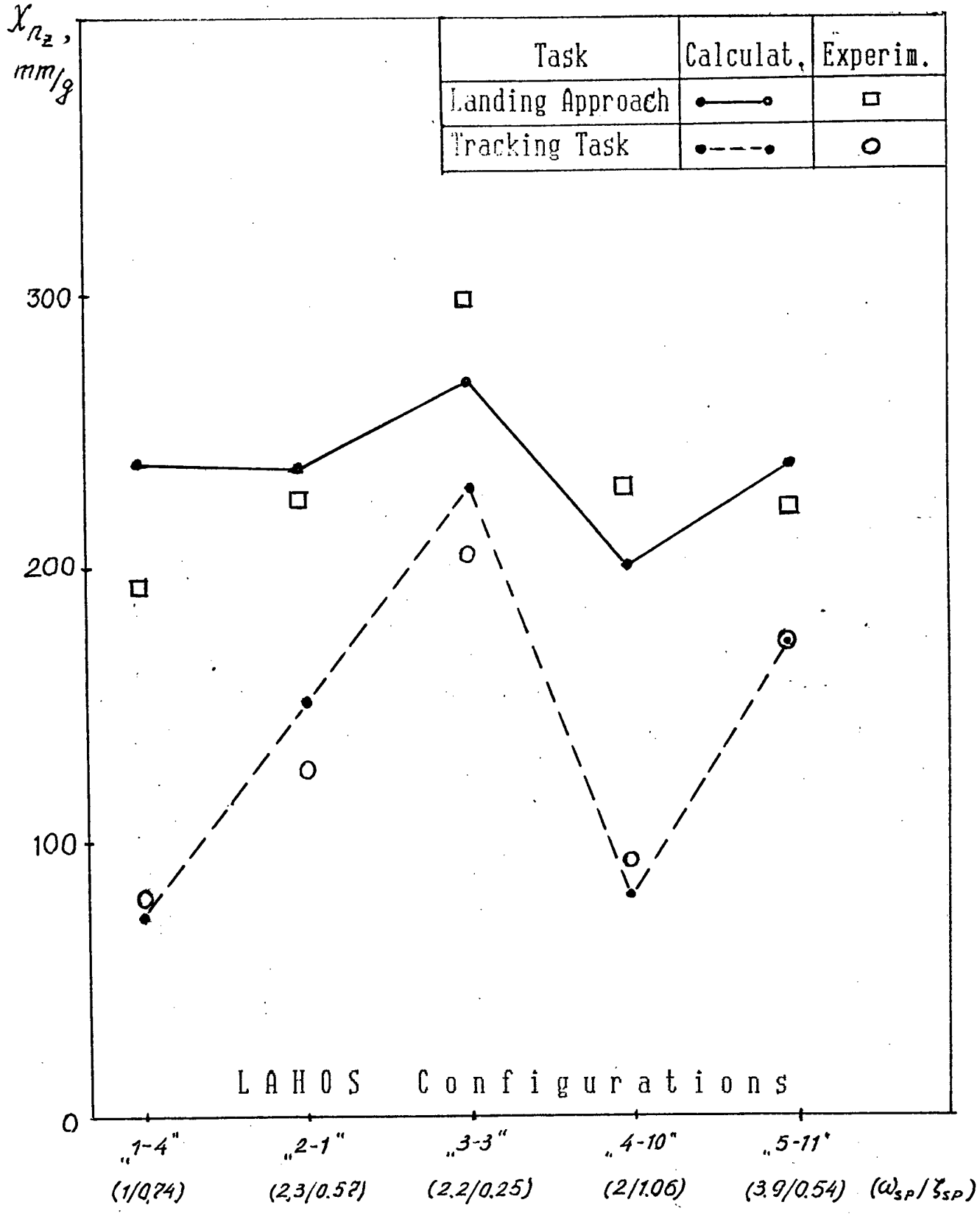

Fig.2.10 Optimum Command-Response Gradients X_{n_z} for 5 LAHOS Configurations for Landing Approach and Tracking Task.

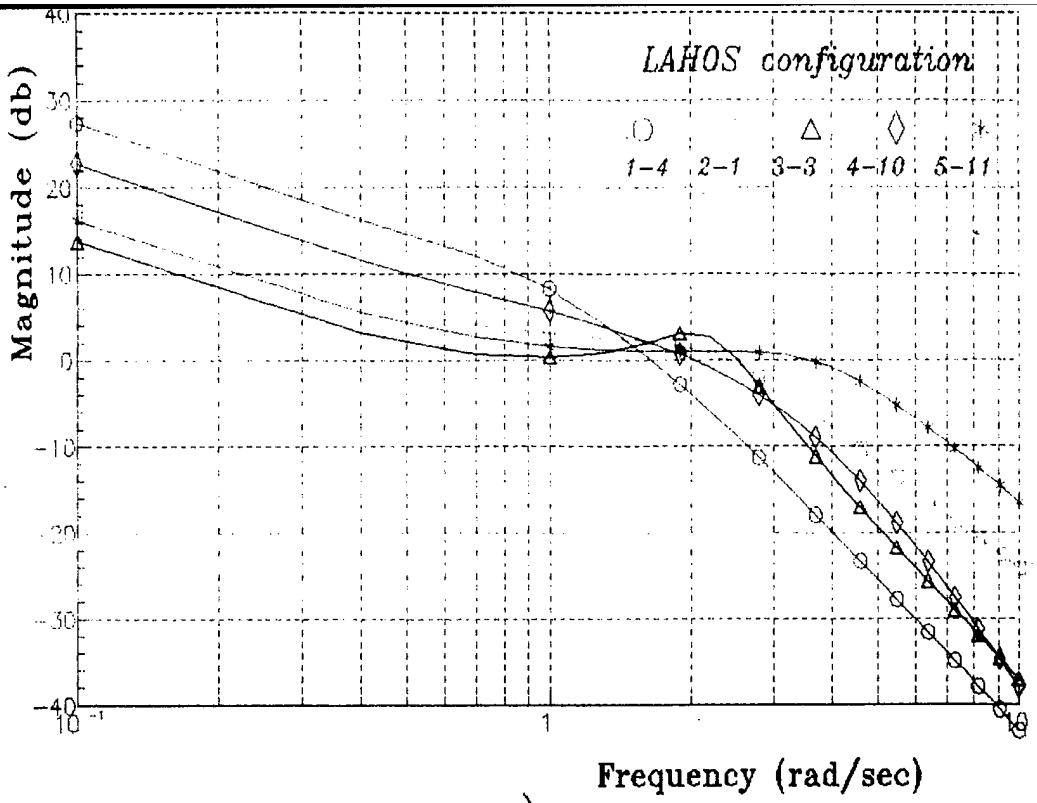

a)

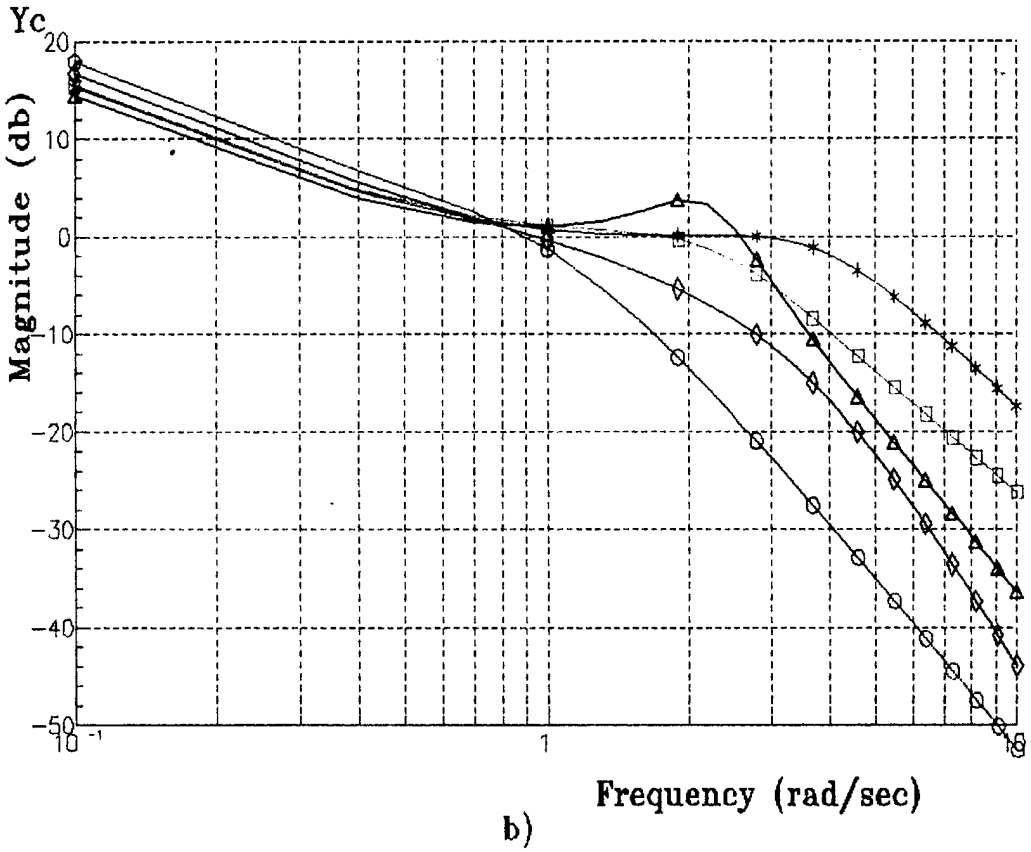

b)

Fig.2.11 Roll transfer function responses for optimal control sensitivity of different dynamic configuration,
a) tracking task
b) landing approach.

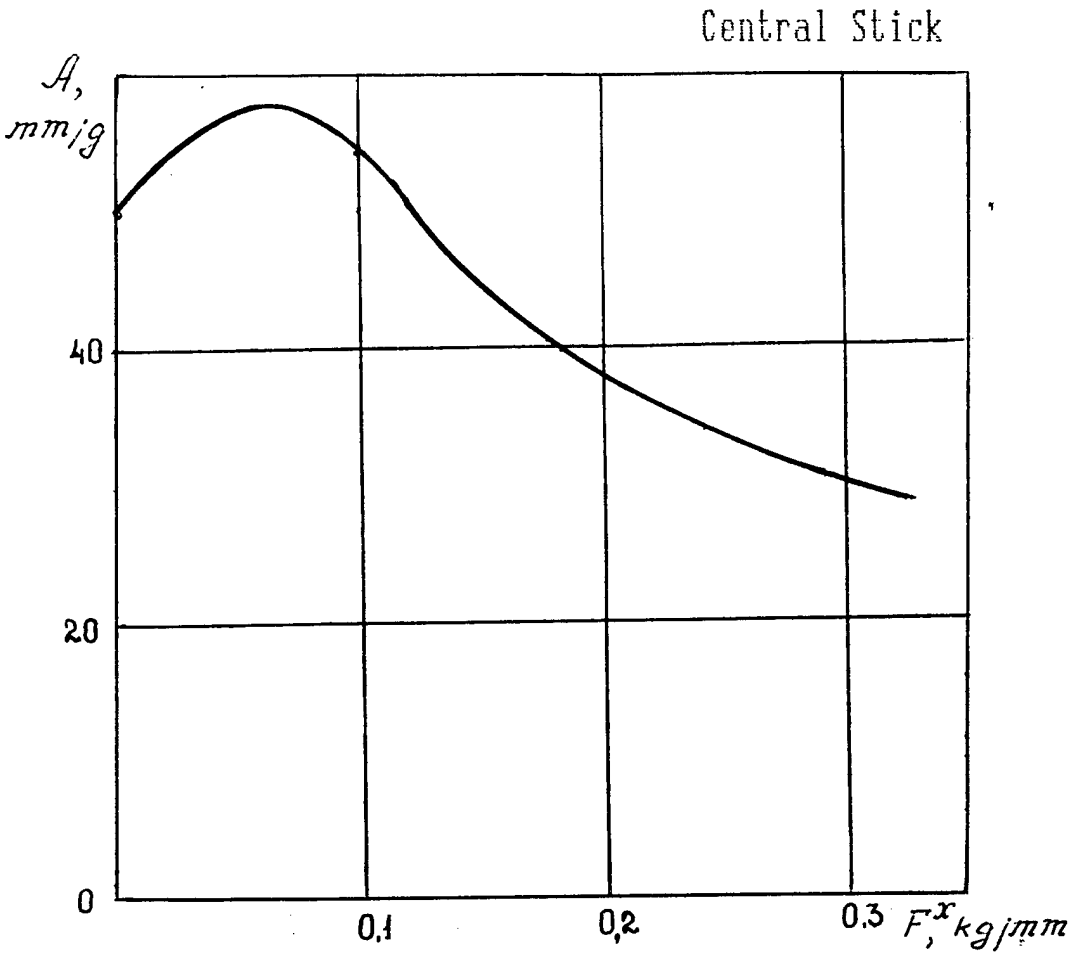

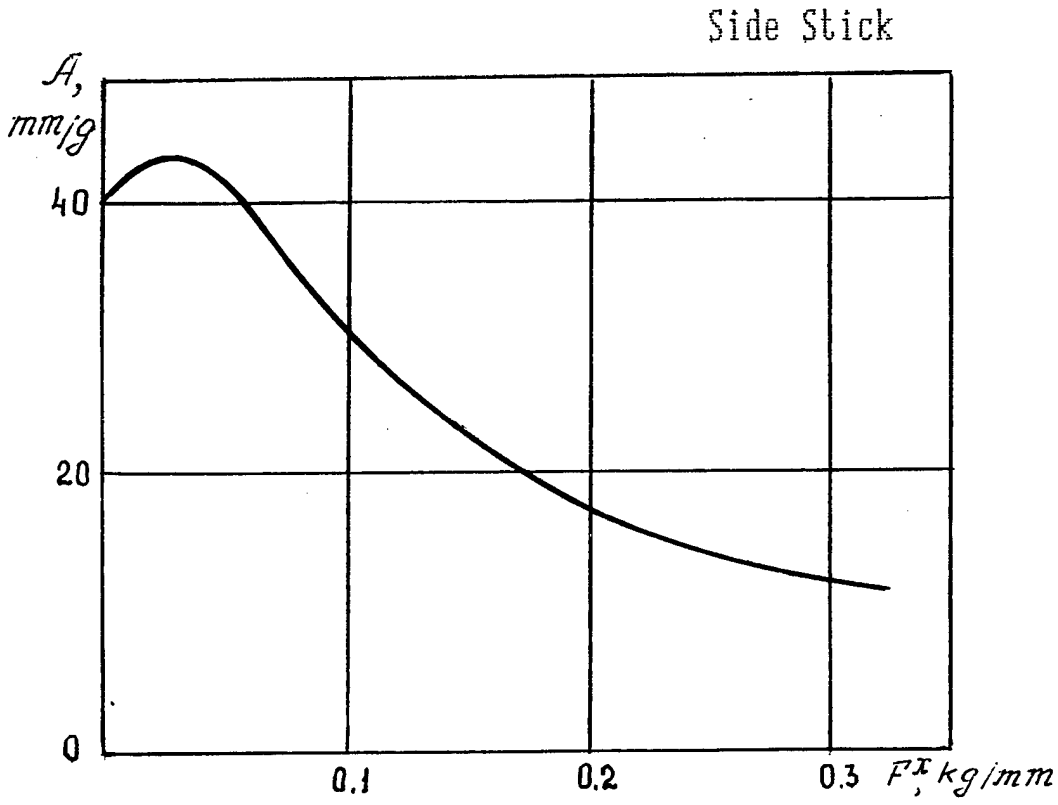

Fig.2.12 Parameter A Depending on Gradient F^x of Central and Side Sticks ($F_{br}=F_{fr}=F^{\dot{x}}=0$)

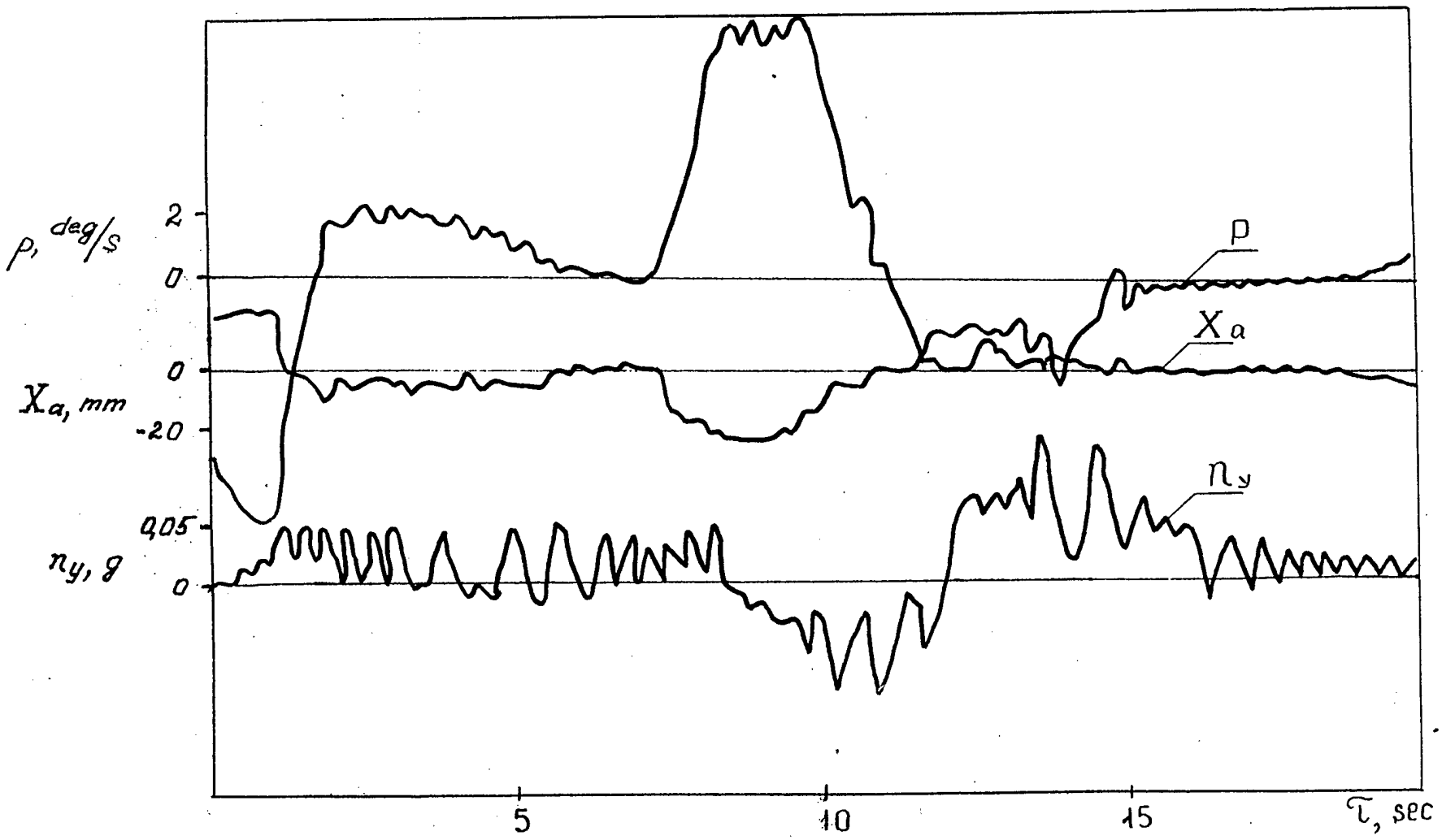

Fig. 3.1. Time Histories for the Ratchet Case.

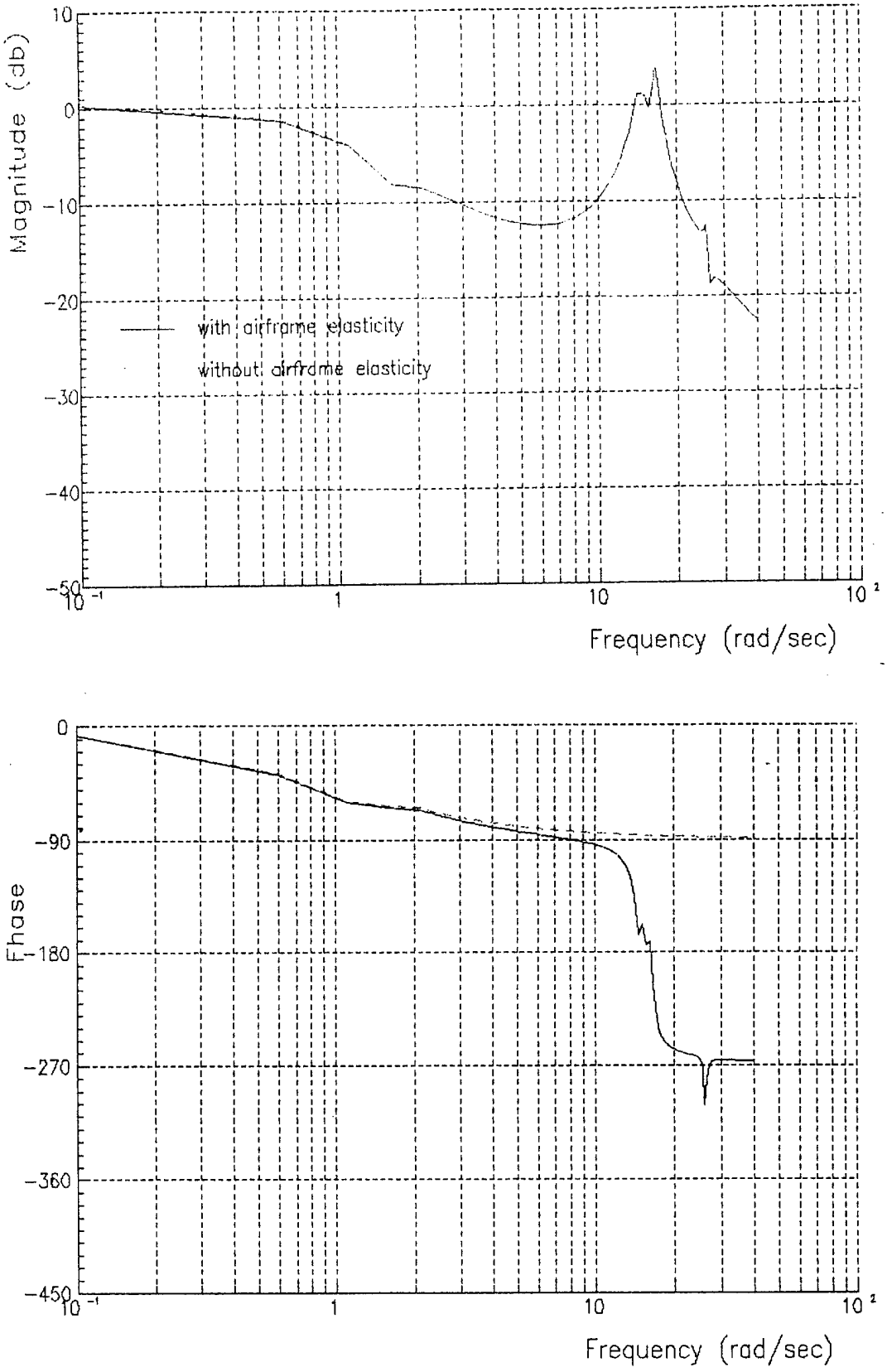

Fig.3.2a Roll-rate transfer function responses for the aircraft with and without airframe elasticity.

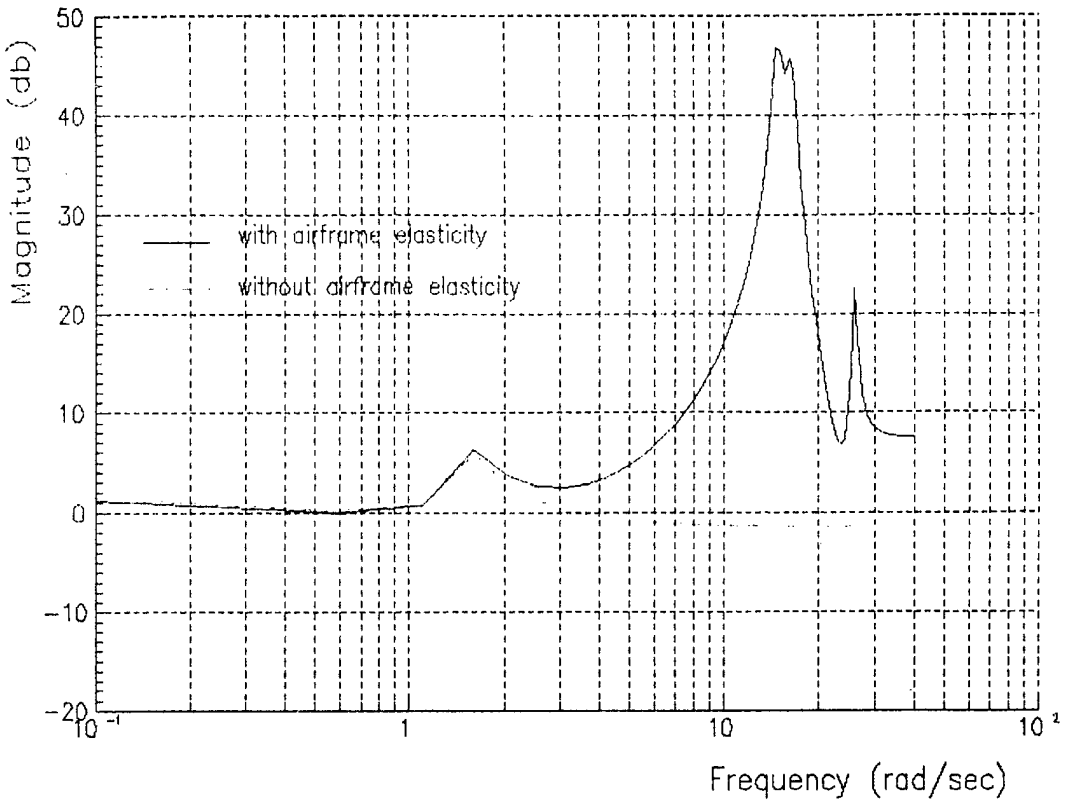

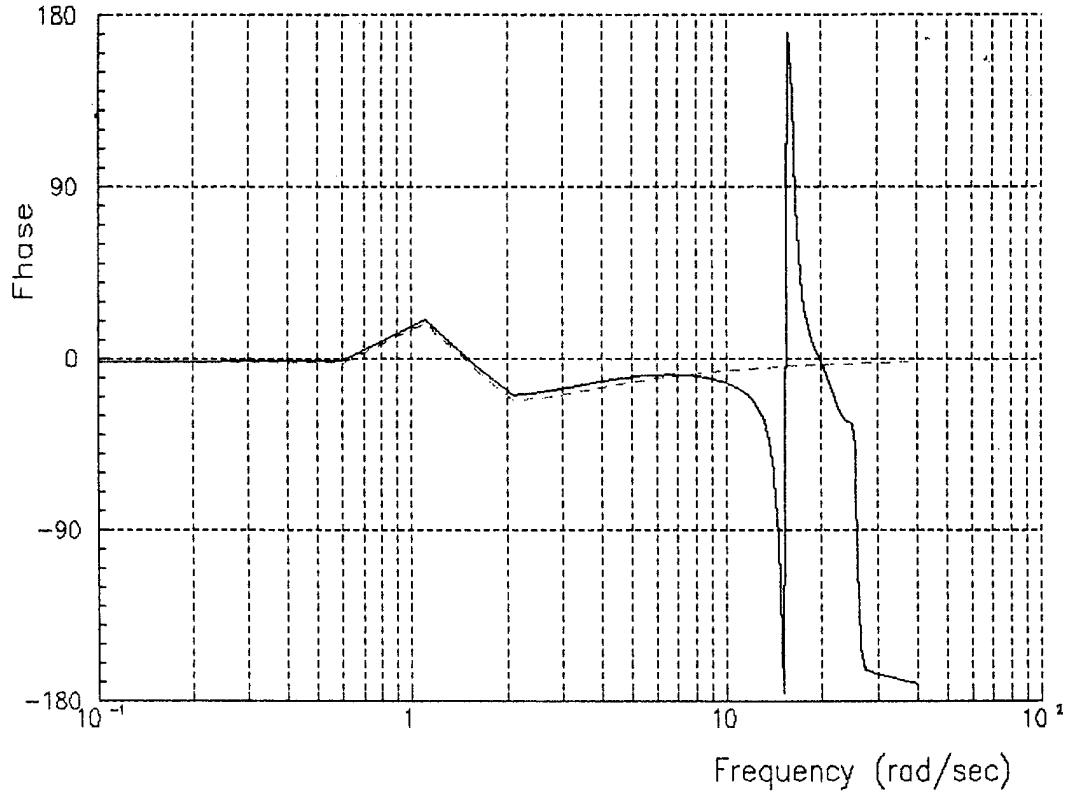

Fig. 3.2b Lateral–acceleration transfer function responses for the aircraft with and without airframe elasticity.

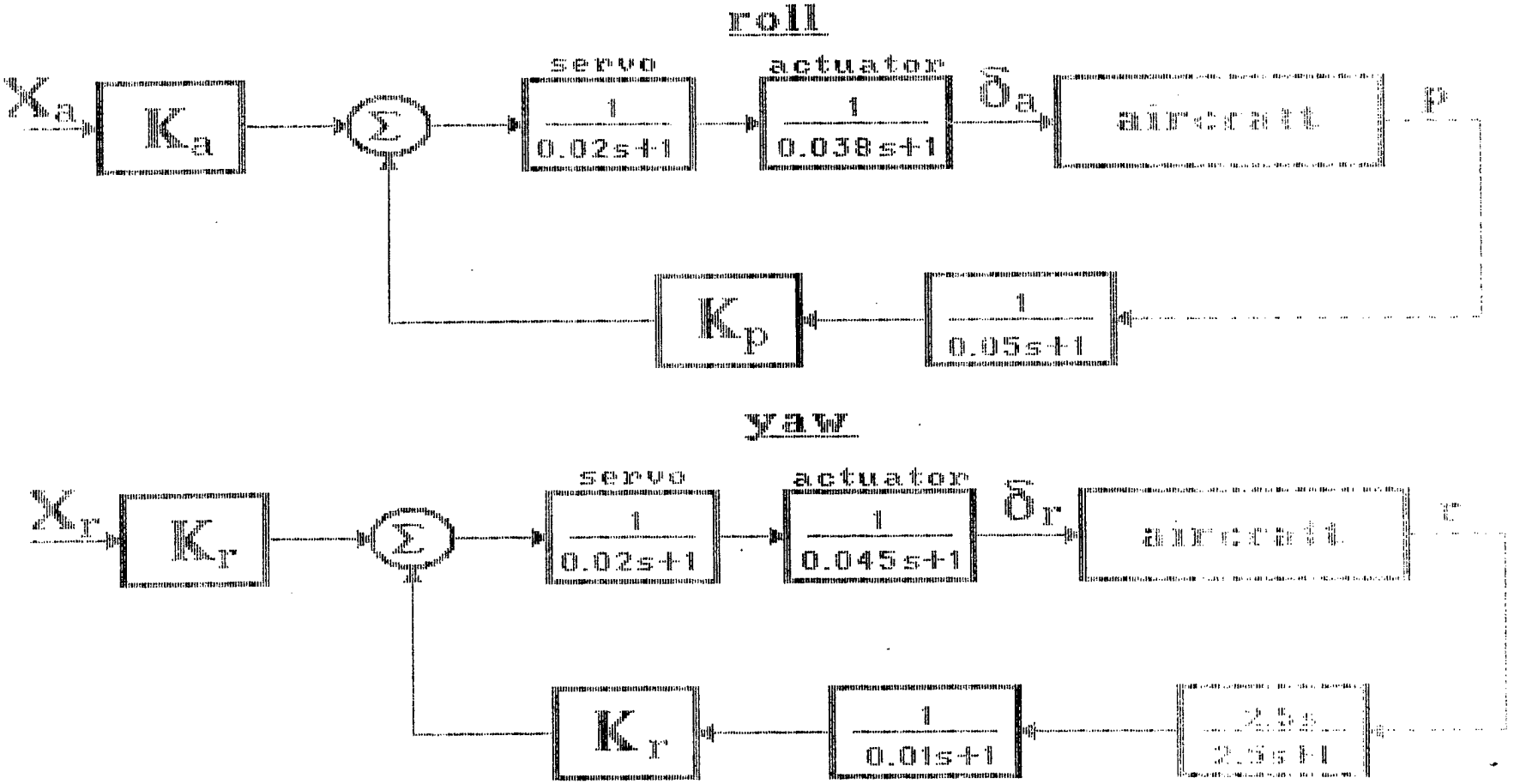

Fig.3.3. Block-diagrams of aircraft lateral control system.

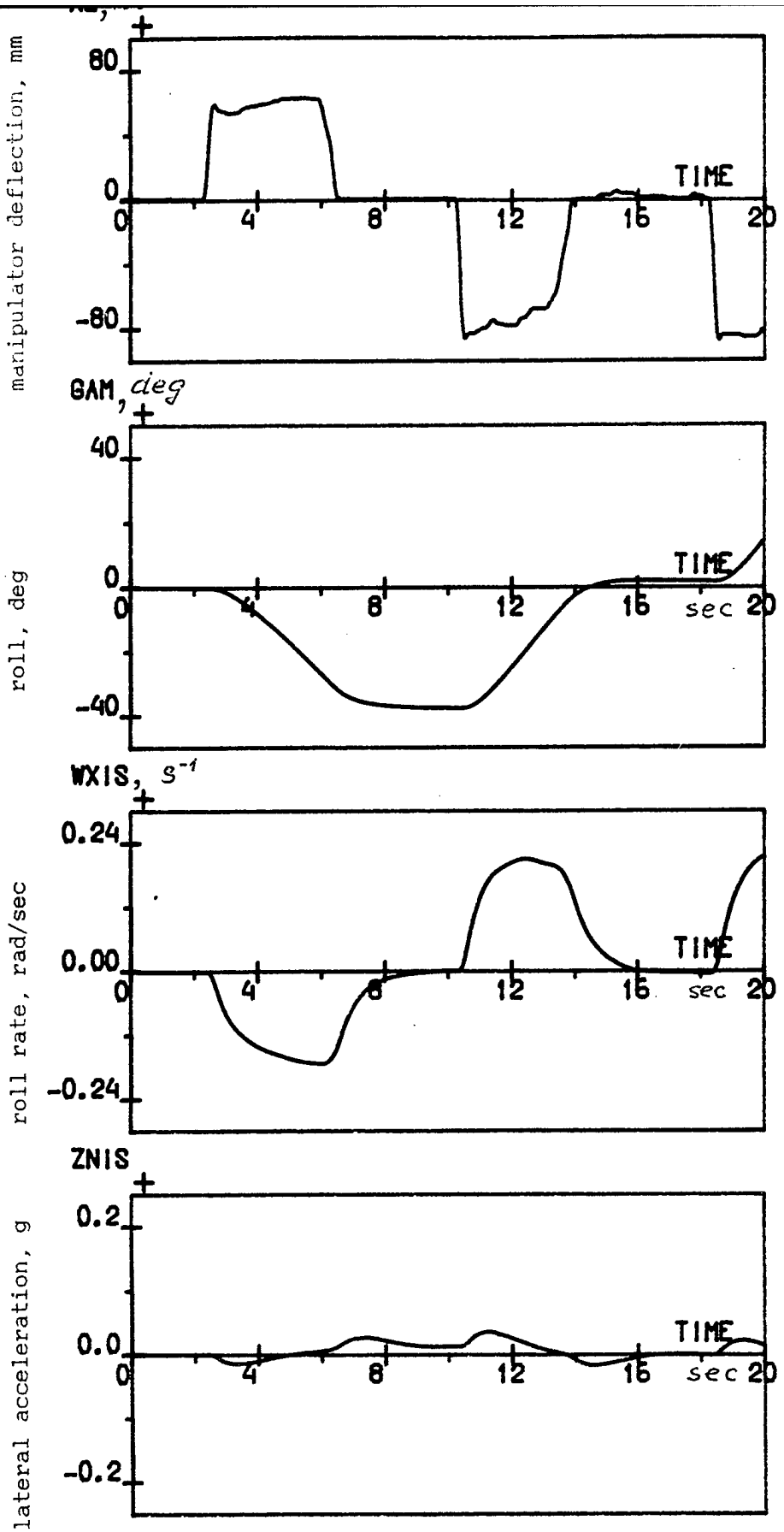

Fig.3.4. Time Histories of Aircraft as Rigid Body.

Elastic mode amplitude: $\bar{A}$ = 0 Manipulator: central stick
Motion simulated: roll, yaw, lat.displ. Aircraft gain: K/Kn = 1

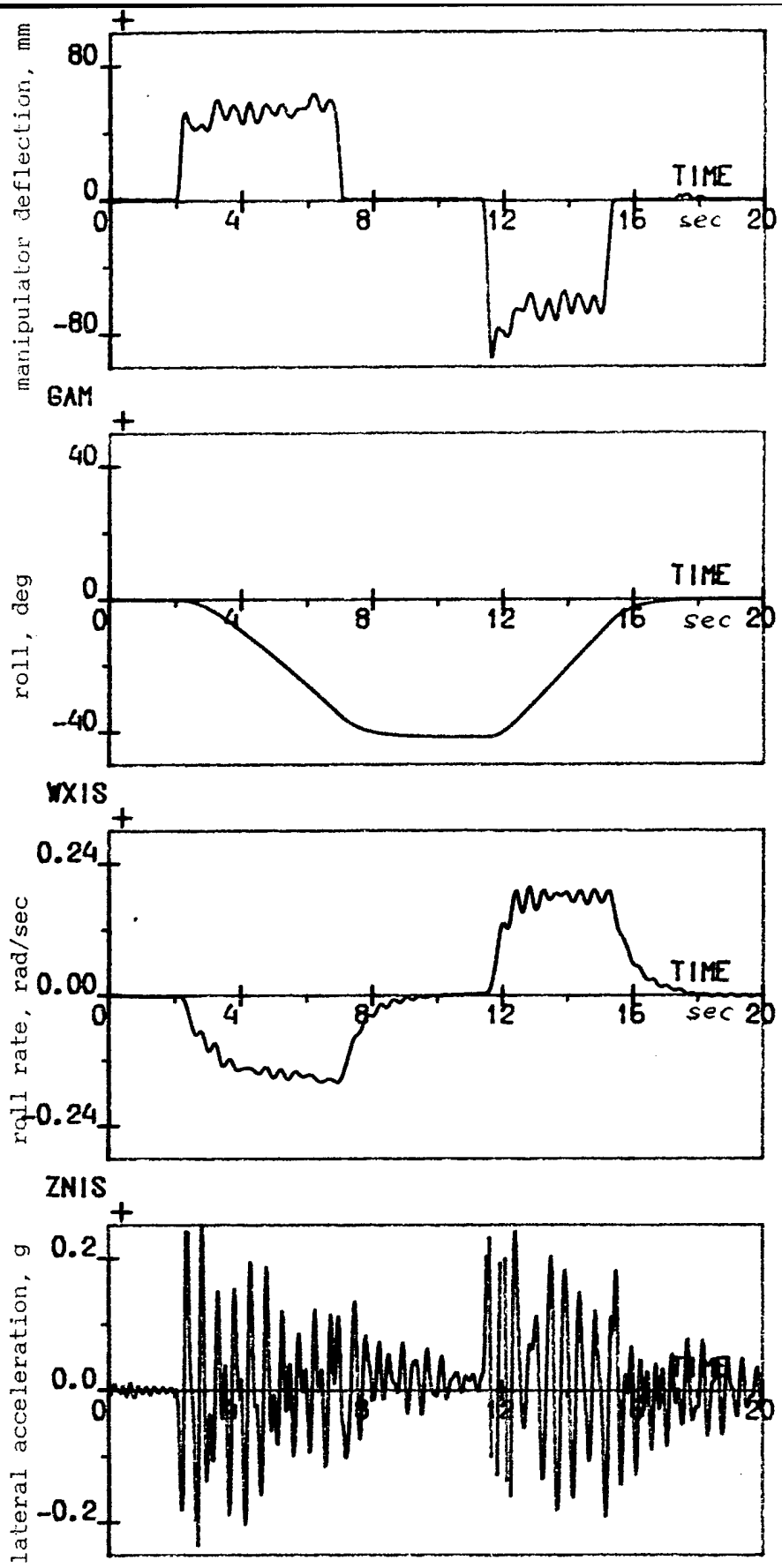

Fig.3.5. Time Histories of Elastic Aircraft

Elastic mode amplitude: $\bar{A}$ = 1 Manipulator: central stick
Motion simulated: roll, yaw, lat.displ. Aircraft gain: K/Kn = 1

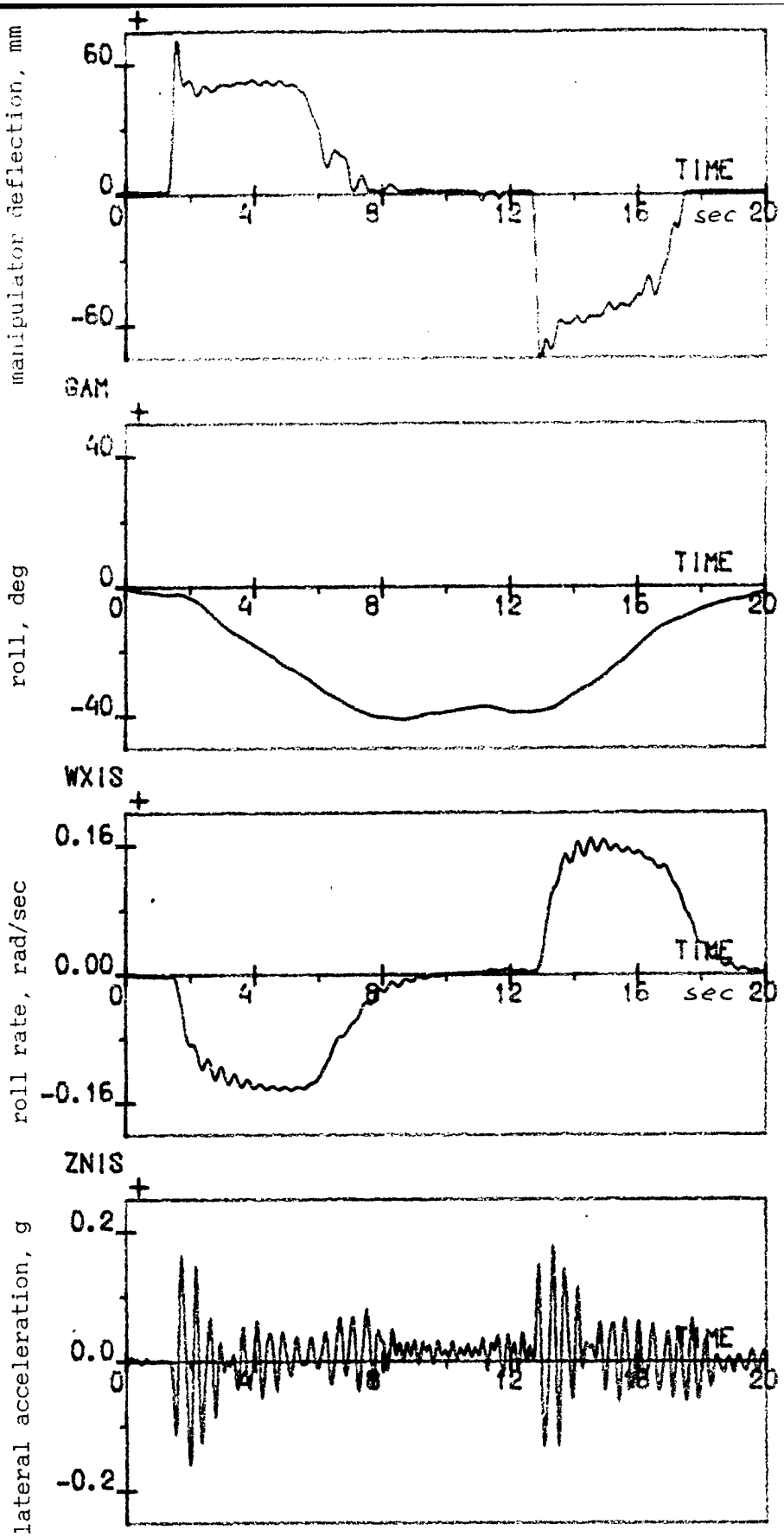

Fig.3.6. Time Histories of Elastic Aircraft

Elastic mode amplitude: $\bar{A}$ = 0.5 Manipulator: central stick
Motion simulated: roll, yaw, lat.displ. Aircraft gain: K/Kn = 1

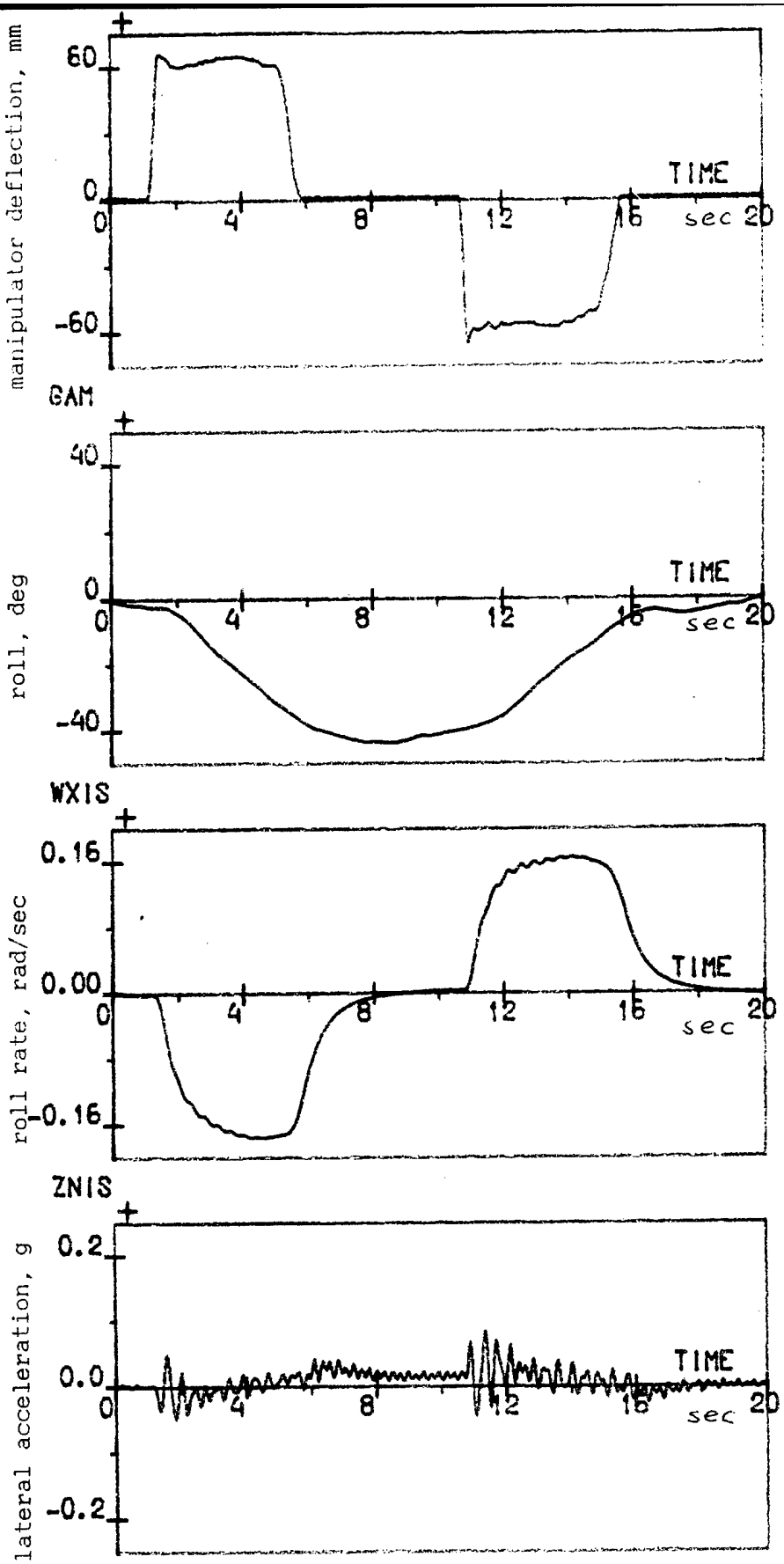

Fig.3.7. Time Histories of Elastic Aircraft

Elastic mode amplitude: $\bar{A}$ = 0.25 Manipulator: central stick
Motion simulated: roll, yaw, lat.displ. Aircraft gain: K/Kn = 1

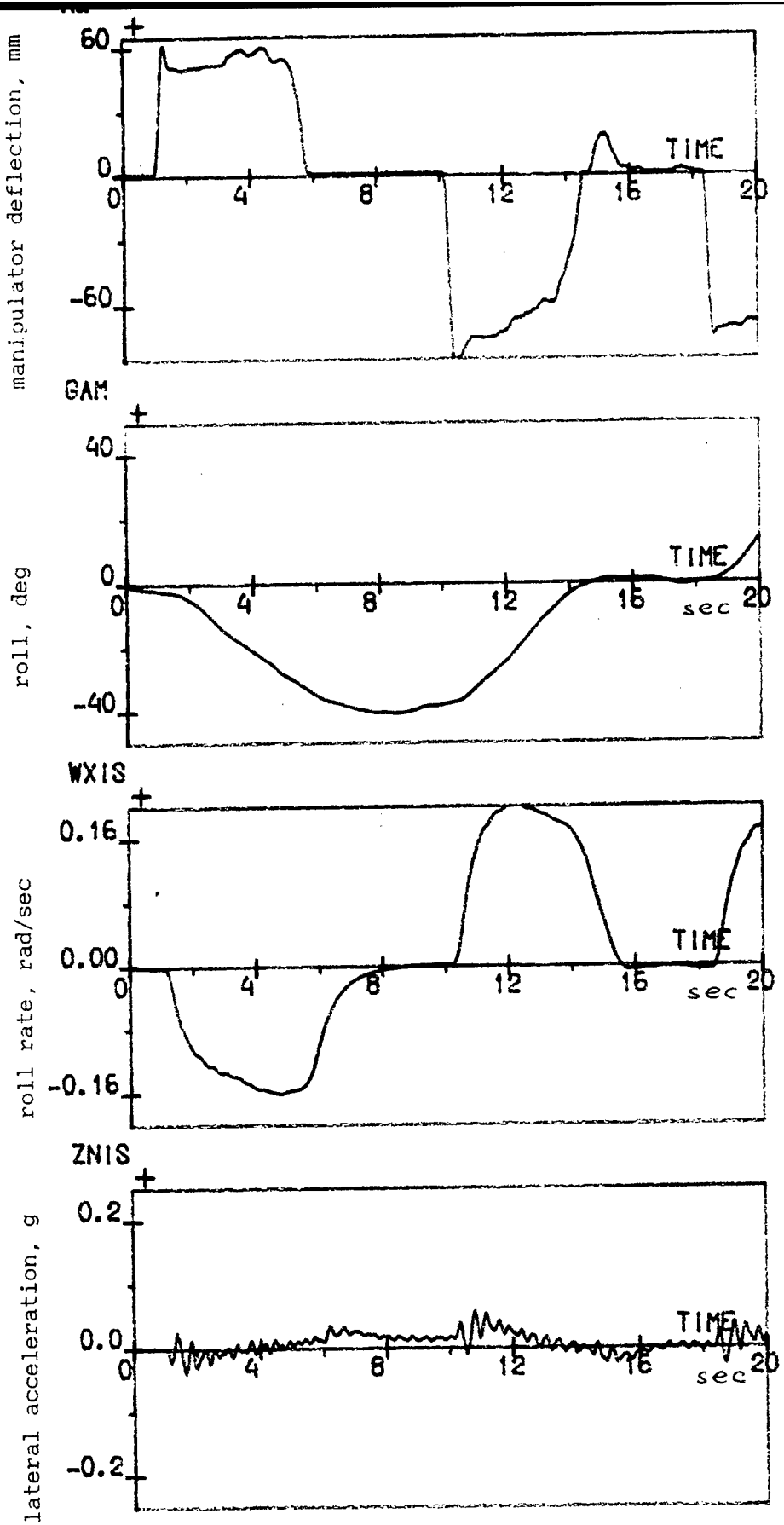

Fig.3.8. Time Histories of Elastic Aircraft

Elastic mode amplitude: $\bar{A}$ = 0.125 Manipulator: central stick
Motion simulated: roll, yaw, lat.displ. Aircraft gain: K/Kn = 1

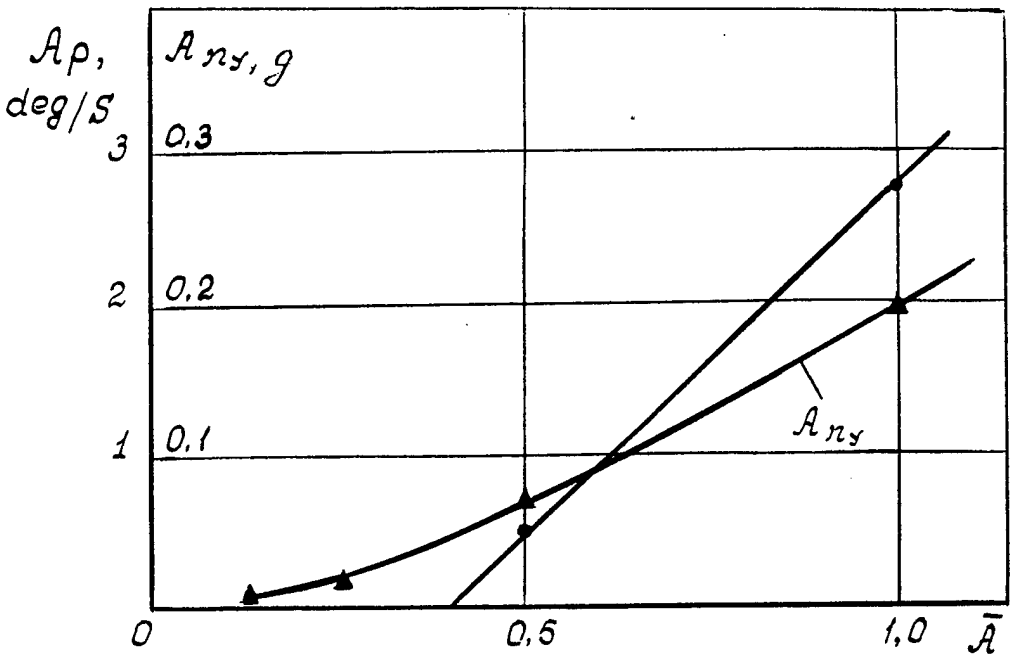

Fig.3.9. Elastic Mode Amplitude $\bar{A}$ Influence on Roll Rate Ap and Lateral Acceleration A_{n_y} Amplitudes.

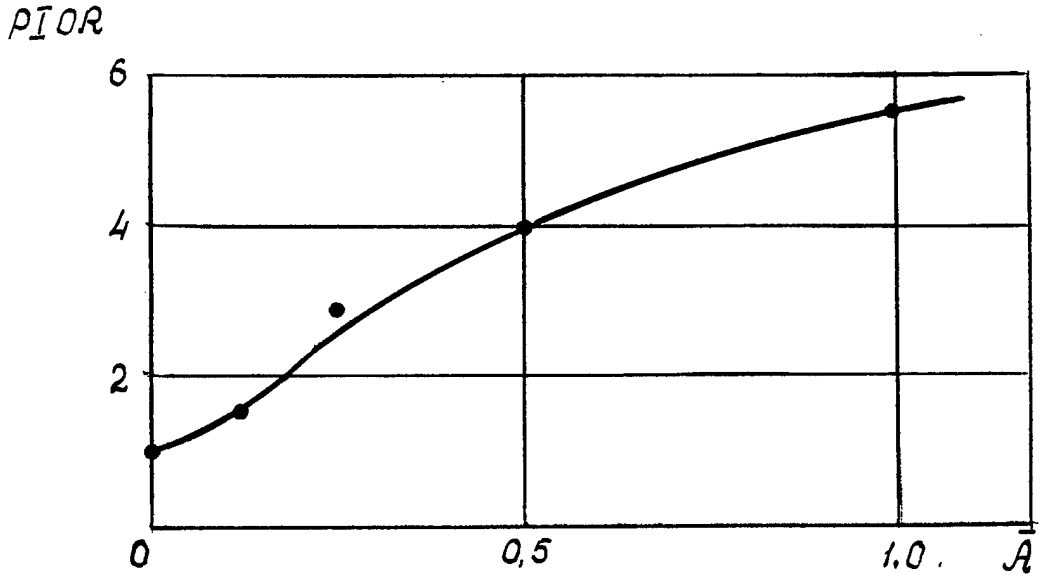

Fig.3.10. PIORs depending on Elastic Mode Amplitude $\bar{A}$.

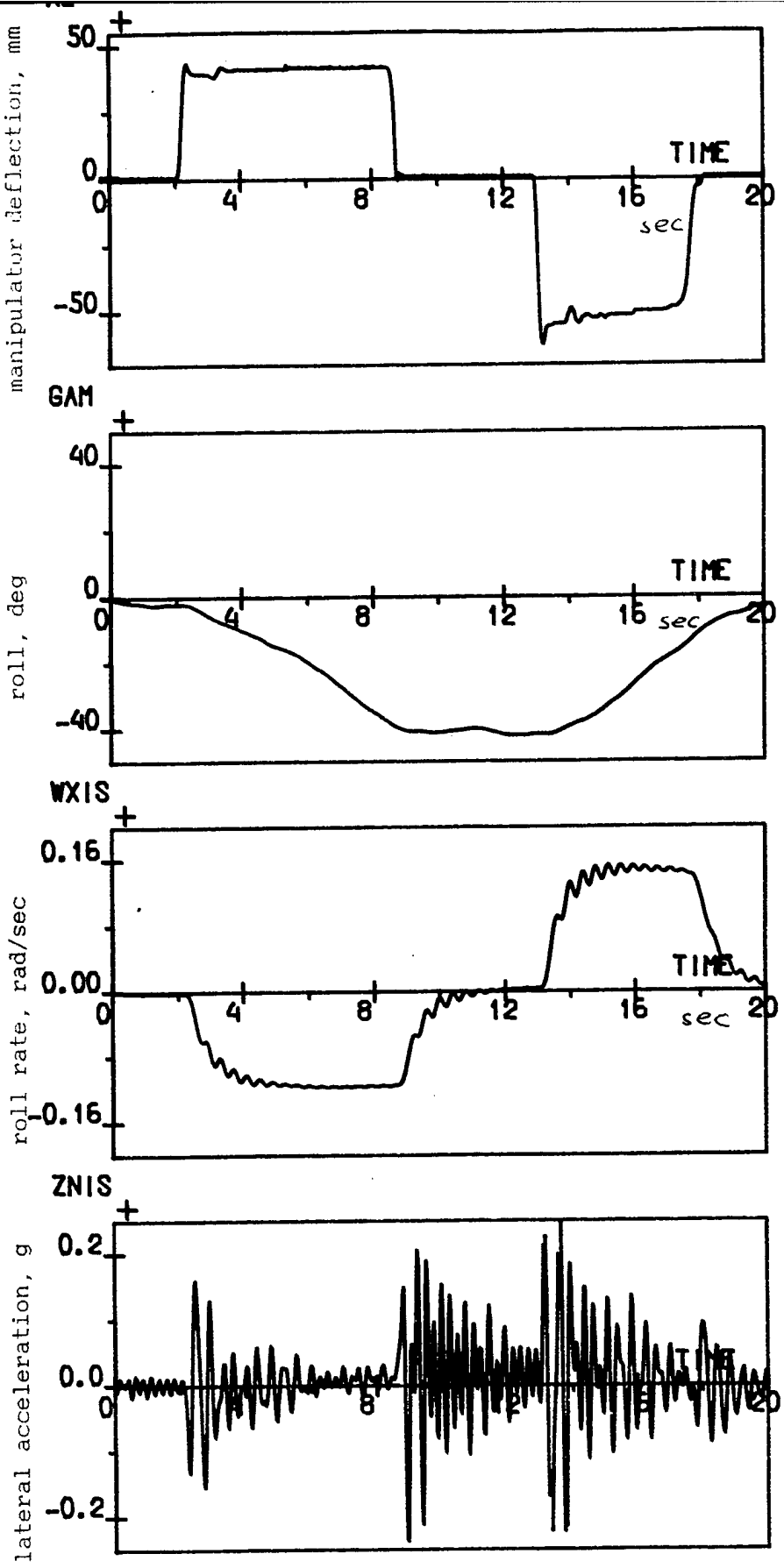

Fig.3.11. Time Histories of Elastic Aircraft

Elastic mode amplitude: $\bar{A}$ = 1
Motion simulated: roll

Manipulator: central stick
Aircraft gain: K/Kn = 1

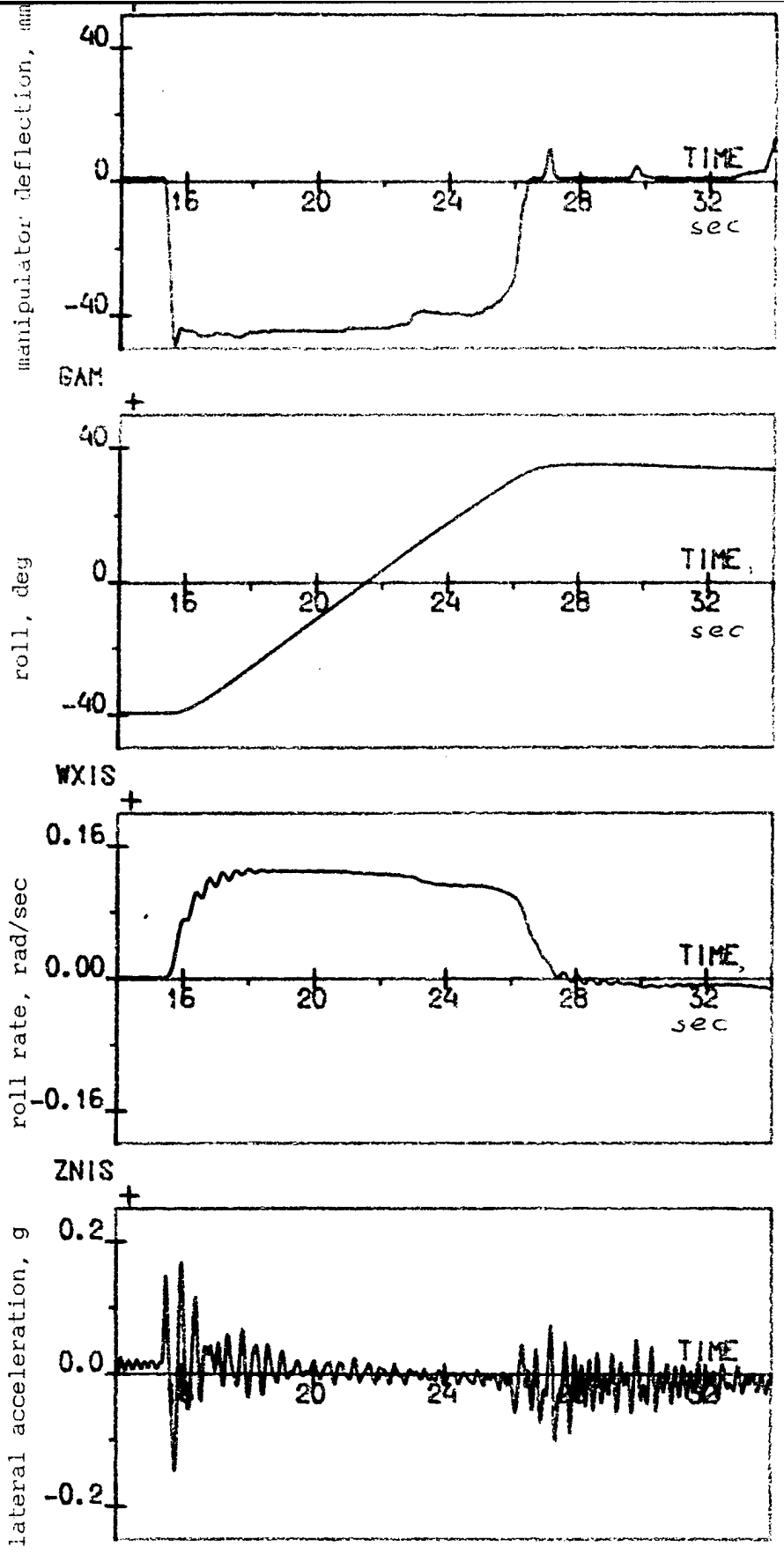

Fig.3.12. Time Histories of Elastic Aircraft

Elastic mode amplitude: $\bar{A} = 1$
Motion simulated: absent

Manipulator: central stick
Aircraft gain: K/Kn = 1

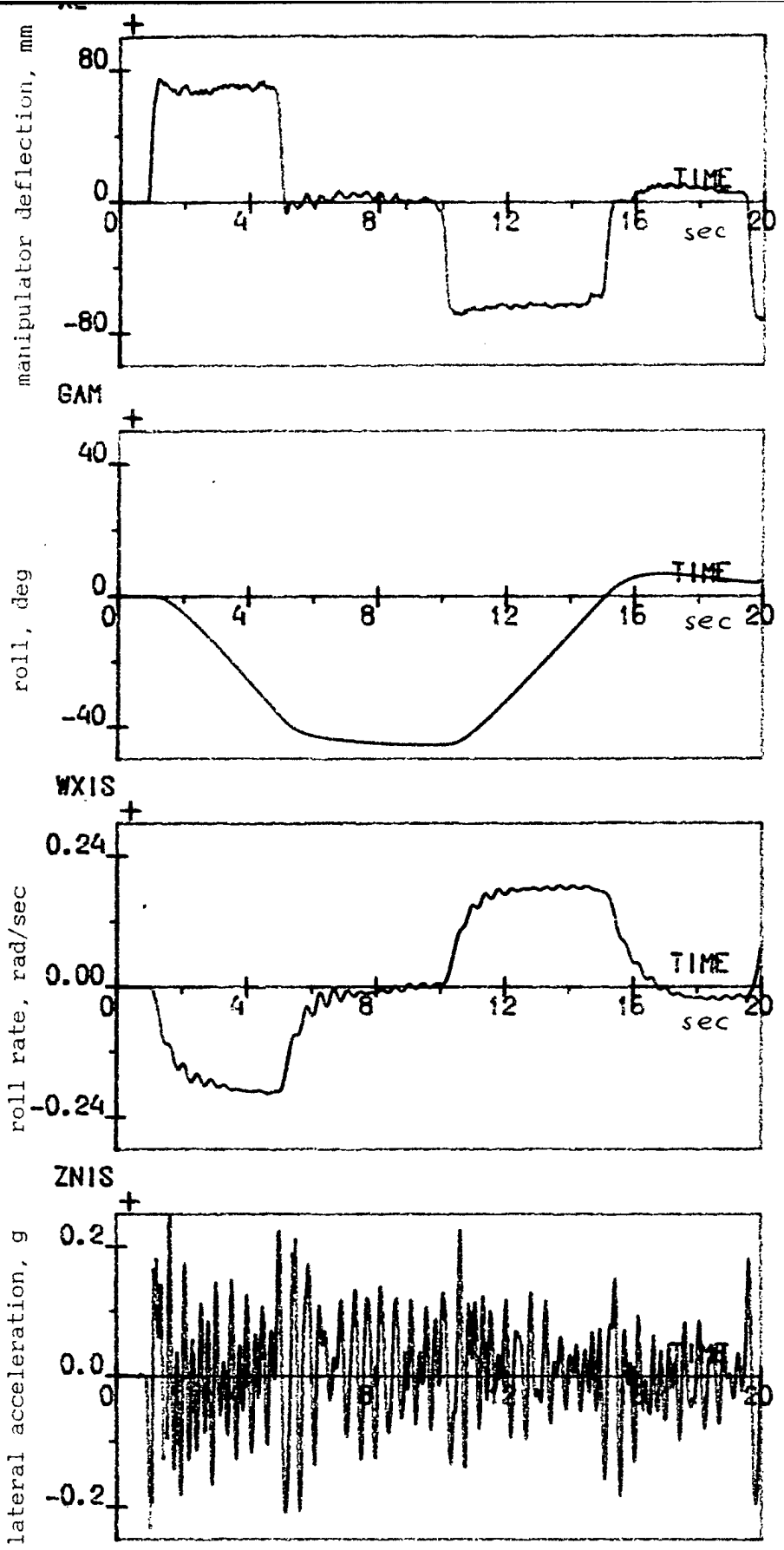

Fig.3.13. Time Histories of Elastic Aircraft

Elastic mode amplitude: $\bar{A}$ = 1 Manipulator: side stick
Motion simulated: roll, yaw, lat.displ. Aircraft gain: K/Kn = 1

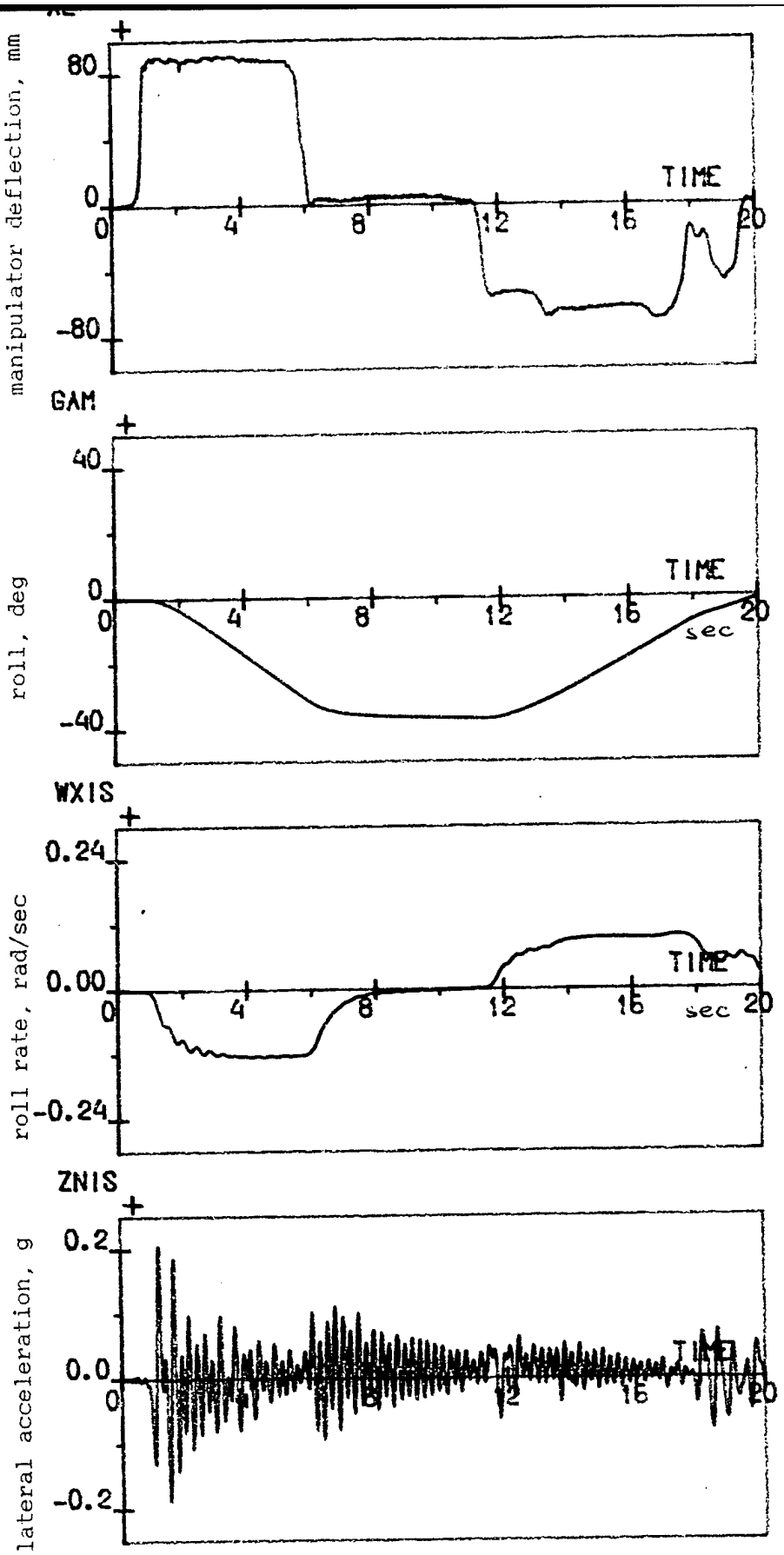

Fig.3.14a. Time Histories of Elastic Aircraft

Elastic mode amplitude: $\bar{A} = 1$ Manipulator: side stick

Motion simulated: roll, yaw, lat.displ. Aircraft gain: K/Kn = 0.5

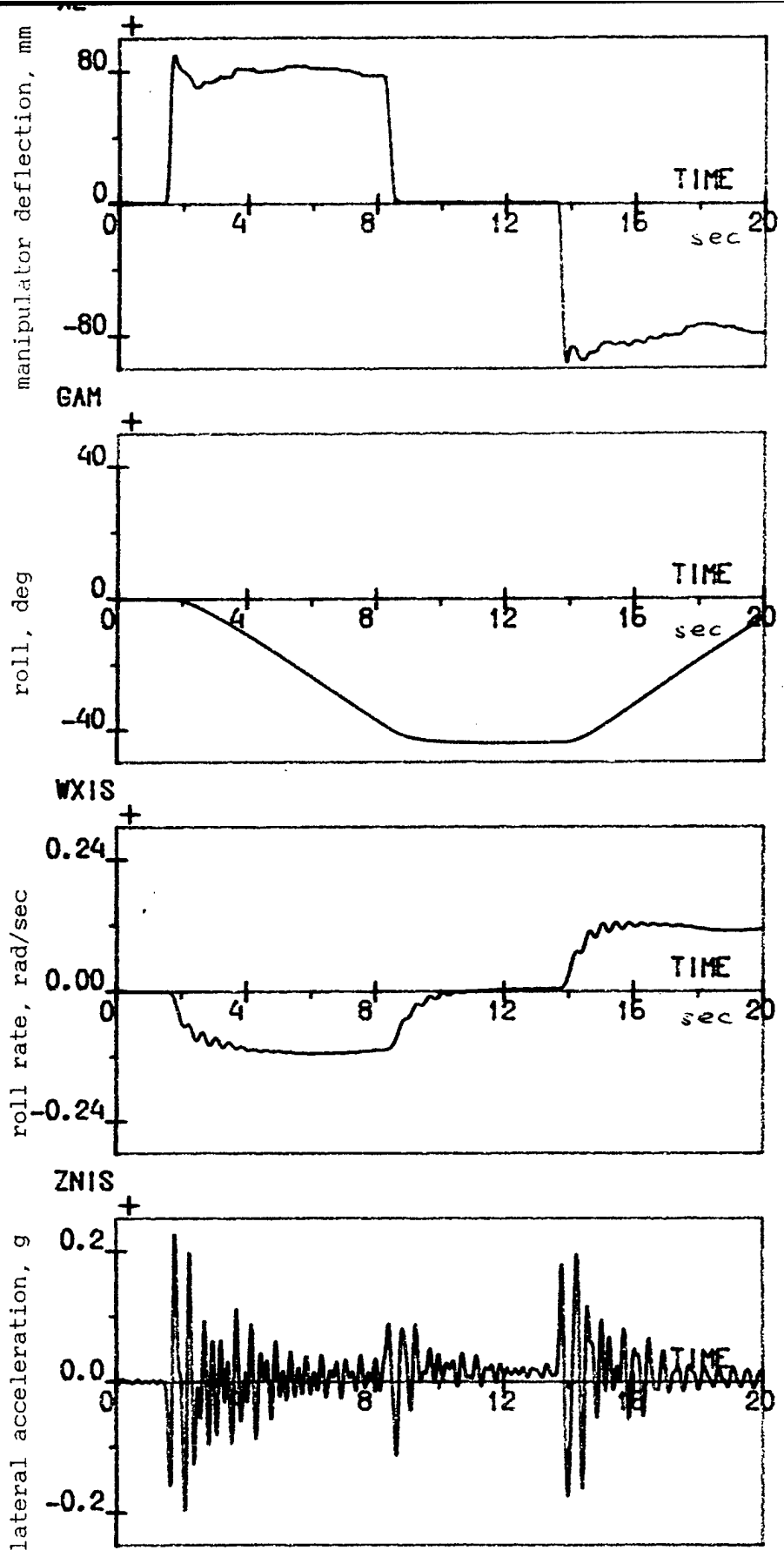

Fig.3.14b. Time Histories of Elastic Aircraft

Elastic mode amplitude: $\bar{A}$ = 1 Manipulator: central stic

Motion simulated: roll, yaw, lat.displ. Aircraft gain: K/Kn = 0.5

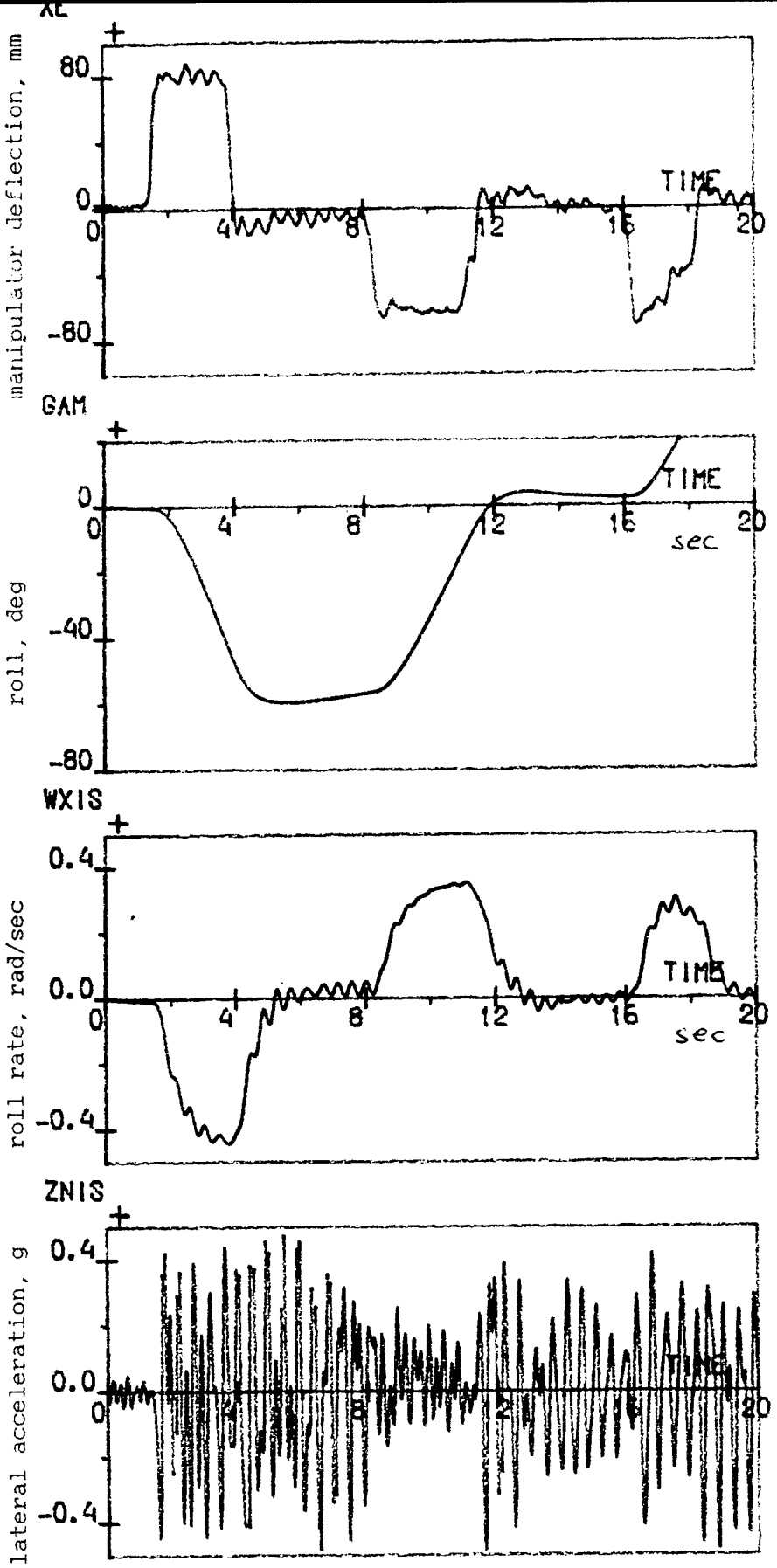

Fig.3.15. Time Histories of Elastic Aircraft

Elastic mode amplitude: $\bar{A}$ = 1 Manipulator: side stick
Motion simulated: roll, yaw, lat.displ. Aircraft gain: K/Kn = 2

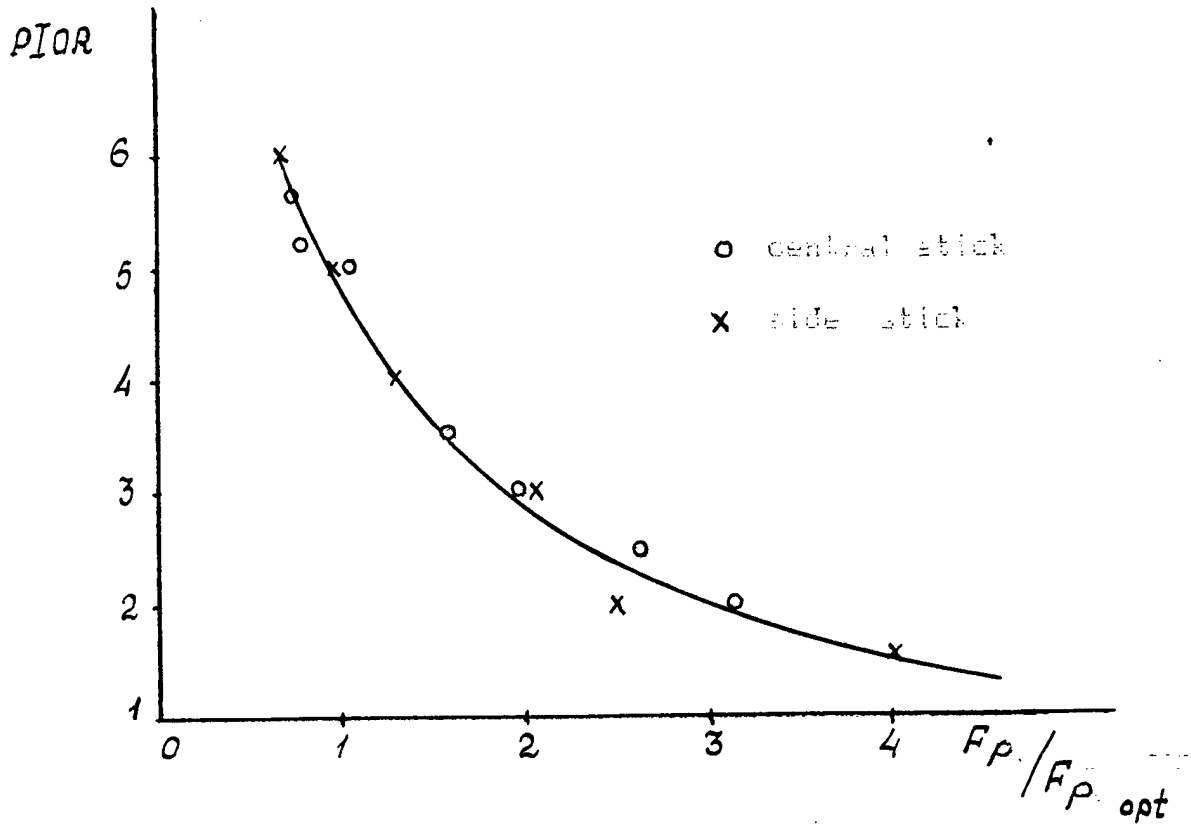

Fig.3.16. Lateral Control Sensitivity Influence on PIOR

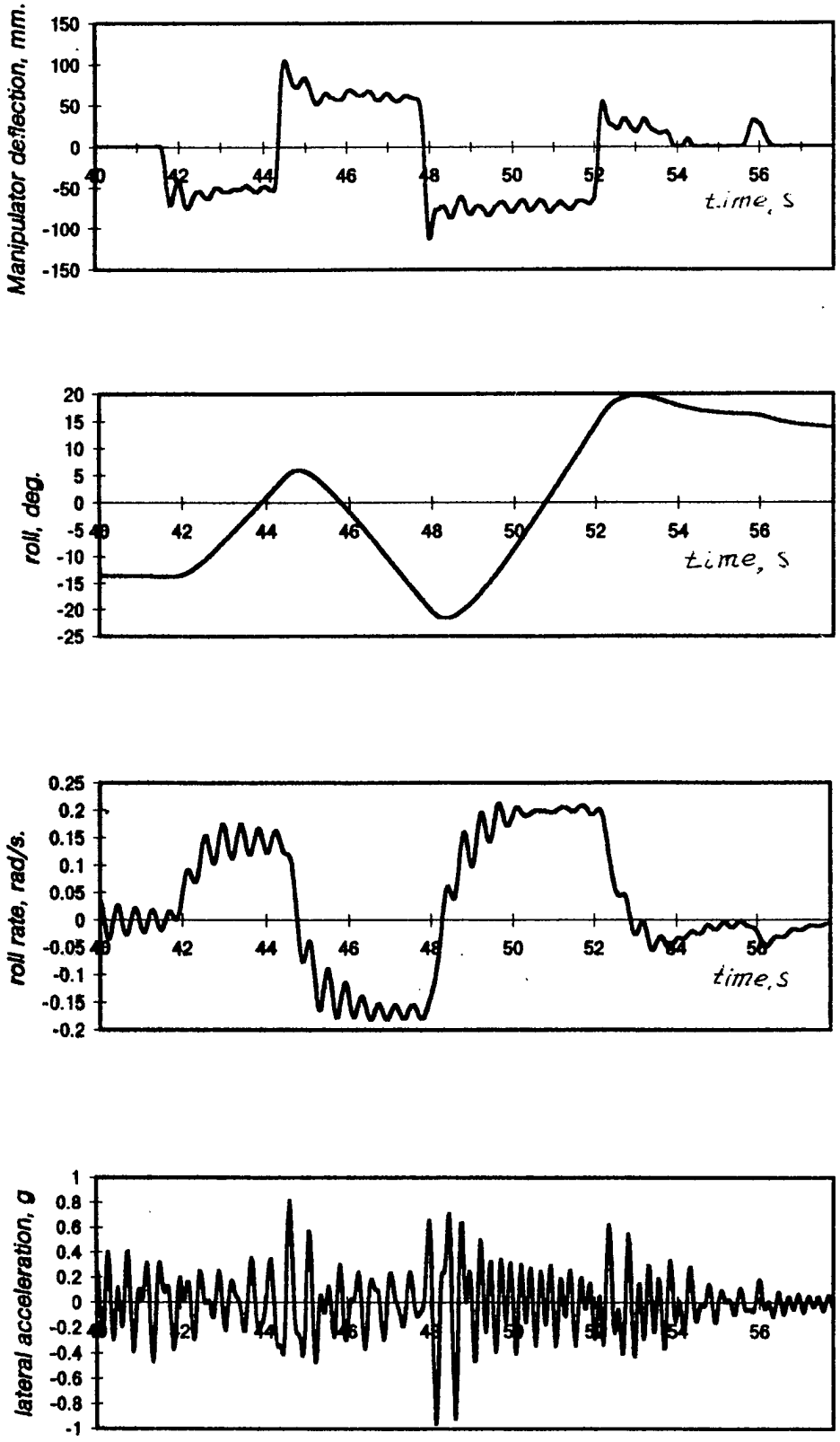

Fig.3.17. Time Histories of Elastic Aircraft

Elastic mode amplitude: $\bar{A}$ = 1
Motion simulated: roll
Manipulator: central stick
Aircraft gain: K/Kn = 1.5

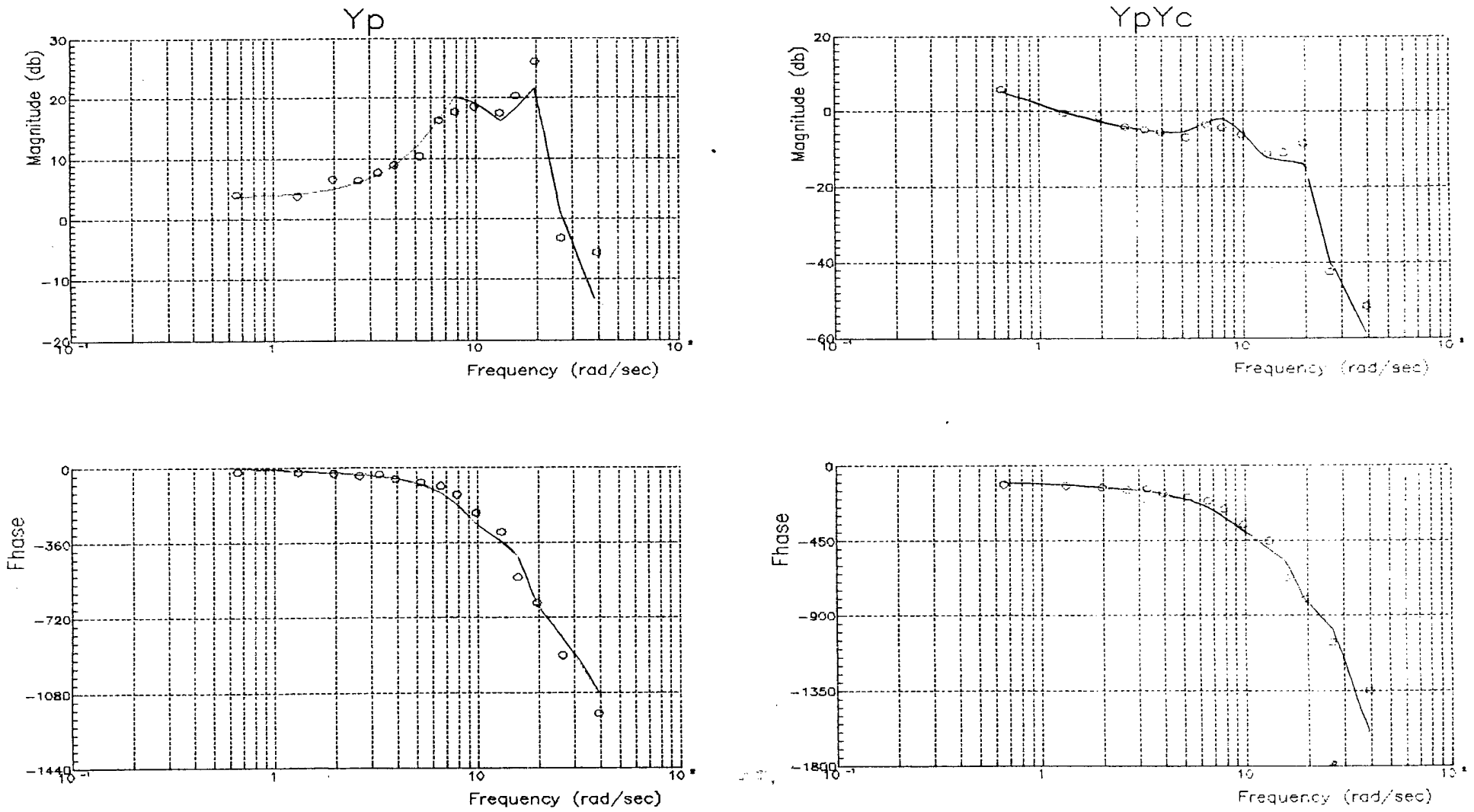

Fig.3.18.Pilot/Pilot—Aircraft describing function (isolated roll, $T_R = 0.1s$)

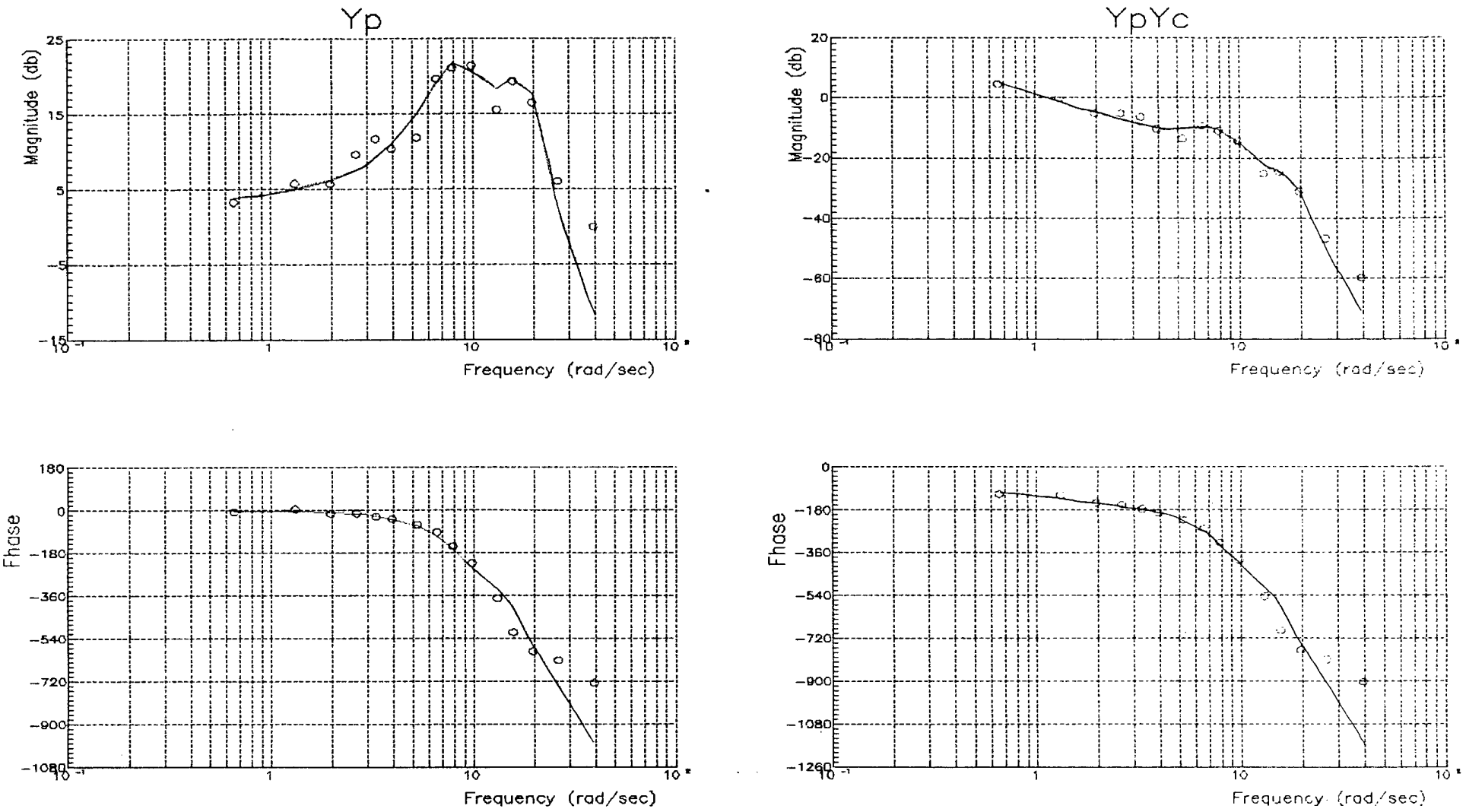

Fig.3.19.Pilot/Pilot—Aircraft describing function
(isolated roll, $T_R = 0.5s$)

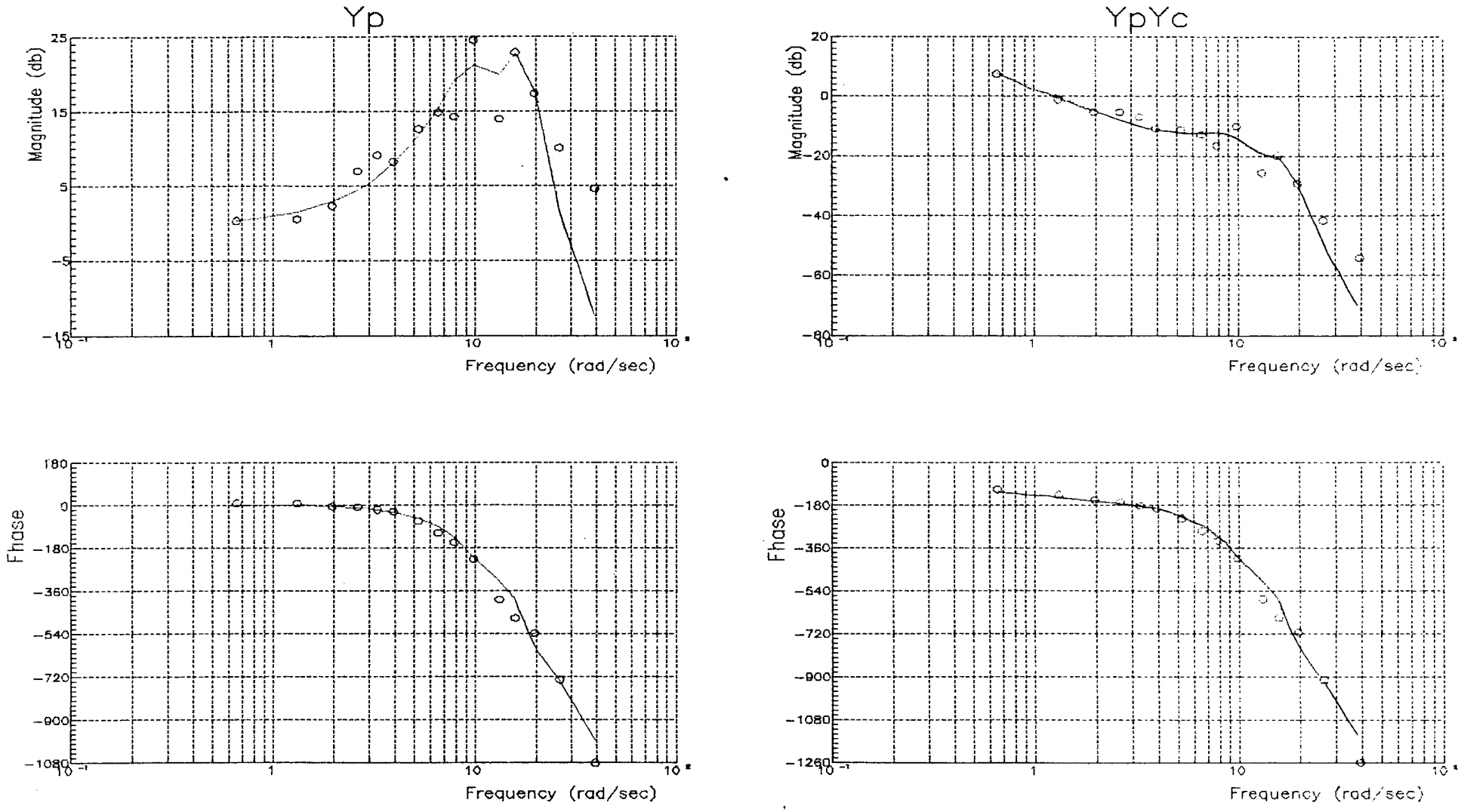

Fig.3.20.Pilot/Pilot—Aircraft describing function (isolated roll, T_R = 1.0s)

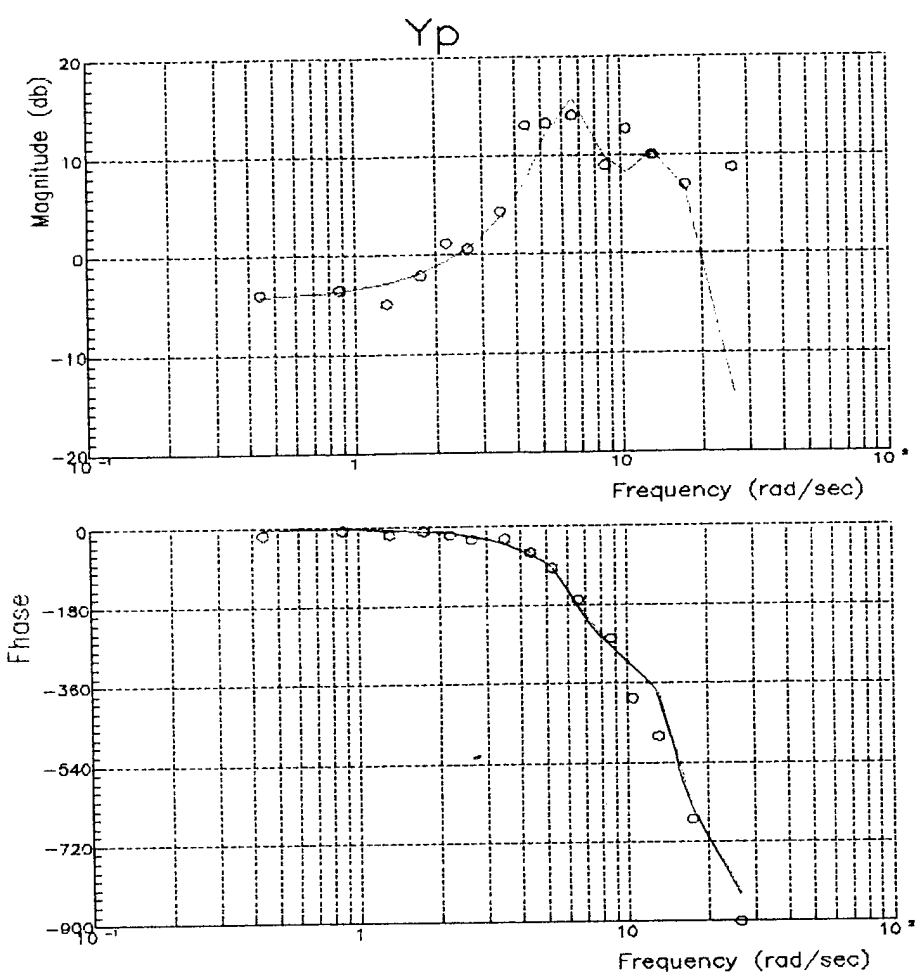

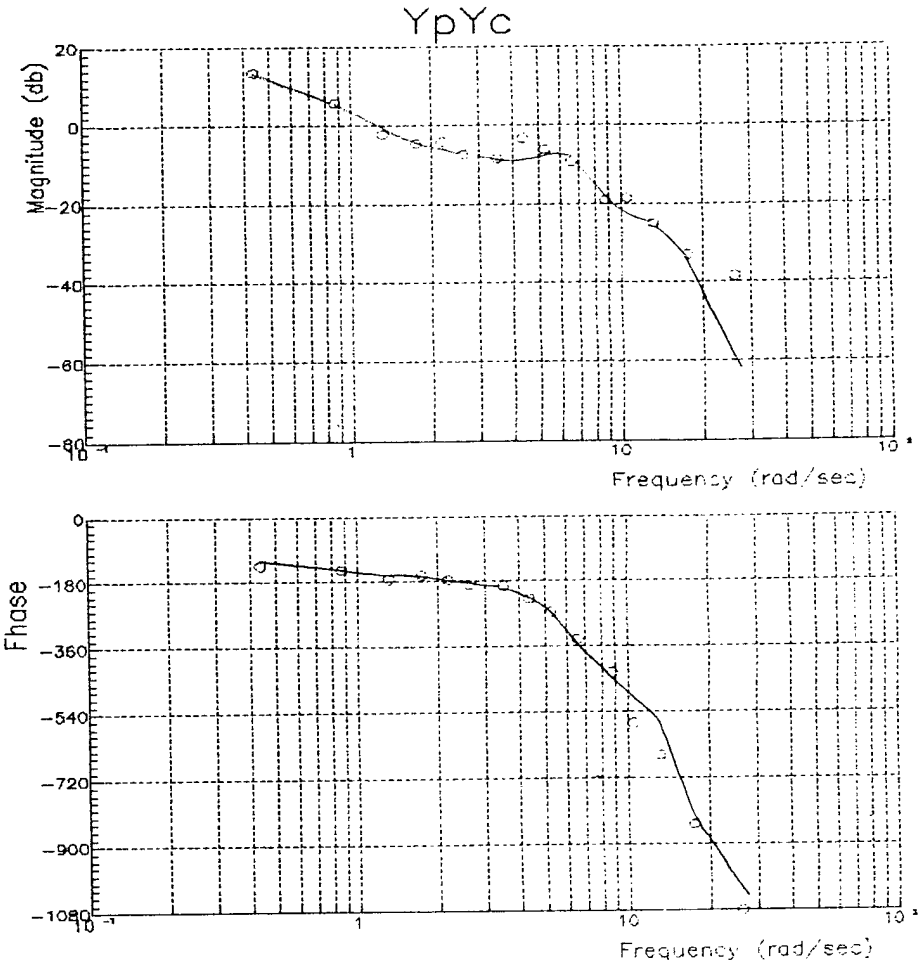

Fig. 3.21. Pilot/Pilot—Aircraft describing function

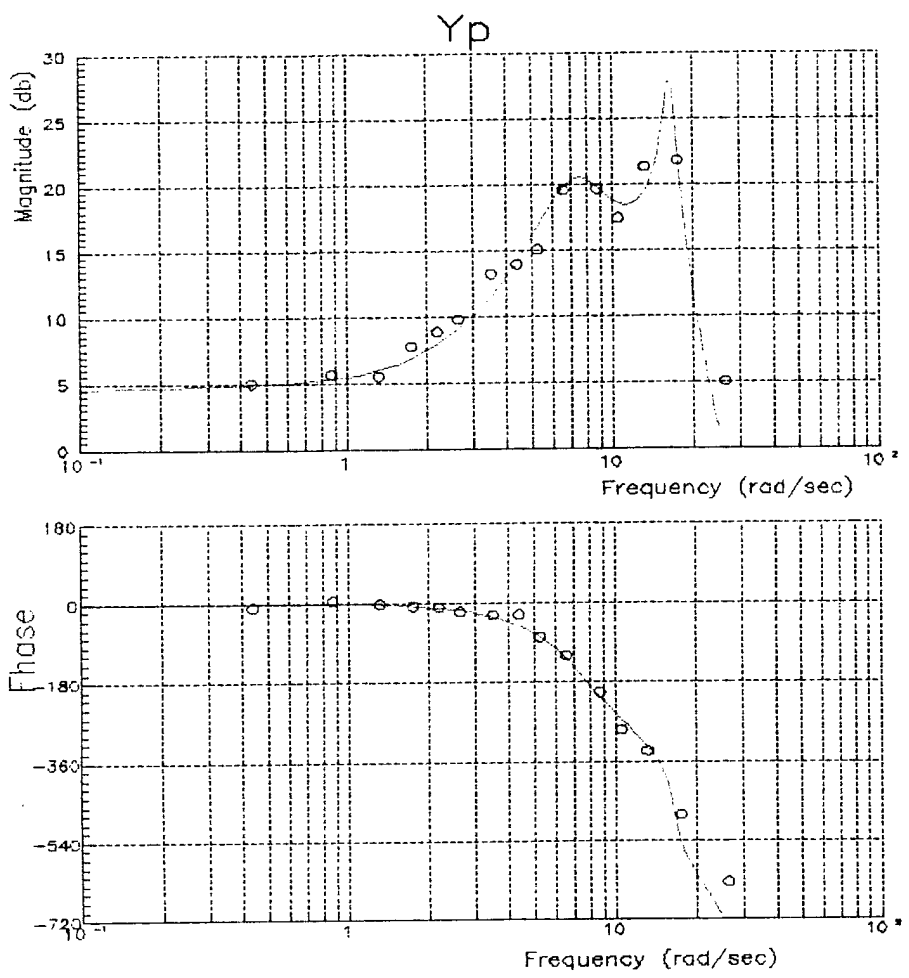

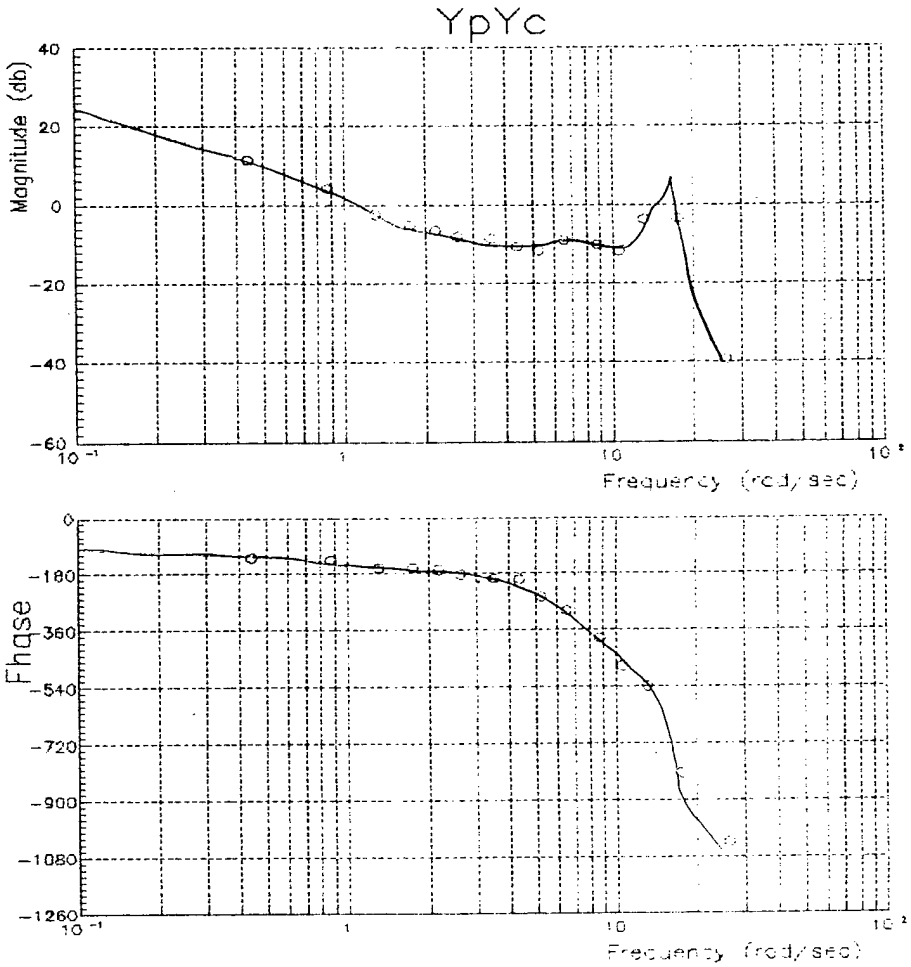

Fig.3.22. Pilot/Pilot—Aircraft describing function (elastic aircraft, equations (3.1)).